CONSTRUCTION MATERIALS CONSULTANTS, INC.

# XRF and XRD Studies of Soils


York Building Products - Belvidere Plant
Cecil County, Maryland

April 7, 2021
CMC 0321116

## TABLE OF CONTENTS

## EXECUTIVE SUMMARY

Twelve (12) soil samples, from BVD 21-10 Wash Pond 11, marked as S-1 through S-12, collected at 4 ft. intervals from 4 ft. to 52 ft. depths were analyzed for chemical (major element oxide) compositions by X-ray fluorescent spectroscopy (XRF), and, mineralogical compositions by X-ray diffraction (XRD).

Samples were originally received in moist conditions, which were dried to constant masses in a laboratory oven. Approximately 8 grams of sample from each depth was pulverized with alcohol to finer than No. 200 mesh, from which 7 grams were used for preparation of pressed pellet in a 25-ton automated press for XRF and remaining gram of pulverized sample was used for preparation of XRD.

XRF studies provided relatively consistent chemical compositions of soils through depth with some intersample (depth wise) variations in silica, alumina, and iron oxides as the three major oxides, and, lime, magnesia, alkalis, titanium, and phosphorus oxides as the minor oxides. Oxides of silicon contents varied between 47 and 63 percent, aluminum 15 to 27 percent, iron 8.5 to 12.5 percent, calcium less than 0.2 percent, magnesium 0.7 to 0.9 percent, sodium less than 0.2 percent, potassium 0.7 to 1.5 percent, titanium 0.6 to less than 1 percent, and phosphorus around 0.1 percent. No sulfate was detected in any sample. Balances corresponding to volatiles (loss on ignition) varied between 10 and 13 percent. Silica contents showed a progressive increase towards the mid-depth samples (S-5, S-6) corresponding to progressive decrease in alumina and iron from the end-depth members (S-1, S-2, S-10, S-11) to the mid-depth ones (S-5, S-6). Such systematic variations in chemical compositions are judged to be partly due to variations in quartz contents which showed highest values at the mid-depth samples (S5, S-6) compared to the end-depth ones, and clay mineralogies from kaolinite-based clays in all samples to illite-based clays in mid-depth and lower-depth ones, as determined from subsequent XRD studies.

Consistent with the chemical compositions, XRD studies showed the abundance of silt and clay-sized quartz as the dominant non-clay fraction, and kaolinite, and illite as the two main clay minerals. XRD studies did not detect any potentially expansive clays (e.g., some montmorillonite-types) in the samples. Muscovite and biotite are two common micas found in the clay-sized fractions associated with kaolinite and illite clays.

Due to the abundance of plate minerals in micas and clays, sample preparation for XRD has a major influence in the phase identifications and quantifications. Therefore, along with the conventional bulk sample powder diffraction of pulverized soil in a sample holder in XRD, a slurry of soil in alcohol was pulverized in McCrone micronizing mill for 10-minutes to create abundant size fractions of less than 10 micron in size, which was subsequently placed as a slurry on a zero background sample holder of XRD for the clay minerals to settle in random orientations from alcohol suspension. Such randomly oriented settled clay minerals from alcohol slurry provided better peaks for clay minerals in the diffraction pattern than the pressed pellets without any new phase than the ones already detected from conventional bulk sample method. However, it is the loosely compacted soil samples (not pressed pellet) in sample holder that have provided the best match of known clay and non-clay fractions to their theoretical diffraction peaks. Therefore, results obtained from loosely compacted soil were eventually used for the final results.

## INTRODUCTION

Reported herein are the results of chemical and mineralogical compositions of twelve soil samples collected from the surface through 52 ft. deep at 4 ft. intervals, determined from energy-dispersive X-ray fluorescence spectroscopy (XRF), and X-ray diffraction (XRD), respectively. XRF provided the major element oxide compositions of soil, whereas XRD provided the types and semi-quantitative estimates of clay and non-clay components of soil.

## SAMPLES

Figure 1 shows the samples as received in plastic Ziploc bags for XRF and XRD.

Samples were oven dried, then representative portions of each sample weighing 8 grams were selected for pulverization in a Rocklab pulverizer with alcohol as the coolant.


Figure 1: Twelve soil samples received from 4 ft. to 52 ft. depth that were dried in a laboratory oven to constant mass prior to the sample preparation for XRD and XRF studies.

## METHODOLOGIES

### X-RAY FLUORESCENCE SPECTROSCOPY

X-ray fluorescence (XRF) was used for determining the major element oxide compositions of soil, which provide clues about the clay and non-clay components as well as the presence of any organic or volatile constituents in the soil.

A series of standards from Portland cements, lime, gypsum to various rocks, and masonry mortars of certified compositions (e.g., from USGS, GSA, NIST, CCRL, Brammer, or measured by ICP) are used to calibrate the instrument for various oxides, and empirical calculations are done from such calibrations to determine oxide compositions of soil.


Figure 2: Rigaku NEX-CG in CMC, which can perform analyses of 9 pressed pellet or fused bead of sample. Soil samples are prepared as pressed pellets.

An energy-dispersive bench-top X-ray fluorescence unit from Rigaku Americas Corporation (NEX-CG) was used (Figure 2). Rigaku NEX CG delivers rapid qualitative and quantitative determination of major and minor atomic elements in a wide variety of sample types with minimal standards. Unlike conventional EDXRF analyzers, the NEX CG was engineered with a unique close-coupled Cartesian Geometry (CG) optical kernel that dramatically increases signal-to-noise. By using monochromatic secondary target excitation, instead of conventional direct excitation, sensitivity is further improved. The resulting dramatic reduction in background noise, and simultaneous increase in element peaks, result in a spectrometer capable of routine trace element analysis even in difficult sample types. The instrument is calibrated by using various certified (CCRL, NIST, GSA, and Brammer) reference standards of cements and rocks.

After oven drying, approximately 8 grams of representative soil samples were pulverized for 3 minutes with alcohol in a pulverizing mill with three wax tablets for preparation of pressed pellets. A 25-ton Spex automated hydraulic press was used for preparation of pressed pellets.

## X-RAY DIFFRACTION

Portions of ground soil left from XRF pellet preparation was compacted in sample holders for XRD studies for bulk mineralogical compositions of soil. The purpose of this study is to detect: (a) the clay and non-clay components in soil, (b) semi-quantitative estimates of clay and non-clay components, and (c) the presence of any potentially expansive clay in the soil.

X-ray diffraction was carried out in a Bruker D2 Phaser (2nd Generation) benchtop Powder diffractometer (Figure 3, Bragg-Brentano geometry) employing a Cu X-ray tube (Cu k-alpha radiation of 1.54 angstroms), a primary slit of 1 mm, a receiving slit of 3 mm, a position sensitive 1D Lynxeye XE-T detector. Generator settings used are 30 kV and 10mA (300 watt).

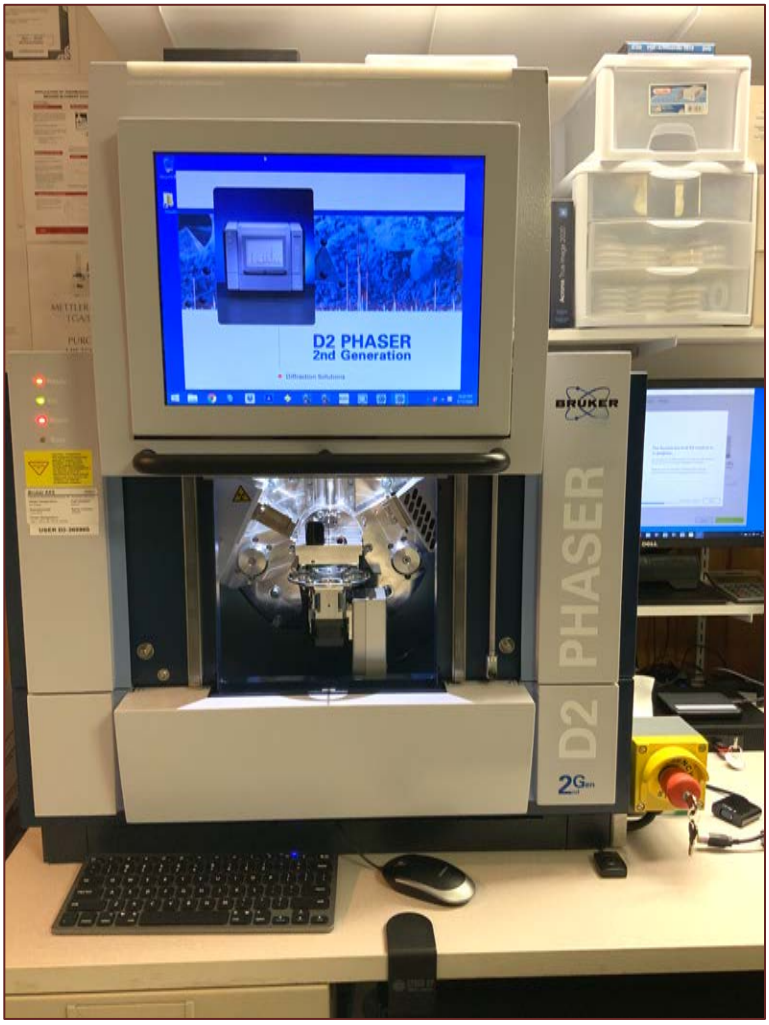


Figure 3: Bruker's D2 Phaser (2nd generation) benchtop X-ray powder diffractometer with Lynxeye 1D position sensitive detector used in X-ray diffraction studies of samples.

In addition to bulk soil XRD studies of all 12 samples, three samples from end-depths and mid-depth locations were selected for additional sample preparation steps to more accurately detect the clay minerals. About 10 grams of soil was first ground by a mortar and pestle and passed through US 325 sieve to collect finer than 44-micron size fraction. About 3-gram of sieved soil fraction (< 45 micron size) was then mixed with 10-gram of ethyl alcohol and pulverized in a McCrone micronizing mill with 44 agate cylinders for 10 minutes. The slurry such prepared was then collected and a few drops were placed in a zero background sample holder, which is an optically polished 111 plane of silicon wafer attached to a stainless steel sample holder for use in the 6-position sample stage of D2 Phaser. Tests were scanned at 2θ from 8° to 64° with a step of 0.05° 2θ integrated at 0.05 sec. step$^{-1}$ dwell time.

The resulting diffraction patterns were collected by Bruker's Diffrac.Measurement software. Phase identification was done with Bruker's Diffrac.EVA software with the search-match database from Crystallographic Open Database (COD). Additional phase identification, and Rietveld quantitative analyses were carried out with Match! software.

## X-RAY FLUORESCENCE SPECTROSCOPY (XRF)

**XRF Analyses of Soil Samples**

| | Depth (ft.) | $SiO_2$ | $Al_2O_3$ | CaO | MgO | $Na_2O$ | $K_2O$ | $Fe_2O_3$ | $TiO_2$ | $P_2O_5$ | $SO_3$ | Balance | Total |
|---|---|---|---|---|---|---|---|---|---|---|---|---|---|
| S-1 | 4-8 | 47.7 | 25.5 | 0.111 | 0.759 | ND | 0.974 | 11.5 | 0.634 | 0.172 | ND | 12.8 | 100 |
| S-2 | 8-12 | 47.8 | 26.8 | 0.125 | 0.827 | ND | 1.260 | 10.5 | 0.764 | 0.146 | ND | 11.9 | 100 |
| S-3 | 12-16 | 48.4 | 26.1 | 0.137 | 0.861 | ND | 1.270 | 11.1 | 0.774 | 0.142 | ND | 11.4 | 100 |
| S-4 | 16-20 | 47.3 | 25.6 | 0.138 | 0.830 | 0.158 | 1.210 | 12.4 | 0.730 | 0.135 | ND | 11.8 | 100 |
| S-5 | 20-24 | 60.5 | 16.7 | 0.120 | 0.765 | ND | 0.939 | 8.9 | 0.694 | 0.110 | ND | 11.4 | 100 |
| S-6 | 24-28 | 62.5 | 15.2 | 0.097 | 0.713 | ND | 0.783 | 8.6 | 0.628 | 0.109 | ND | 11.7 | 100 |
| S-7 | 28-32 | 49.8 | 25.3 | 0.151 | 0.930 | 0.175 | 1.500 | 11.0 | 0.865 | 0.110 | ND | 10.4 | 100 |
| S-8 | 32-36 | 47.7 | 26.4 | 0.115 | 0.818 | 0.155 | 1.070 | 10.7 | 0.726 | 0.133 | ND | 12.5 | 100 |
| S-9 | 36-40 | 51.5 | 23.9 | 0.122 | 0.947 | 0.188 | 1.270 | 9.3 | 0.974 | 0.125 | ND | 12.0 | 100 |
| S-10 | 40-44 | 50.4 | 25.4 | 0.127 | 0.937 | 0.186 | 1.170 | 9.6 | 0.899 | 0.133 | ND | 11.5 | 100 |
| S-11 | 44-48 | 46.2 | 26.3 | 0.128 | 0.910 | 0.153 | 1.210 | 11.1 | 0.897 | 0.141 | ND | 13.2 | 100 |
| S-12 | 48-52 | 55.4 | 19.8 | 0.123 | 0.882 | 0.174 | 1.130 | 10.1 | 0.749 | 0.135 | ND | 11.8 | 100 |

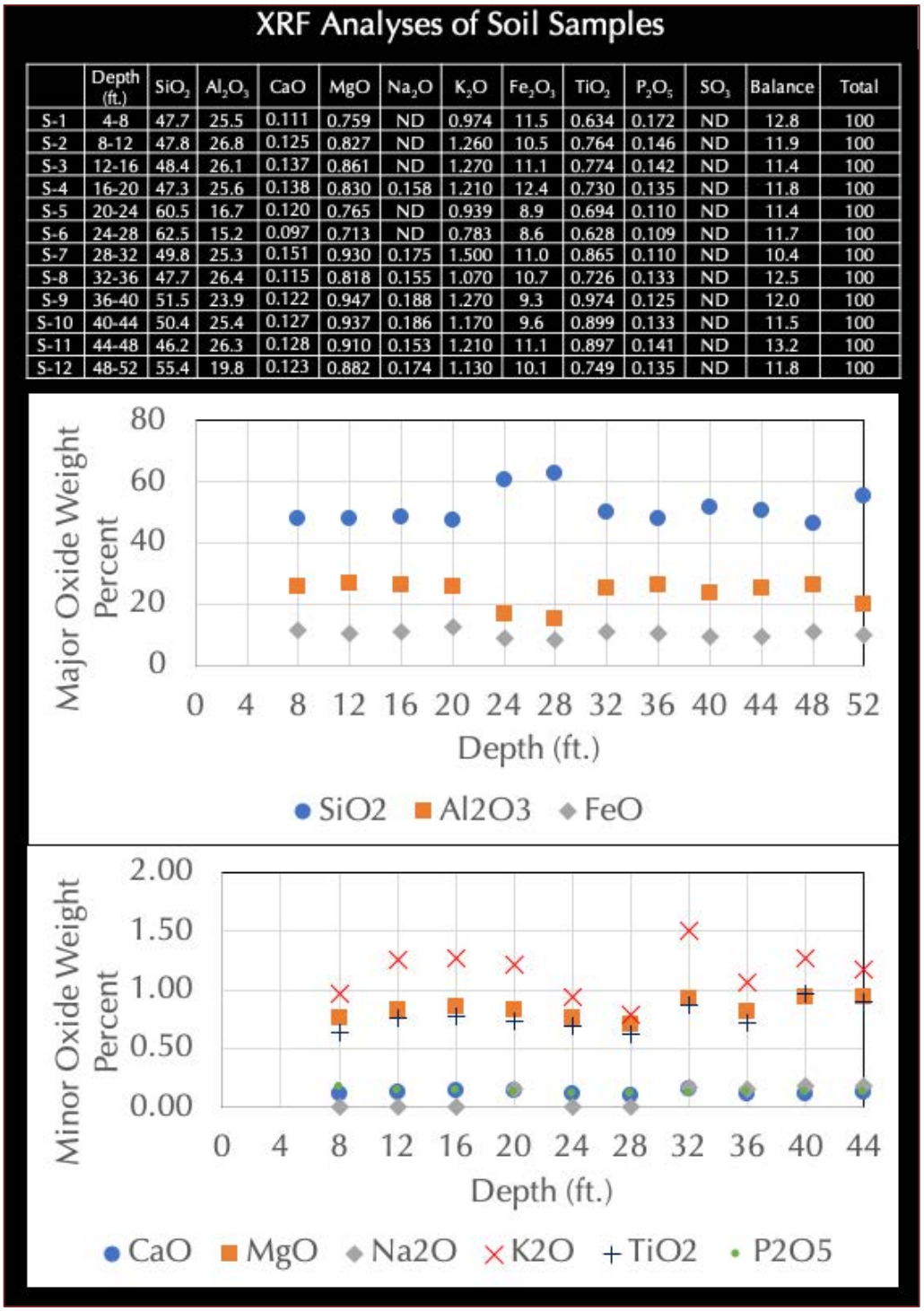


Figure 4: Results of chemical (oxide) compositions of soil samples determined from X-ray fluorescence spectroscopy (XRF). The middle and bottom plots show respective compositional variations of major and minor oxide components of soil through depth.

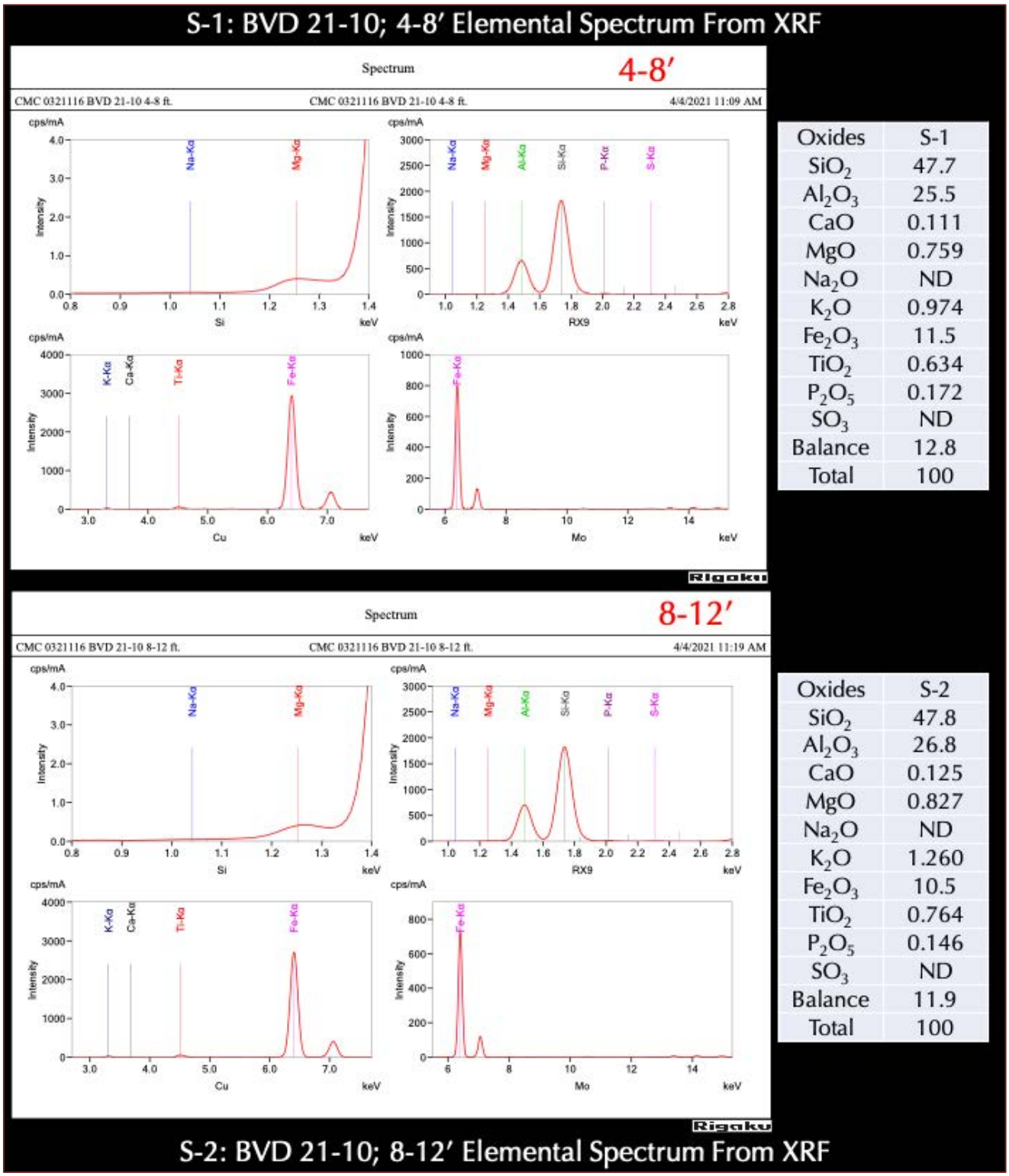


| Oxides | S-1 |
|---|---|
| $SiO_2$ | 47.7 |
| $Al_2O_3$ | 25.5 |
| CaO | 0.111 |
| MgO | 0.759 |
| $Na_2O$ | ND |
| $K_2O$ | 0.974 |
| $Fe_2O_3$ | 11.5 |
| $TiO_2$ | 0.634 |
| $P_2O_5$ | 0.172 |
| $SO_3$ | ND |
| Balance | 12.8 |
| Total | 100 |

| Oxides | S-2 |
|---|---|
| $SiO_2$ | 47.8 |
| $Al_2O_3$ | 26.8 |
| CaO | 0.125 |
| MgO | 0.827 |
| $Na_2O$ | ND |
| $K_2O$ | 1.260 |
| $Fe_2O_3$ | 10.5 |
| $TiO_2$ | 0.764 |
| $P_2O_5$ | 0.146 |
| $SO_3$ | ND |
| Balance | 11.9 |
| Total | 100 |

Figure 5: XRF analyses of soil samples S-1 and S-2 from 4 to 8 ft. depths and 8 to 12 ft. depths, respectively.

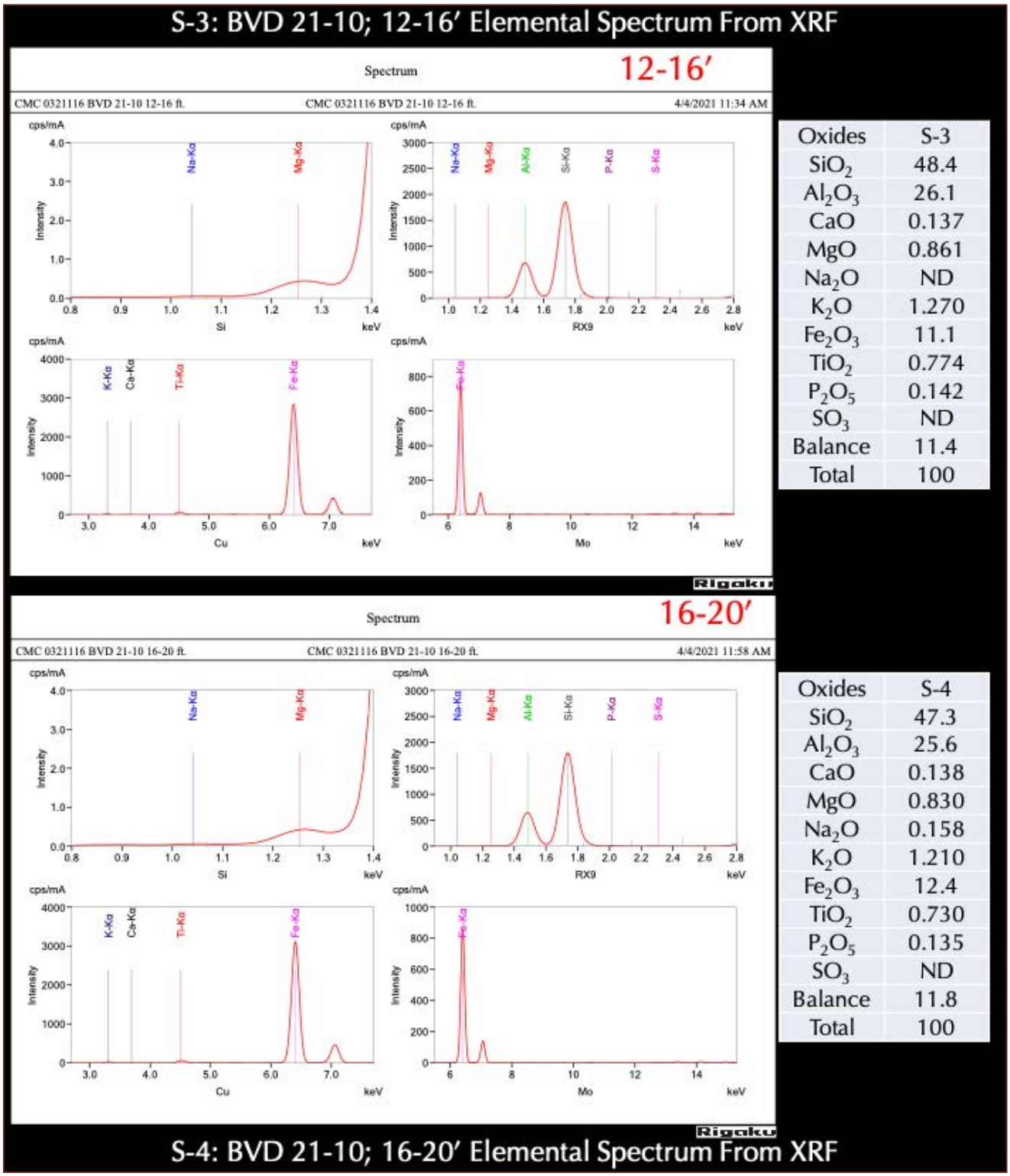


| Oxides | S-3 |
|---|---|
| $SiO_2$ | 48.4 |
| $Al_2O_3$ | 26.1 |
| CaO | 0.137 |
| MgO | 0.861 |
| $Na_2O$ | ND |
| $K_2O$ | 1.270 |
| $Fe_2O_3$ | 11.1 |
| $TiO_2$ | 0.774 |
| $P_2O_5$ | 0.142 |
| $SO_3$ | ND |
| Balance | 11.4 |
| Total | 100 |

| Oxides | S-4 |
|---|---|
| $SiO_2$ | 47.3 |
| $Al_2O_3$ | 25.6 |
| CaO | 0.138 |
| MgO | 0.830 |
| $Na_2O$ | 0.158 |
| $K_2O$ | 1.210 |
| $Fe_2O_3$ | 12.4 |
| $TiO_2$ | 0.730 |
| $P_2O_5$ | 0.135 |
| $SO_3$ | ND |
| Balance | 11.8 |
| Total | 100 |

Figure 6: XRF analyses of soil samples S-3 and S-4 from 12 to 16 ft. and 16 to 20 ft. depths, respectively.

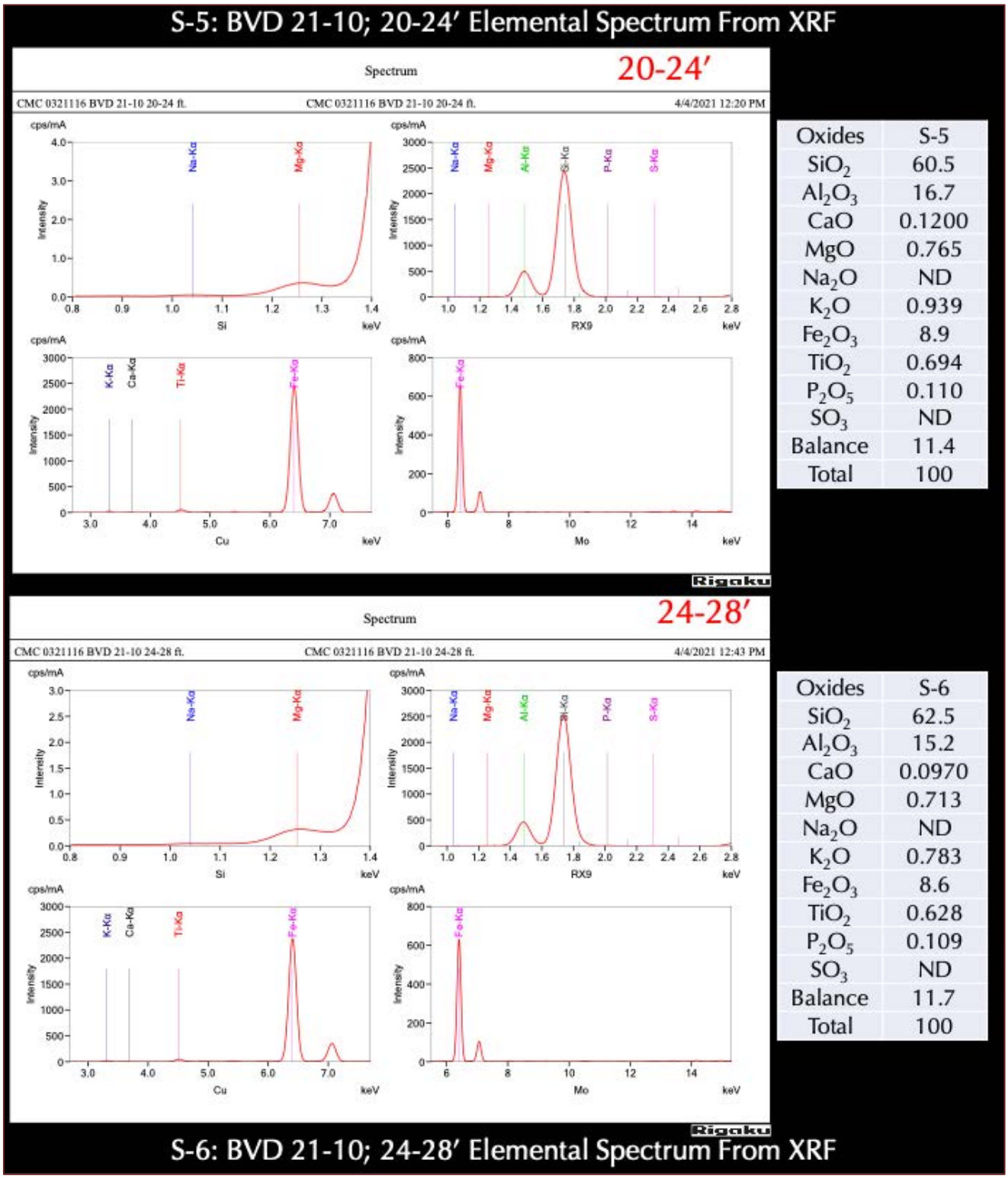


| Oxides | S-5 |
|---|---|
| $SiO_2$ | 60.5 |
| $Al_2O_3$ | 16.7 |
| CaO | 0.1200 |
| MgO | 0.765 |
| $Na_2O$ | ND |
| $K_2O$ | 0.939 |
| $Fe_2O_3$ | 8.9 |
| $TiO_2$ | 0.694 |
| $P_2O_5$ | 0.110 |
| $SO_3$ | ND |
| Balance | 11.4 |
| Total | 100 |

| Oxides | S-6 |
|---|---|
| $SiO_2$ | 62.5 |
| $Al_2O_3$ | 15.2 |
| CaO | 0.0970 |
| MgO | 0.713 |
| $Na_2O$ | ND |
| $K_2O$ | 0.783 |
| $Fe_2O_3$ | 8.6 |
| $TiO_2$ | 0.628 |
| $P_2O_5$ | 0.109 |
| $SO_3$ | ND |
| Balance | 11.7 |
| Total | 100 |

Figure 7: XRF analyses of soil samples S-5 and S-6 from 20 to 24 ft. and 24 to 28 ft. depths, respectively.

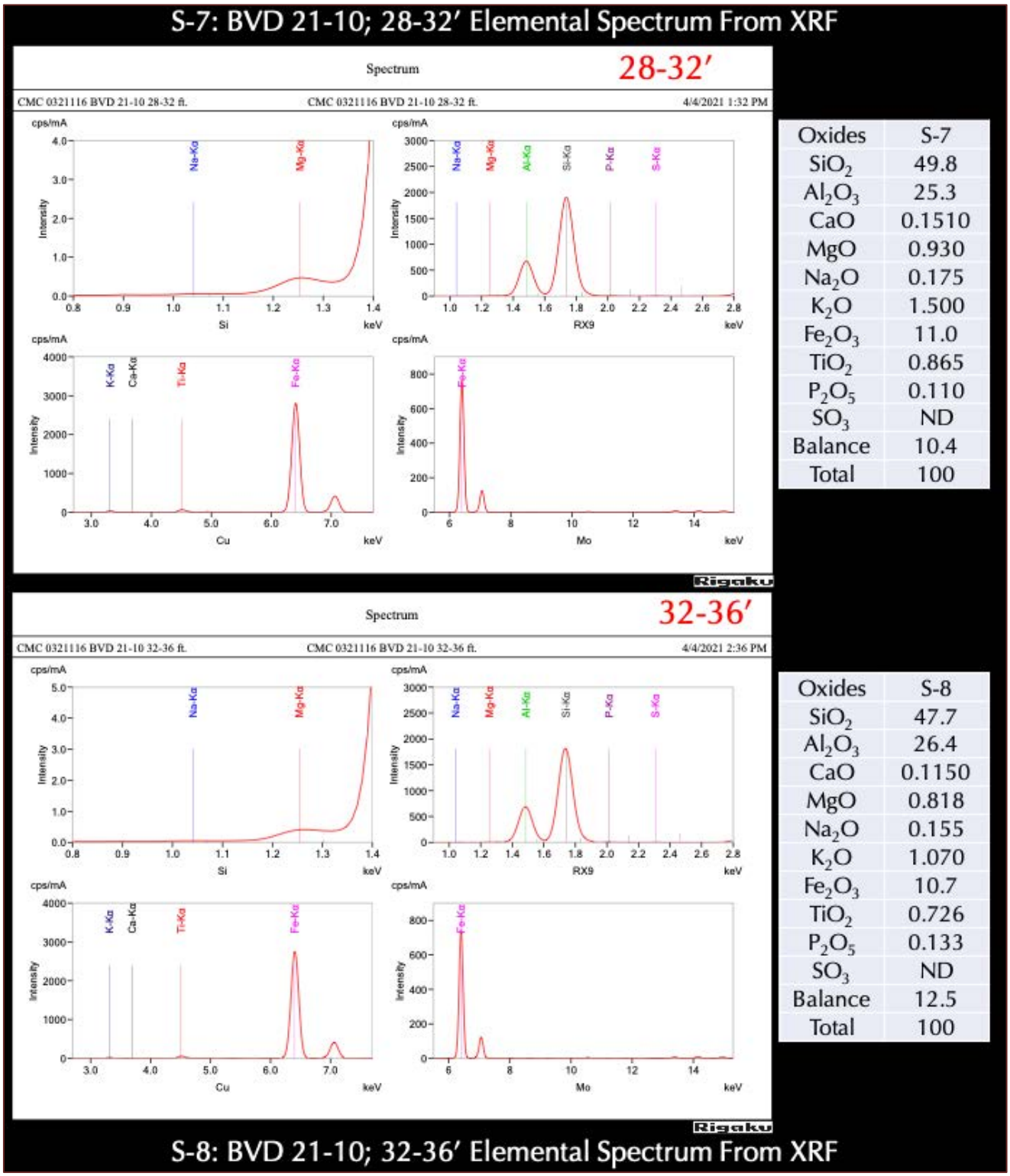


| Oxides | S-7 |
|---|---|
| $SiO_2$ | 49.8 |
| $Al_2O_3$ | 25.3 |
| CaO | 0.1510 |
| MgO | 0.930 |
| $Na_2O$ | 0.175 |
| $K_2O$ | 1.500 |
| $Fe_2O_3$ | 11.0 |
| $TiO_2$ | 0.865 |
| $P_2O_5$ | 0.110 |
| $SO_3$ | ND |
| Balance | 10.4 |
| Total | 100 |

| Oxides | S-8 |
|---|---|
| $SiO_2$ | 47.7 |
| $Al_2O_3$ | 26.4 |
| CaO | 0.1150 |
| MgO | 0.818 |
| $Na_2O$ | 0.155 |
| $K_2O$ | 1.070 |
| $Fe_2O_3$ | 10.7 |
| $TiO_2$ | 0.726 |
| $P_2O_5$ | 0.133 |
| $SO_3$ | ND |
| Balance | 12.5 |
| Total | 100 |

Figure 8: XRF analyses of soil samples S-7 and S-8 from 28 to 32 ft. and 32 to 36 ft. depths, respectively.

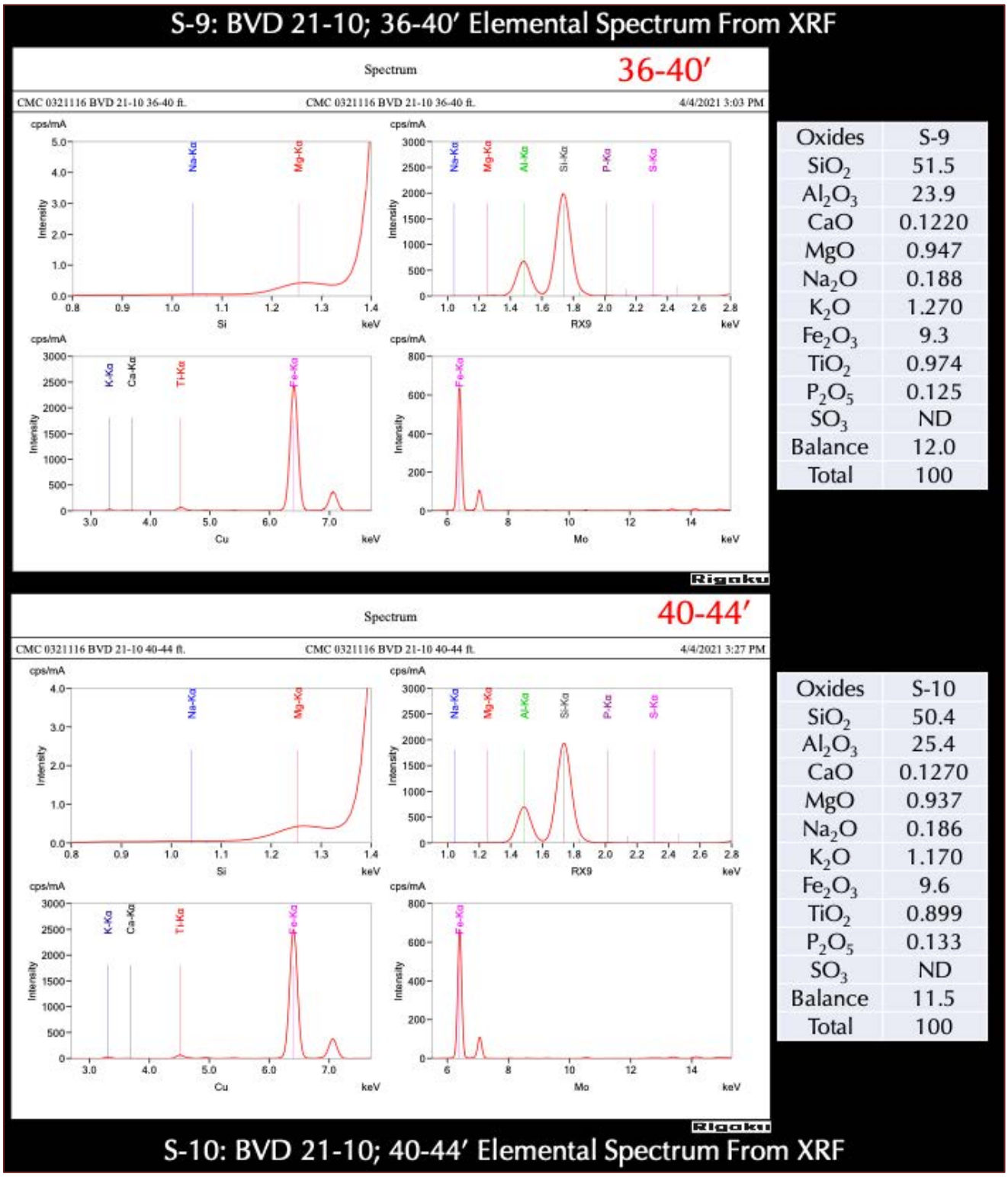


| Oxides | S-9 |
|---|---|
| $SiO_2$ | 51.5 |
| $Al_2O_3$ | 23.9 |
| CaO | 0.1220 |
| MgO | 0.947 |
| $Na_2O$ | 0.188 |
| $K_2O$ | 1.270 |
| $Fe_2O_3$ | 9.3 |
| $TiO_2$ | 0.974 |
| $P_2O_5$ | 0.125 |
| $SO_3$ | ND |
| Balance | 12.0 |
| Total | 100 |

| Oxides | S-10 |
|---|---|
| $SiO_2$ | 50.4 |
| $Al_2O_3$ | 25.4 |
| CaO | 0.1270 |
| MgO | 0.937 |
| $Na_2O$ | 0.186 |
| $K_2O$ | 1.170 |
| $Fe_2O_3$ | 9.6 |
| $TiO_2$ | 0.899 |
| $P_2O_5$ | 0.133 |
| $SO_3$ | ND |
| Balance | 11.5 |
| Total | 100 |

Figure 9: XRF analyses of soil samples S-9 and S-10 from 36 to 40 ft. and 40 to 44 ft. depths, respectively.

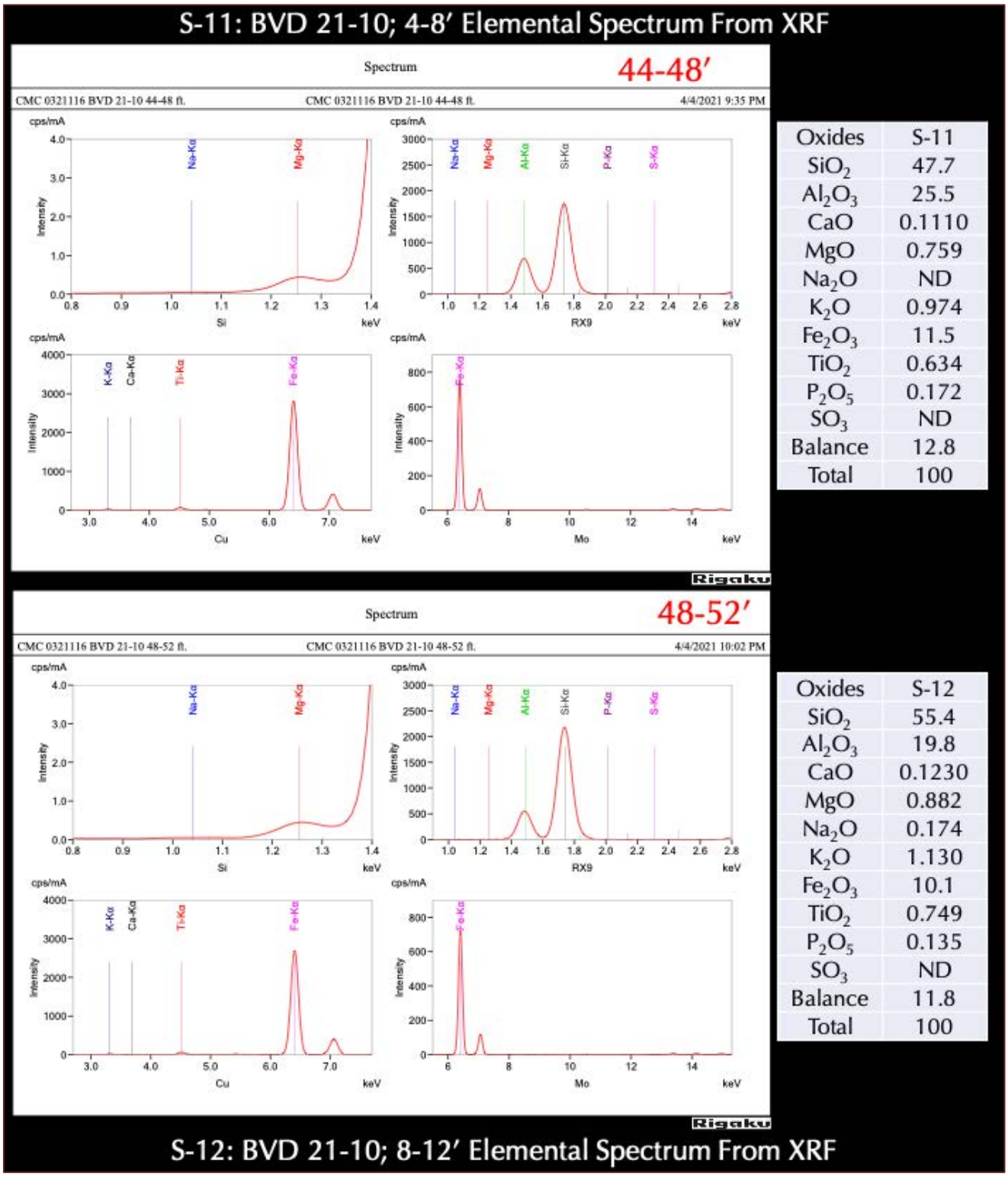


| Oxides | S-11 |
|---|---|
| $SiO_2$ | 47.7 |
| $Al_2O_3$ | 25.5 |
| CaO | 0.1110 |
| MgO | 0.759 |
| $Na_2O$ | ND |
| $K_2O$ | 0.974 |
| $Fe_2O_3$ | 11.5 |
| $TiO_2$ | 0.634 |
| $P_2O_5$ | 0.172 |
| $SO_3$ | ND |
| Balance | 12.8 |
| Total | 100 |

| Oxides | S-12 |
|---|---|
| $SiO_2$ | 55.4 |
| $Al_2O_3$ | 19.8 |
| CaO | 0.1230 |
| MgO | 0.882 |
| $Na_2O$ | 0.174 |
| $K_2O$ | 1.130 |
| $Fe_2O_3$ | 10.1 |
| $TiO_2$ | 0.749 |
| $P_2O_5$ | 0.135 |
| $SO_3$ | ND |
| Balance | 11.8 |
| Total | 100 |

Figure 10: XRF analysis of soil samples S-11 and S-12 from 44 to 48 ft. and 48 to 52 ft. depths, respectively.

## X-RAY DIFFRACTION (XRD)

XRD Analyses of Soil Samples

| | Depth (ft.) | Quartz | Kaolinite | Kaolin | Illite | Muscovite | Biotite | Chloritoid | Gibbsite | Goethite | Phlogopite | Chlorite | Hematite |
|---|---|---|---|---|---|---|---|---|---|---|---|---|---|
| S-1 | 4-8 | 44.0 | 14.4 | 11.4 | | 15.0 | | 7.4 | 5.1 | 2.7 | | | |
| S-2 | 8-12 | 47.4 | 19.4 | 15.2 | | 2.9 | | 8.4 | 4.3 | 2.5 | | | |
| S-3 | 12-16 | 47.9 | 13.0 | 10.5 | | 15.3 | | 6.5 | 4.3 | 2.3 | | | |
| S-4 | 16-20 | 53.7 | 12.9 | 10.3 | | | 2.8 | 7.6 | 5.2 | 2.8 | | | |
| S-5 | 20-24 | 42.7 | 4.2 | 3.2 | 43.5 | 1.3 | 1.6 | 2.4 | | 0.9 | | | |
| S-6 | 24-28 | 39.2 | 2.4 | 1.8 | 46.9 | 1.1 | 5.0 | 1.3 | | 0.7 | 1.6 | | |
| S-7 | 28-32 | 31.3 | 6.7 | 5.4 | 40.7 | 1.8 | 6.1 | 3.9 | 2.5 | 1.6 | | | |
| S-8 | 32-36 | 47.9 | 16.6 | 12.8 | | 3.9 | | 10.4 | 5.3 | 3.3 | | | |
| S-9 | 36-40 | 50.6 | 12.4 | 9.7 | | 3.0 | 2.6 | 7.0 | 3.9 | 1.9 | 8.9 | | |
| S-10 | 40-44 | 28.3 | 7.8 | 5.8 | 41.1 | 1.9 | | 4.7 | 3.0 | 1.4 | | 5.6 | 0.4 |
| S-11 | 44-48 | 31.2 | 7.0 | 6.0 | 40.8 | 1.8 | 1.6 | 4.0 | 3.2 | 1.4 | 3.1 | | |
| S-12 | 48-52 | 34.2 | 4.1 | 3.2 | 43.1 | 1.8 | 1.9 | 2.8 | 1.8 | 1.1 | 1.8 | | |

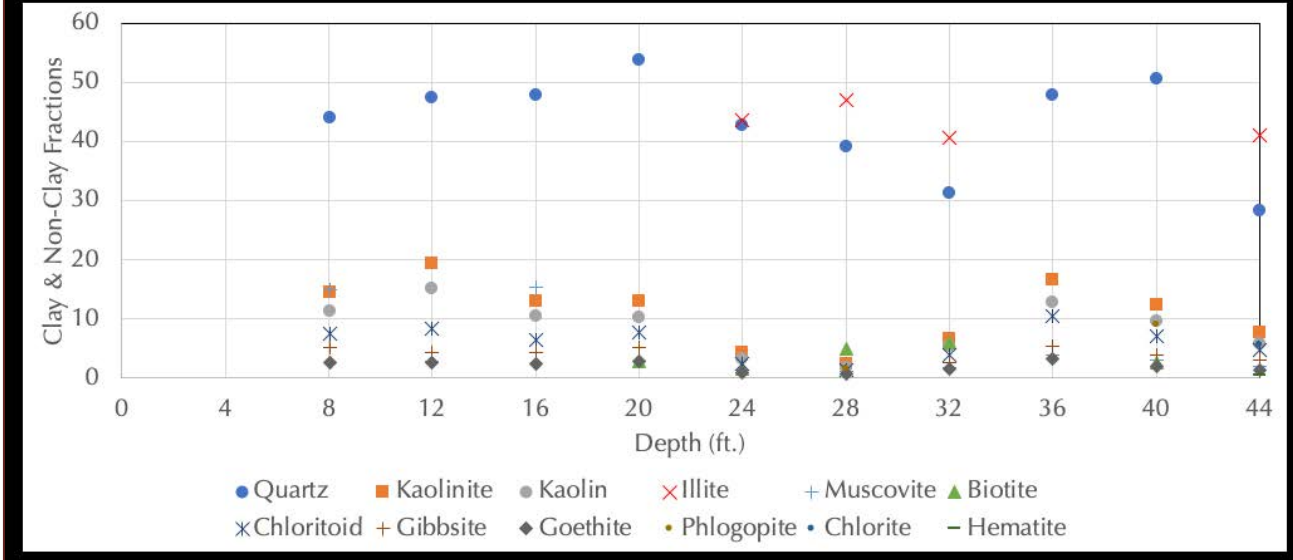


Figure 11: Results of mineralogical compositions of soil samples determined from X-ray diffraction (XRD). The bottom plot shows variations of quartz and clay contents of soil through depth.

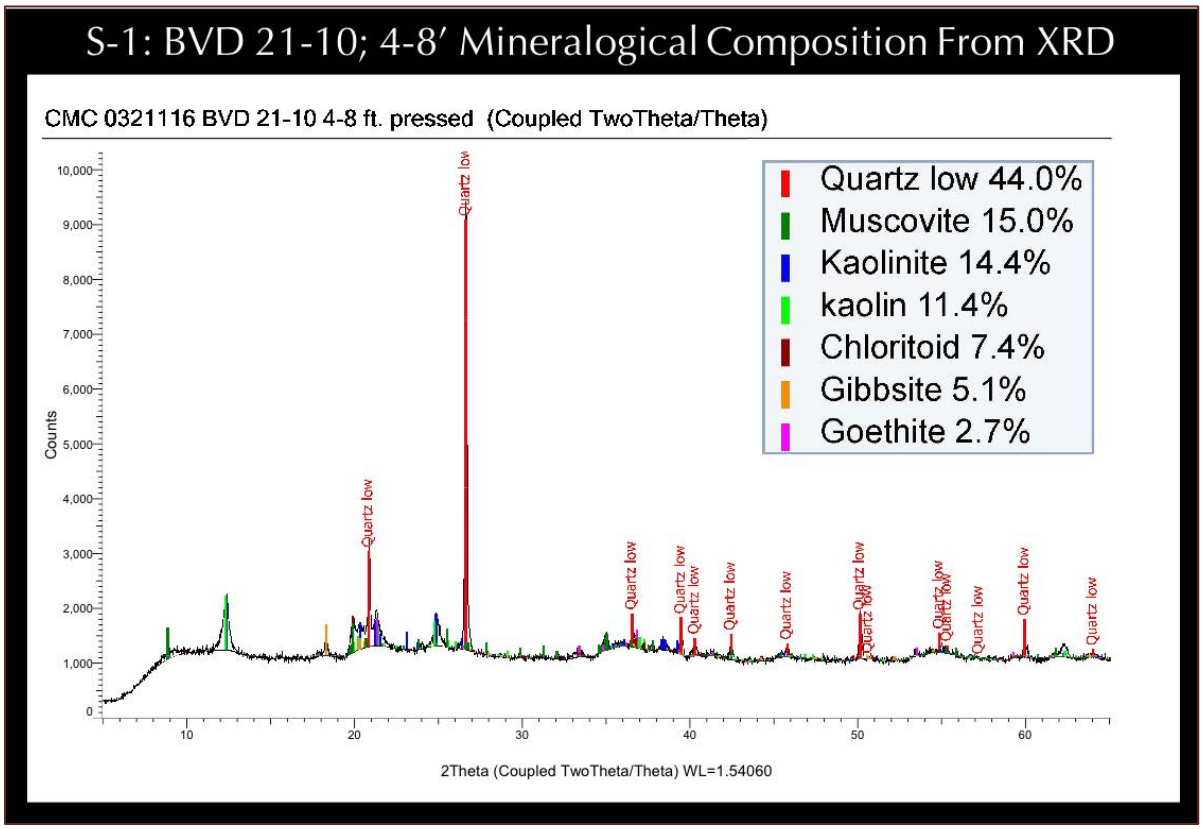


Figure 12: XRD analysis of soil sample S-1 from 4 to 8 ft. depth.

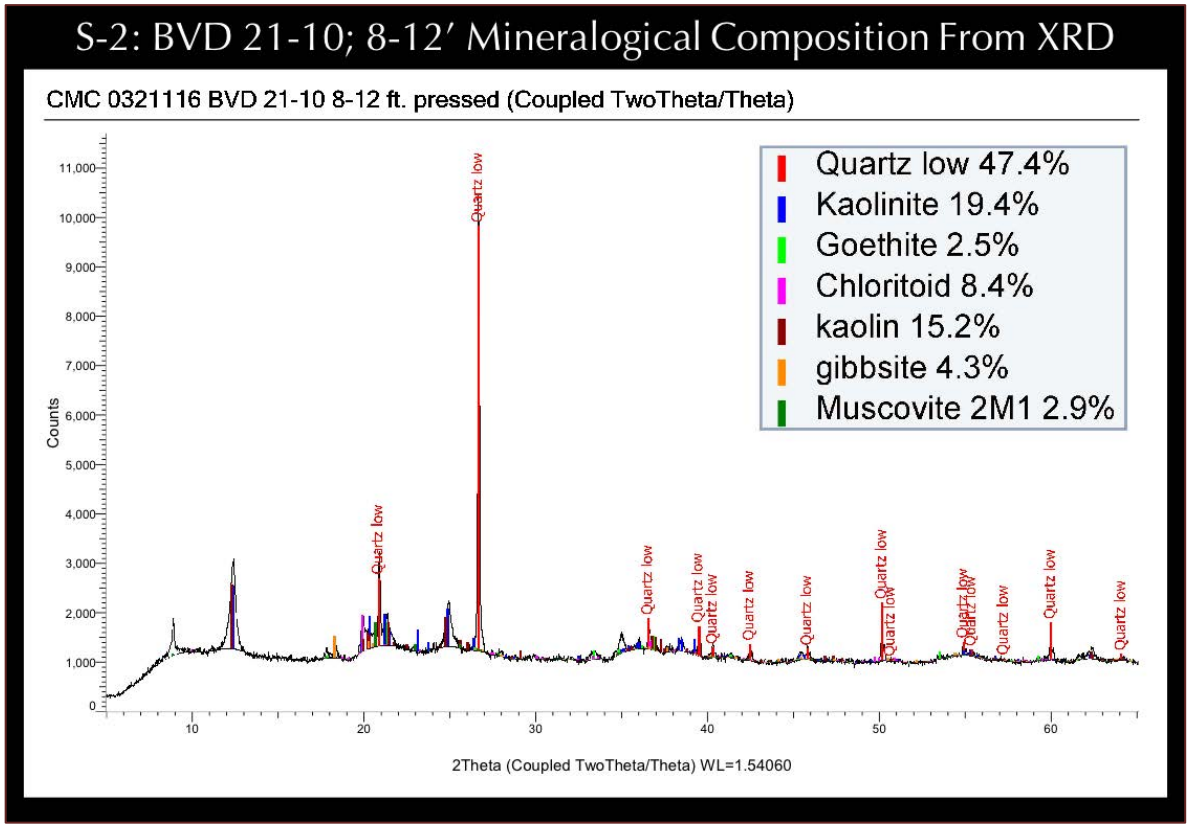


Figure 13: XRD analysis of soil sample S-2 from 8 to 12 ft. depth.

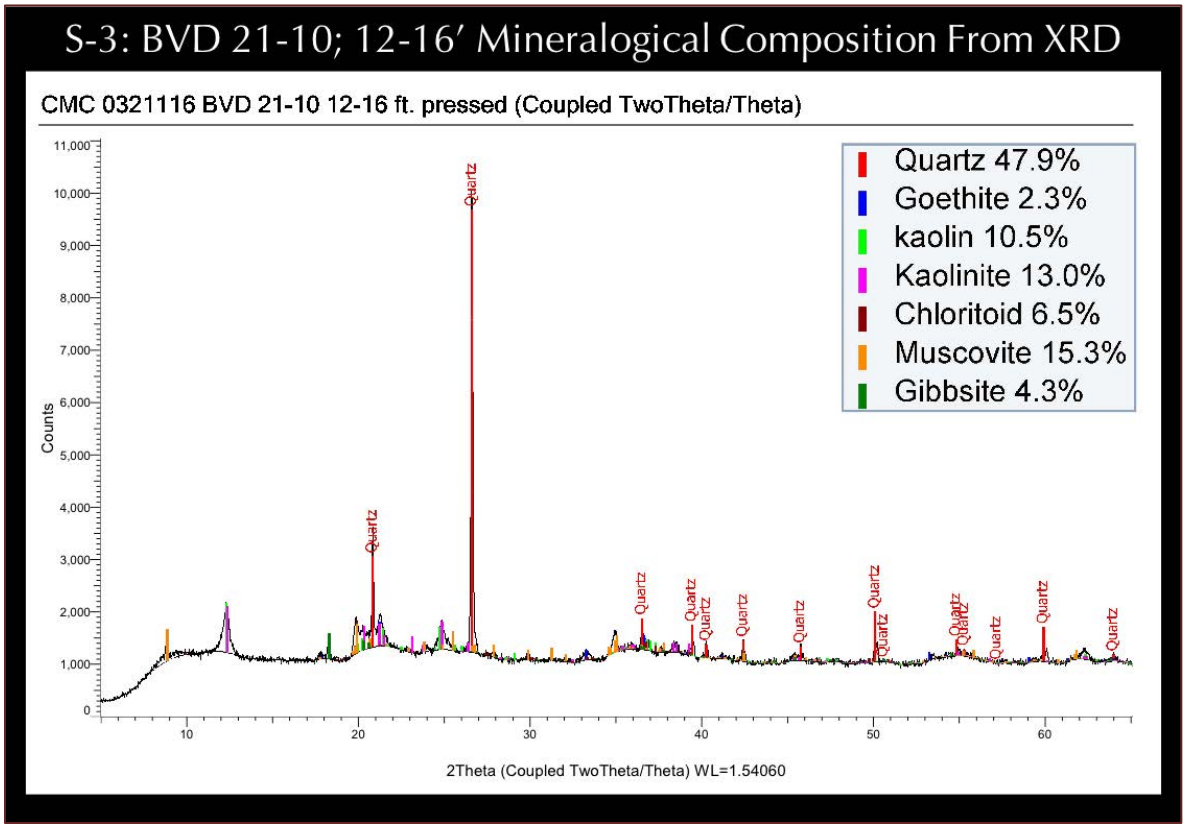


Figure 14: XRD analysis of soil sample S-3 from 12 to 16 ft. depth.

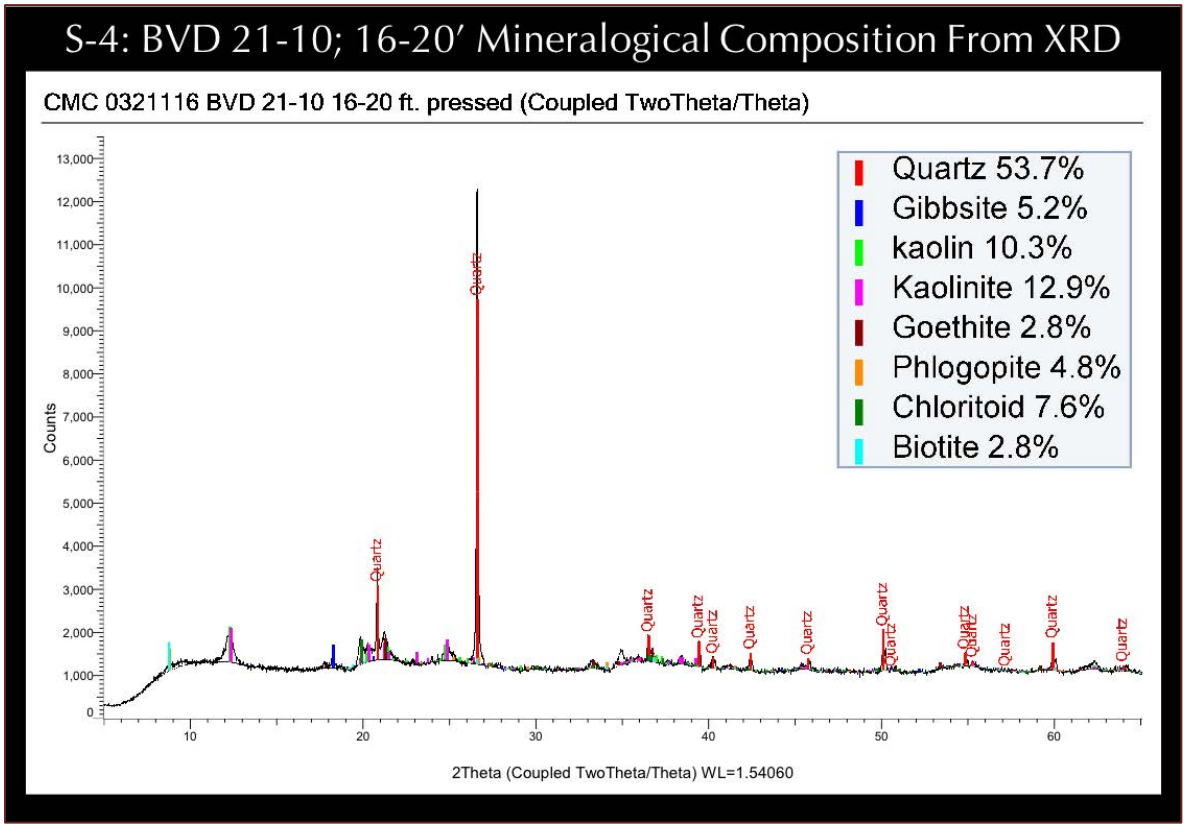


Figure 15: XRD analysis of soil sample S-4 from 16 to 20 ft. depth.

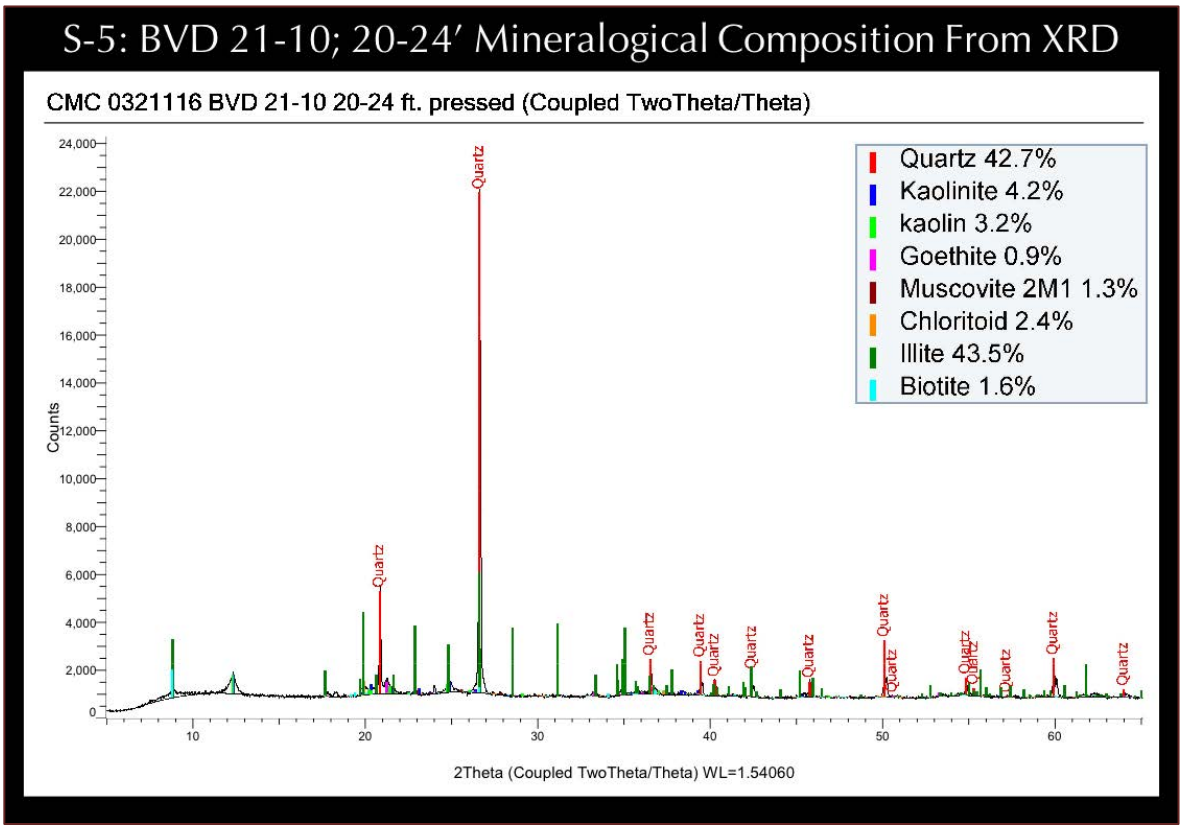


Figure 16: XRD analysis of soil sample S-5 from 20 to 24 ft. depth.

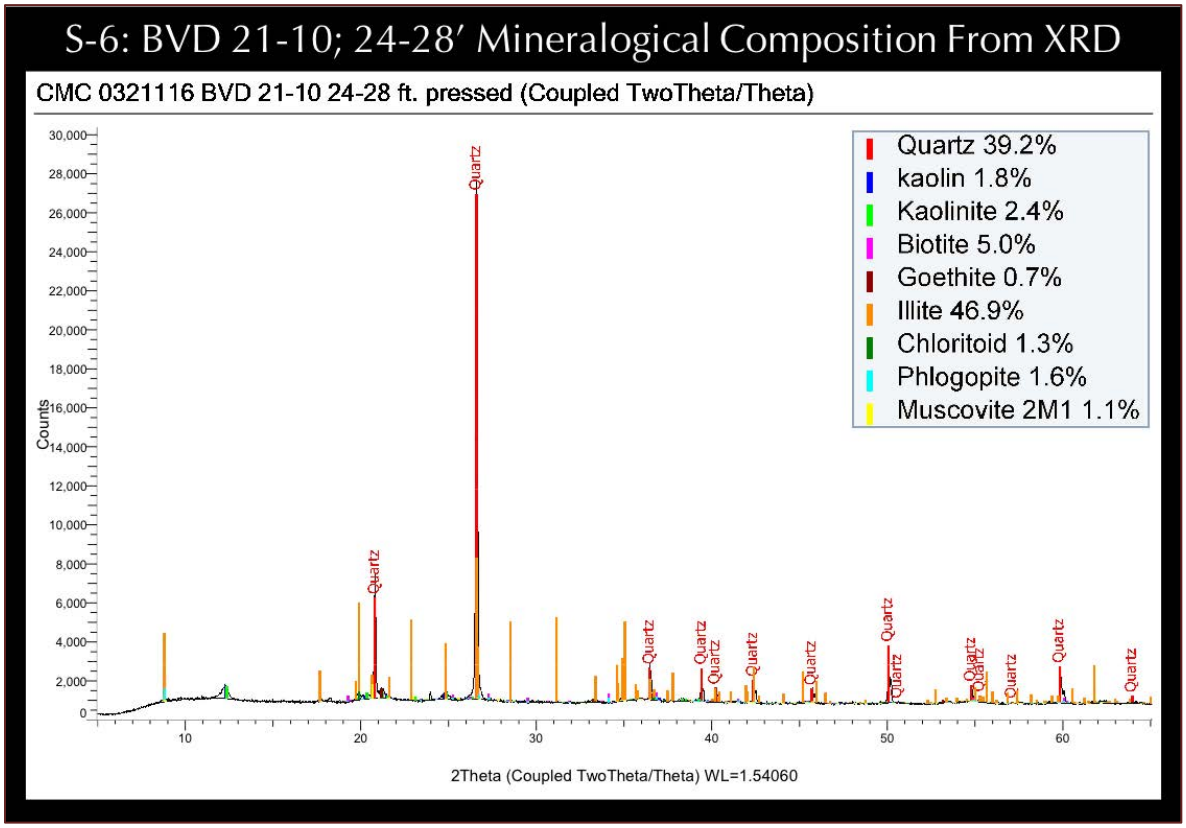


Figure 17: XRD analysis of soil sample S-6 from 24 to 28 ft. depth.

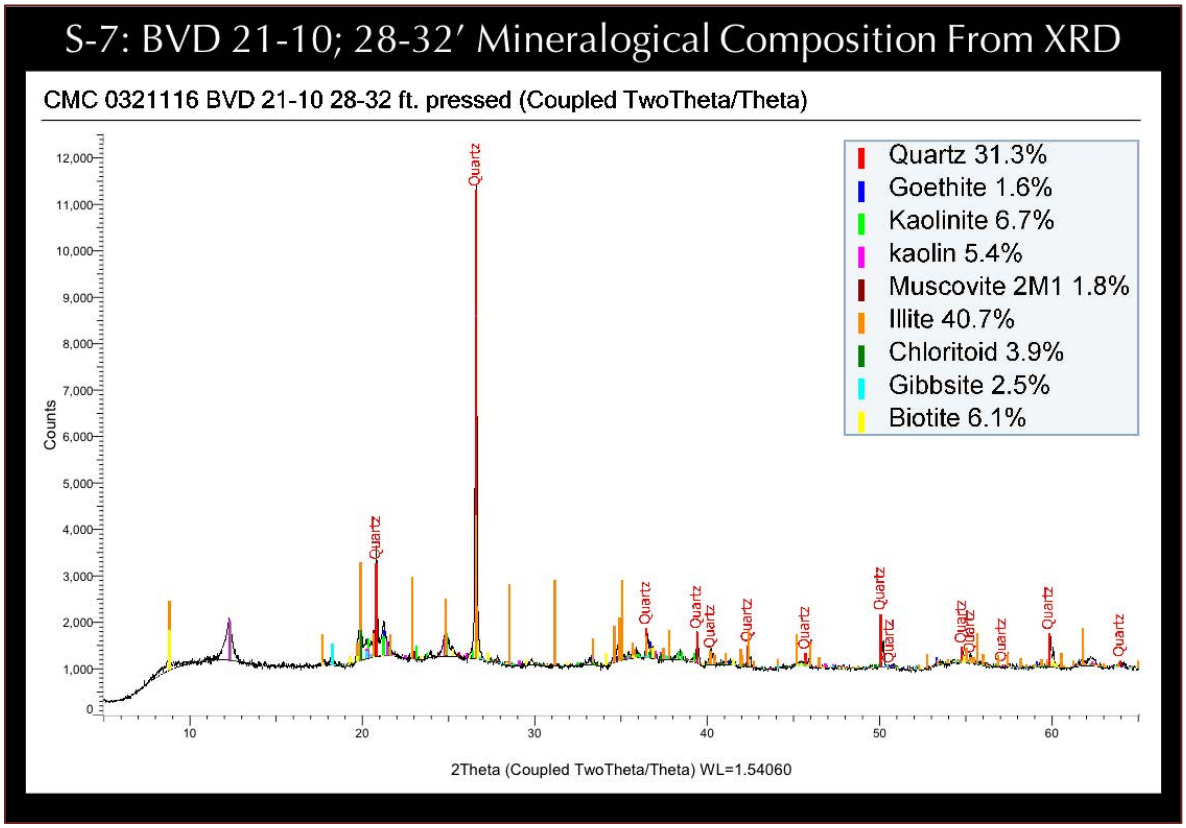


Figure 18: XRD analysis of soil sample S-8 from 28 to 32 ft. depth.

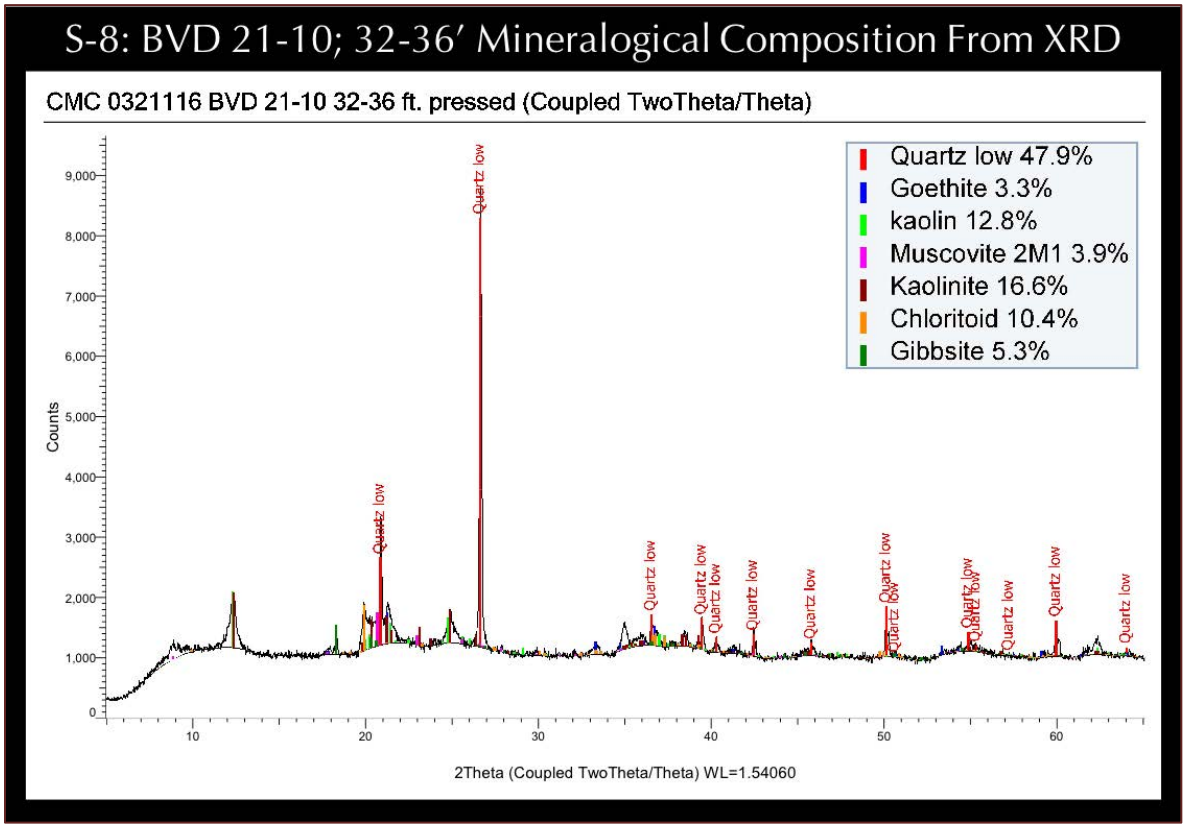


Figure 19: XRD analysis of soil sample S-8 from 32 to 36 ft. depth.

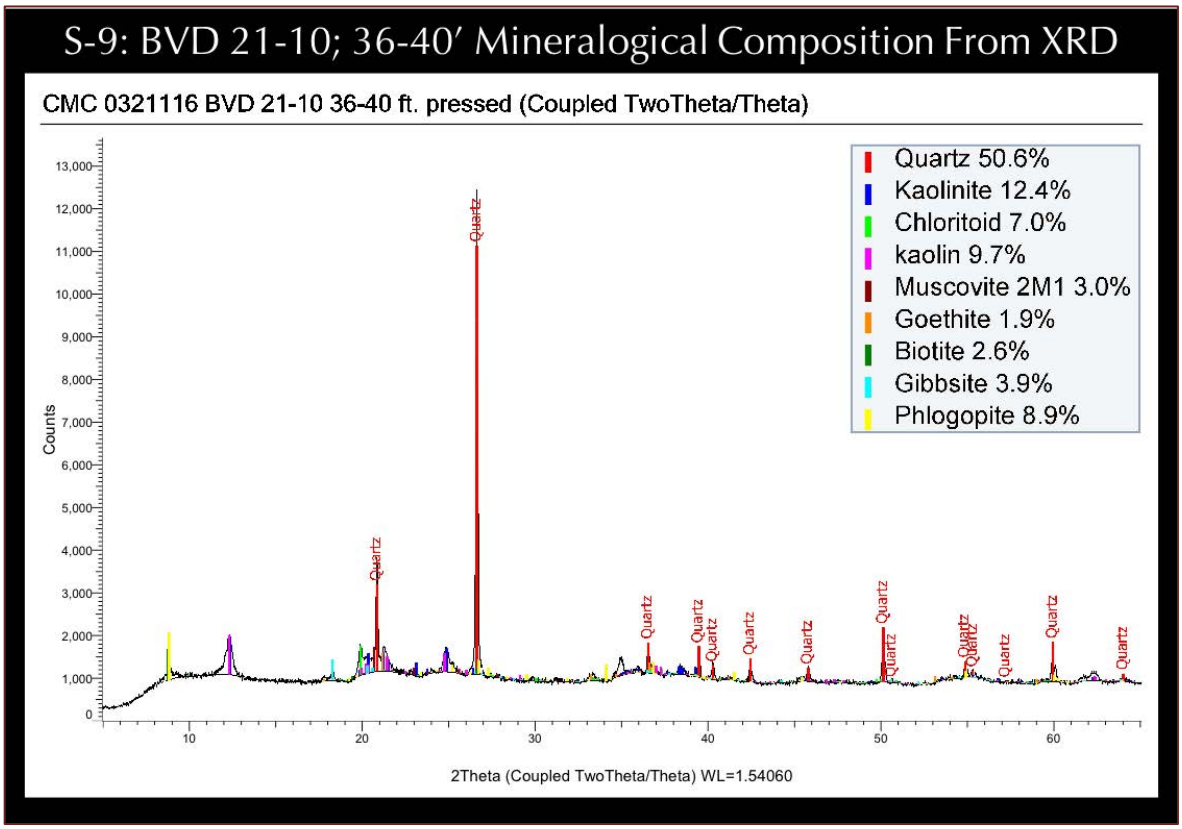


Figure 20: XRD analysis of soil sample S-9 from 36 to 40 ft. depth.

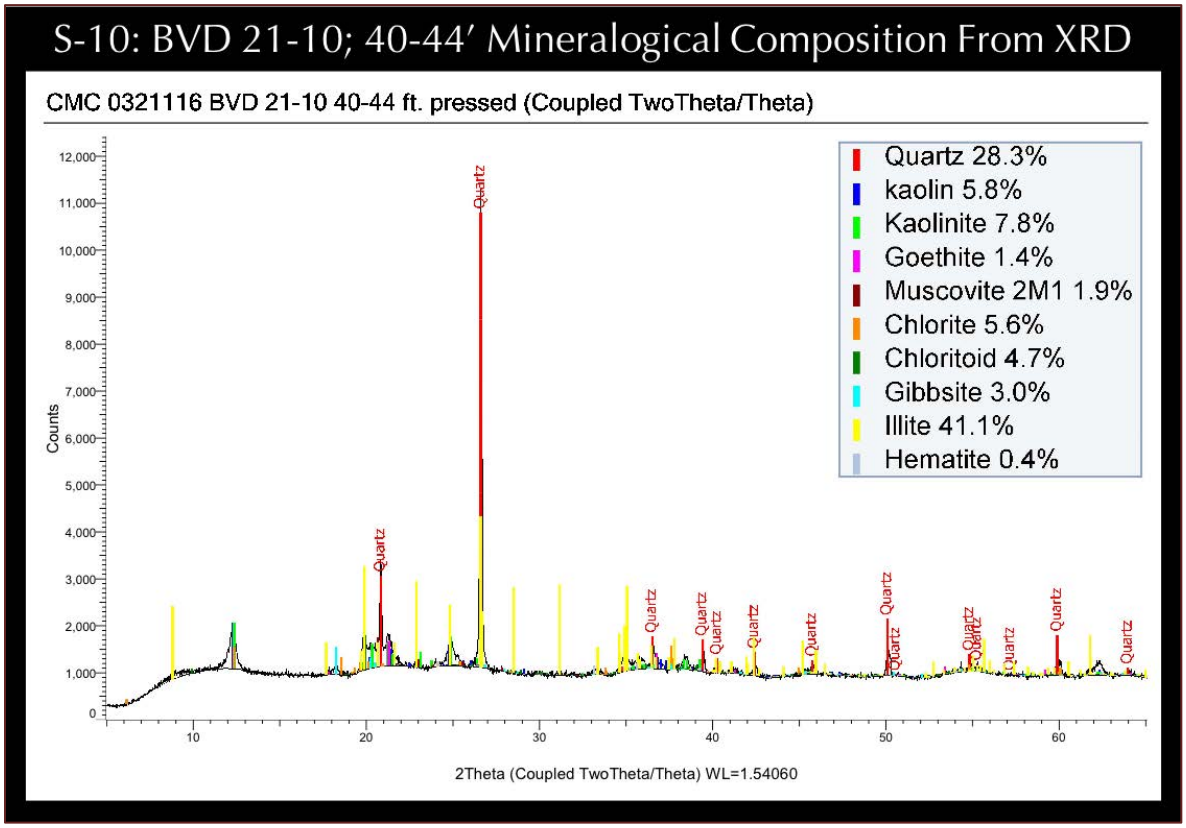


Figure 21: XRD analysis of soil sample S-10 from 40 to 44 ft. depth.

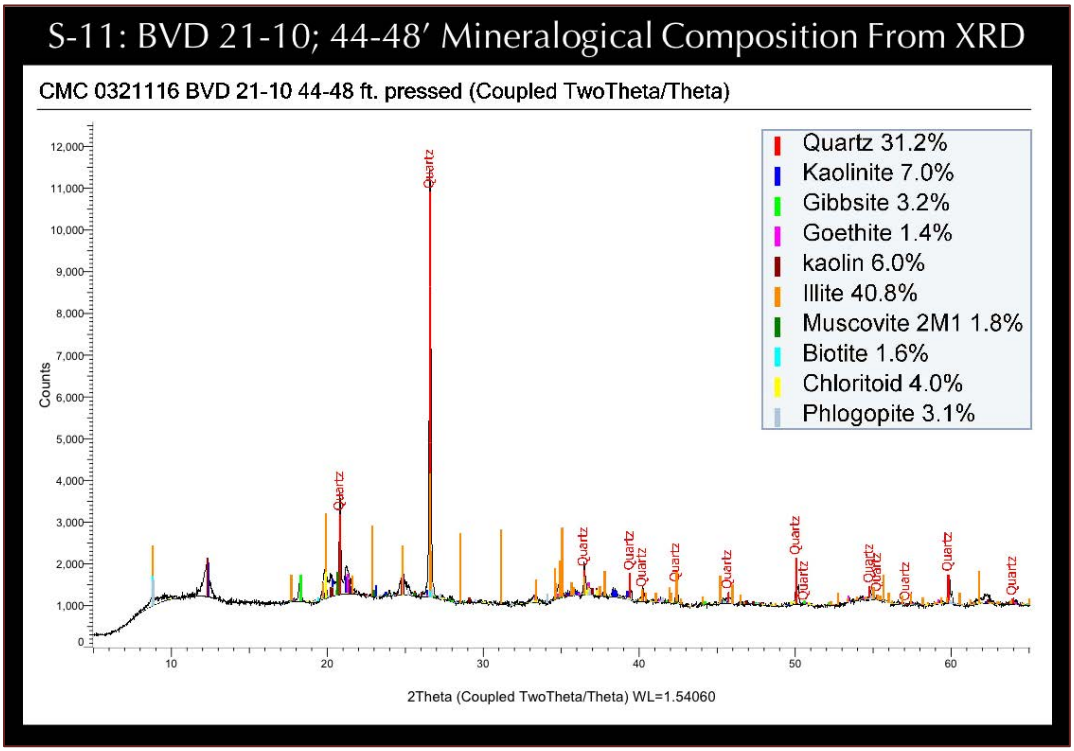


Figure 22: XRD analysis of soil sample S-11 from 44 to 48 ft. depth.

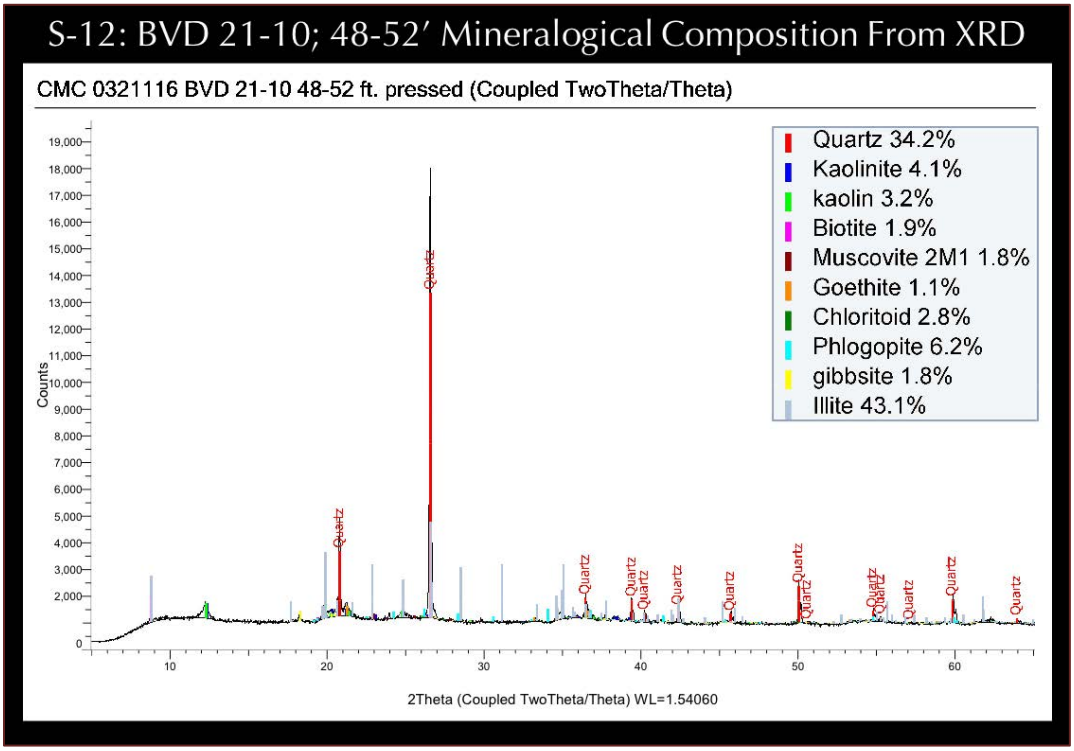


Figure 23: XRD analysis of soil sample S-12 from 48 to 52 ft. depth.

The above conclusions are based solely on the information and samples provided at the time of this investigation. The conclusion may expand or modify upon receipt of further information, field evidence, or samples. All reports are the confidential property of clients, and information contained herein may not be published or reproduced pending our written approval. Neither CMC nor its employees assume any obligation or liability for damages, including, but not limited to, consequential damages arising out of, or, in conjunction with the use, or inability to use this resulting information.

# END OF REPORT[1]

[1] The CMC logo is made using a lapped polished section of a 1930's concrete from an underground tunnel in the U.S. Capitol.

CONSTRUCTION MATERIALS CONSULTANTS, INC.

# Thermal Analyses (TGA-DSC-DTG) of Soils


York Building Products - Belvidere Plant
Cecil County, Maryland

May 04, 2021
CMC 0321116

## TABLE OF CONTENTS

## EXECUTIVE SUMMARY

Thirty-five (35) soil samples, from BVD 21-3, 21-7, and 21-10 Wash Pond 11, collected at 4 ft. intervals from surface to 52 ft. depths were analyzed by thermal analysis from: (a) thermogravimetric studies (TGA) during heating related to decomposition of a phase of interest at a specific temperature that is characteristic of the phase from which both the phase composition and the abundance can be determined, (b) differential thermal analysis (DTA, or first derivative of TGA i.e. DTG) measuring temperature difference between the sample and an inert standard ($Al_2O_3$) both are heated at the same rate and time where endothermic peaks are recorded when the standard continues to increase in temperature during heating but the sample does not due to decompositions (e.g., dehydration of hydrous or decarbonation of carbonate phases); the endothermic or exothermic transitions are characteristic of particular phase, which can be identified and quantified using DTA (or DTG), and (c) differential scanning calorimetry (DSC) which follows the same basic principle as DTA, whereas temperature differences are measured in DTA, during heating using DSC energy is added to maintain the same and the reference material ($Al_2O_3$) at the same temperature; this energy use is recorded and used as a measure of the calorific value of the thermal transitions that the sample experiences; this is particularly useful for detection of quartz that undergoes polymorphic (α to β form) transitions and no weight loss. Simultaneous TGA and DSC analyses are done in a Mettler Toledo TGA/DSC 1 unit on 30-80 mg of moist soil sample in alumina crucible (70 µl, no lid) from 35°C to 1000°C at a heating rate of 20°C/min with high purity nitrogen as purge gas at a flow rate of 75.0 ml/min.

All samples show pretty consistent similar endotherms of weight losses that are indicative of their inherent compositional similarities not only in their decomposed phases but also in their inherent moisture conditions. Maximum weight losses due to loss of free and bound moisture from illitic clay has occurred within 200°C after which major endothermic peaks at 280-300°C and 540-550°C are related to dihydroxylation of other clay minerals (e.g., kaolinite dihydroxylation between 530 and 590°C) in the samples.

## INTRODUCTION

Reported herein are the results of thermal analyses of thirty-five (35) soil samples at successively deeper intervals from surface at locations BVD 21-3, 21-7,and 21-10.

## SAMPLES

Figure 1 shows the soil samples as received in plastic Ziploc bags for thermal analysis.

Representative portions of each soil sample was removed from the sealed plastic Ziploc bags in their pristine moisture conditions and loaded into 70 micron alumina crucible for thermal analysis.

Approximately 30 to 80 milligrams of moist soil samples were loaded in the crucible and subjected to heating from the ambient condition to 1000 degrees C at 20 degrees C per min heating rate. The furnace was purged with an ultrapure nitrogen gas.

Simultaneous TGA and DSC analyses were done in a Mettler Toledo TGA/DSC 1 unit (Figure 2) on 30-80 mg of moist soil sample in alumina crucible (70 µl, no lid) from 35°C to 1000°C at a heating rate of 20°C/min with high purity nitrogen as purge gas at a flow rate of 75.0 ml/min.

Instead of automated analysis of multiple samples each sample was treated individually before loading the next sample to avoid drying out of samples in the queue in the sample tray of automated robot-controlled loading of samples in the furnace.


Figure 1: Soil samples received in sealed plastic bags for thermal analysis.

## METHODOLOGIES

### THERMAL ANALYSES

Thermal analyses encompass: (1) thermogravimetric analysis (TGA), which measures the weight loss during heating related to decomposition of a phase of interest at a specific temperature that is characteristic of the phase from which both the phase composition and the abundance can be determined; (2) differential thermal analysis (DTA, or first derivative of TGA i.e. DTG) measuring temperature difference between the sample and an inert standard ($Al_2O_3$) both are heated at the same rate and time where endothermic peaks are recorded when the standard continues to increase in temperature during heating but the sample does not due to decompositions (e.g., dehydration of hydrous or decarbonation of carbonate phases); the endothermic or exothermic transitions are characteristic of particular phase, which can be identified and quantified using DTA (or DTG); and (3) differential scanning calorimetry (DSC), which follows the same basic principle as DTA, whereas temperature differences are measured in DTA, during heating using DSC energy is added to maintain the same and the reference material ($Al_2O_3$) at the same temperature; this energy use is recorded and used as a measure of the calorific value of the thermal transitions that the sample experiences; this is particularly useful for detection of quartz that undergoes polymorphic (α to β form) transitions and no weight loss.

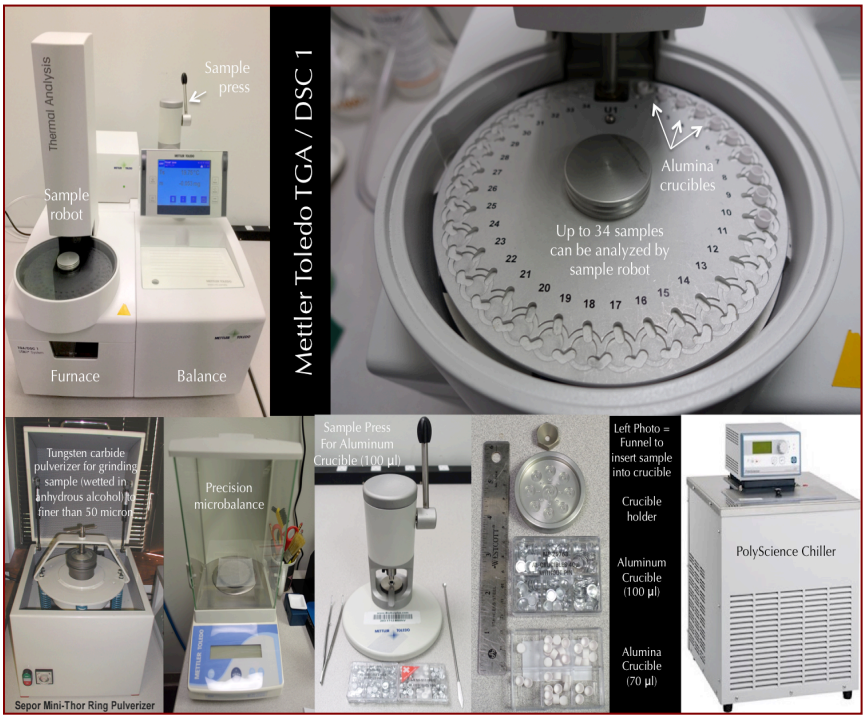


Figure 2: Mettler-Toledo simultaneous TGA/DSC1 unit in CMC that can accommodate 32 samples. The top left photo shows the TGA/DSC1 unit with sample robot for automation as well as the sample holder for pressing aluminum sample holders. Sample is pulverized in a ring pulverizer shown in the bottom left, then a small amount (usually 30-70 mg) is weighed in a precision balance (shown 2nd from left in bottom row) and taken in an alumina sample holder (without lid). For DSC measurements up to 600°C, sometimes sample is taken in an aluminum holder and pressed in sample press (3rd from left in bottom row) and pierced with a needle for release of volatiles from decomposition. A PolyScience chiller (rightmost one in the bottom row) is used to cool the furnace. An ultrapure nitrogen gas is purged through the system during analyses.

# RESULTS OF THERMAL ANALYSES OF SOIL SAMPLES

## TGA

## DSC

## DTG CURVES

| Sample | Depth | DTG Peak T (ºC) | % wt. loss | DTG Peak T (ºC) | % wt. loss | DTG Peak T (ºC) | % wt. loss | DTG Peak T (ºC) | % wt. loss |
|---|---|---|---|---|---|---|---|---|---|
| 21-3 | 0-4 | 62.66 | 26.44 | 112.00 | 15.94 | 276.72 | 0.74 | 539.39 | 2.04 |
| | 4-8 | 77.72 | 29.34 | 147.96 | 15.93 | 290.89 | 1.00 | 545.55 | 2.12 |
| | 8-12 | 90.80 | 29.56 | 166.81 | 10.38 | 284.62 | 0.92 | 536.30 | 1.99 |
| | 12-16 | 89.89 | 24.13 | 144.71 | 15.17 | 287.54 | 1.06 | 544.05 | 2.50 |
| | 16-20 | 85.75 | 20.17 | 129.59 | 15.90 | 283.52 | 0.83 | 539.10 | 2.39 |
| | 20-24 | 89.17 | 14.95 | 141.71 | 17.41 | 286.47 | 0.78 | 547.81 | 2.19 |
| | 24-28 | 84.91 | 21.08 | 137.14 | 8.17 | 291.05 | 0.99 | 549.30 | 2.63 |
| | 28-32 | 101.23 | 23.41 | 158.04 | 5.19 | 287.05 | 0.75 | 534.94 | 1.28 |
| | 32-36 | 96.39 | 19.84 | 155.83 | 5.29 | 289.46 | 0.76 | 537.22 | 1.25 |
| | 36-40 | 93.34 | 16.38 | 127.47 | 6.84 | 289.11 | 0.93 | 536.75 | 1.57 |
| | 40-41 | 122.24 | 22.80 | - | - | 283.88 | 0.92 | 532.26 | 1.91 |
| Average | | | | | | **286.39** | **0.88** | **540.24** | **1.99** |
| StDev | | | | | | 4.14 | 0.11 | 5.59 | 0.46 |
| 21-7 | 0-4 | 62.91 | 26.74 | 119.95 | 13.73 | 280.02 | 0.92 | 529.49 | 2.03 |
| | 4-8 | 80.96 | 29.04 | 154.51 | 14.77 | 278.91 | 1.08 | 528.86 | 2.19 |
| | 8-12 | 100.70 | 40.17 | 181.37 | 10.52 | 284.33 | 0.97 | 534.30 | 2.00 |
| | 12-16 | 83.99 | 31.38 | 145.06 | 12.33 | 274.68 | 0.99 | 524.27 | 2.19 |
| | 16-20 | 85.36 | 34.93 | 121.45 | 13.07 | 280.53 | 0.89 | 532.01 | 2.12 |
| | 20-24 | 92.65 | 23.84 | 137.81 | 16.52 | 287.63 | 0.96 | 543.23 | 2.52 |
| | 24-28 | 84.46 | 23.17 | 137.34 | 18.51 | 283.21 | 1.11 | 543.39 | 3.04 |
| | 28-32 | 82.19 | 18.76 | 126.08 | 17.70 | 283.58 | 0.95 | 540.21 | 3.48 |
| | 32-36 | 71.64 | 15.97 | 112.75 | 16.86 | 265.44 | 0.93 | 519.38 | 3.12 |
| | 36-40 | 105.65 | 29.71 | - | - | 277.25 | 1.29 | 526.17 | 3.06 |
| | 40-44 | 80.49 | 11.59 | 131.62 | 19.54 | 294.31 | 1.92 | 545.58 | 2.91 |
| | 44-45 | 114.94 | 29.85 | - | - | 287.00 | 1.79 | 531.89 | 2.89 |
| Average | | | | | | **281.41** | **1.15** | **533.23** | **2.63** |
| StDev | | | | | | 7.26 | 0.35 | 8.33 | 0.51 |
| 21-10 | 4-8 | 83.14 | 29.99 | 152.21 | 13.01 | 281.38 | 1.28 | 532.76 | 2.51 |
| | 8-12 | 84.62 | 29.86 | 133.63 | 15.29 | 279.18 | 0.85 | 537.20 | 2.57 |
| | 12-16 | 74.55 | 36.80 | 134.61 | 8.64 | 262.98 | 0.78 | 517.36 | 2.18 |
| | 16-20 | 84.87 | 13.01 | 160.37 | 6.24 | 278.77 | 0.47 | 527.05 | 1.00 |
| | 20-24 | 79.91 | 20.83 | 119.85 | 14.33 | 278.51 | 0.77 | 533.58 | 1.65 |
| | 24-28 | 110.98 | 34.01 | - | - | 283.39 | 0.82 | 537.03 | 1.71 |
| | 28-32 | 80.24 | 19.48 | 124.23 | 18.83 | 279.90 | 0.91 | 534.02 | 2.83 |
| | 32-36 | 84.51 | 23.85 | 121.50 | 16.61 | 275.84 | 0.77 | 530.20 | 2.89 |
| | 36-40 | 80.46 | 21.59 | 120.28 | 16.45 | 273.75 | 0.78 | 531.48 | 2.56 |
| | 40-44 | 73.33 | 19.49 | 117.74 | 15.87 | 268.47 | 0.75 | 523.22 | 2.80 |
| | 44-48 | 80.50 | 17.86 | 124.46 | 16.68 | 283.66 | 1.30 | 533.85 | 2.74 |
| | 48-52 | 106.50 | 18.90 | - | - | 277.05 | 0.68 | 526.40 | 1.61 |
| Average | | | | | | **276.91** | **0.85** | **530.35** | **2.25** |
| StDev | | | | | | 6.06 | 0.23 | 5.88 | 0.62 |

Table 1: Results of Thermal Analyses of Soil Samples.

Illite dehydroxylation

1. Between 100 and 200ºC: Endothermic escape of adsorbed and interlayer water (stoichiometric factor of reaction is about 25)
2. At around 900ºC endothermic-exothermic peak system destruction of the lattice and formation of spinel

Kaolinite dehydroxylation

1. Between 530-590ºC Endothermic $Al_2Si_2O_5(OH)_4$ = $Al_2O_3.2SiO_2$ (amorphous meta kaolinite) + $H_2O$ (stoichiometric factor of reaction: 7.17)
2. Between 900-1000ºC Exothermic transformation into crystalline phase $Al_2O_3.2SiO_2$ = $2Al_2O_3.3SiO_2$ (primary mullite or pseudomullite: Si-Al spinel with mullite-like composition + amorphous $SiO_2$ + gamma $Al_2O_3$

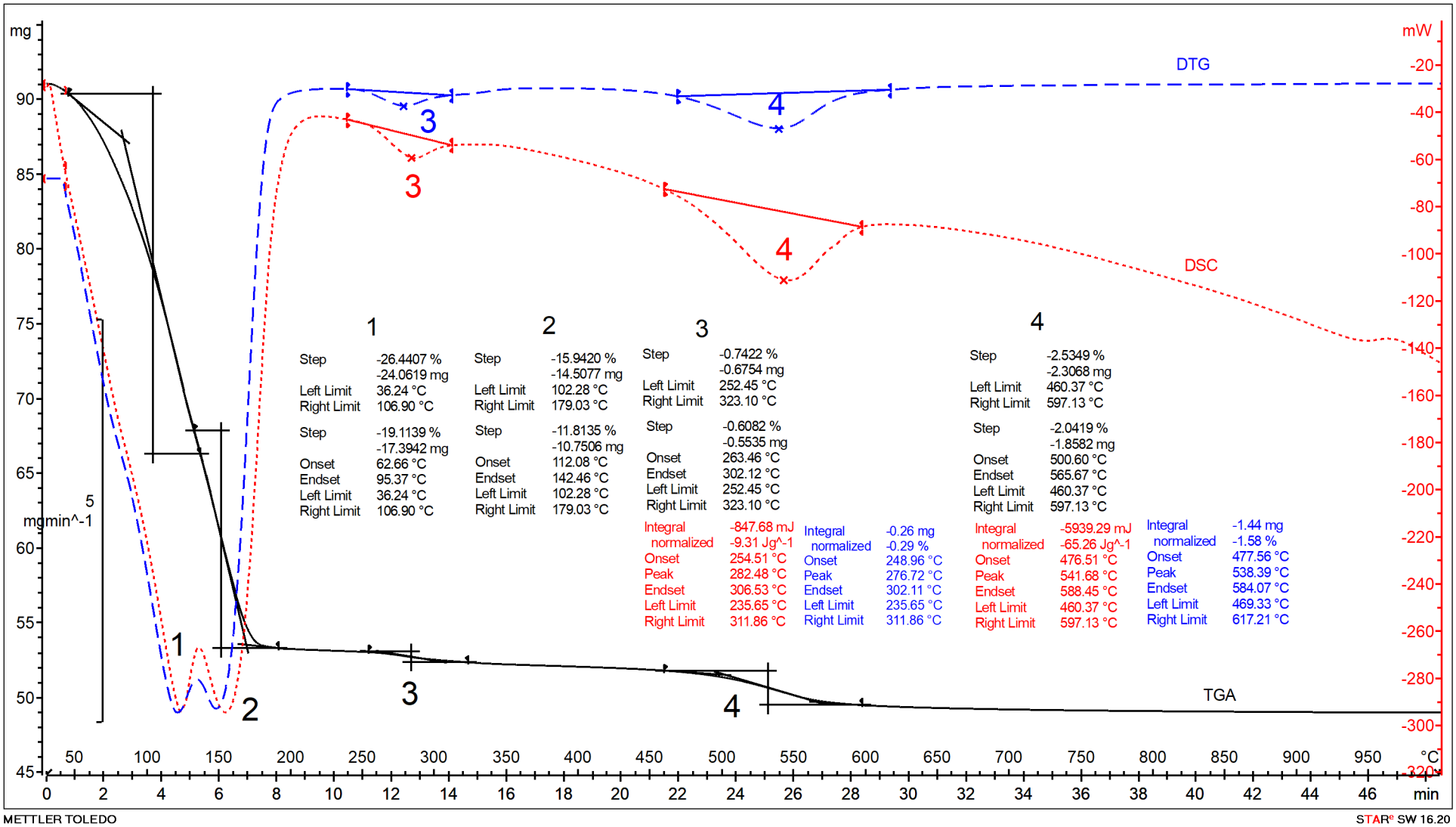


Figure 3: TGA (solid black), DSC (dotted red), and DTG (dashed blue) curves of Soil Sample: BVD 21-3, 0-4 ft. Major endotherms from decompositions (dehydroxylation) of illite-kaolinite clay minerals and other phases in soil are marked as 1 through 4. No polymorphic transition of fine clay-sized quartz particle is found at 573ºC. Results of thermal analyses are also given. Maximum weight loss from loss of free and bound moisture in illitic clay has occurred within 200ºC.

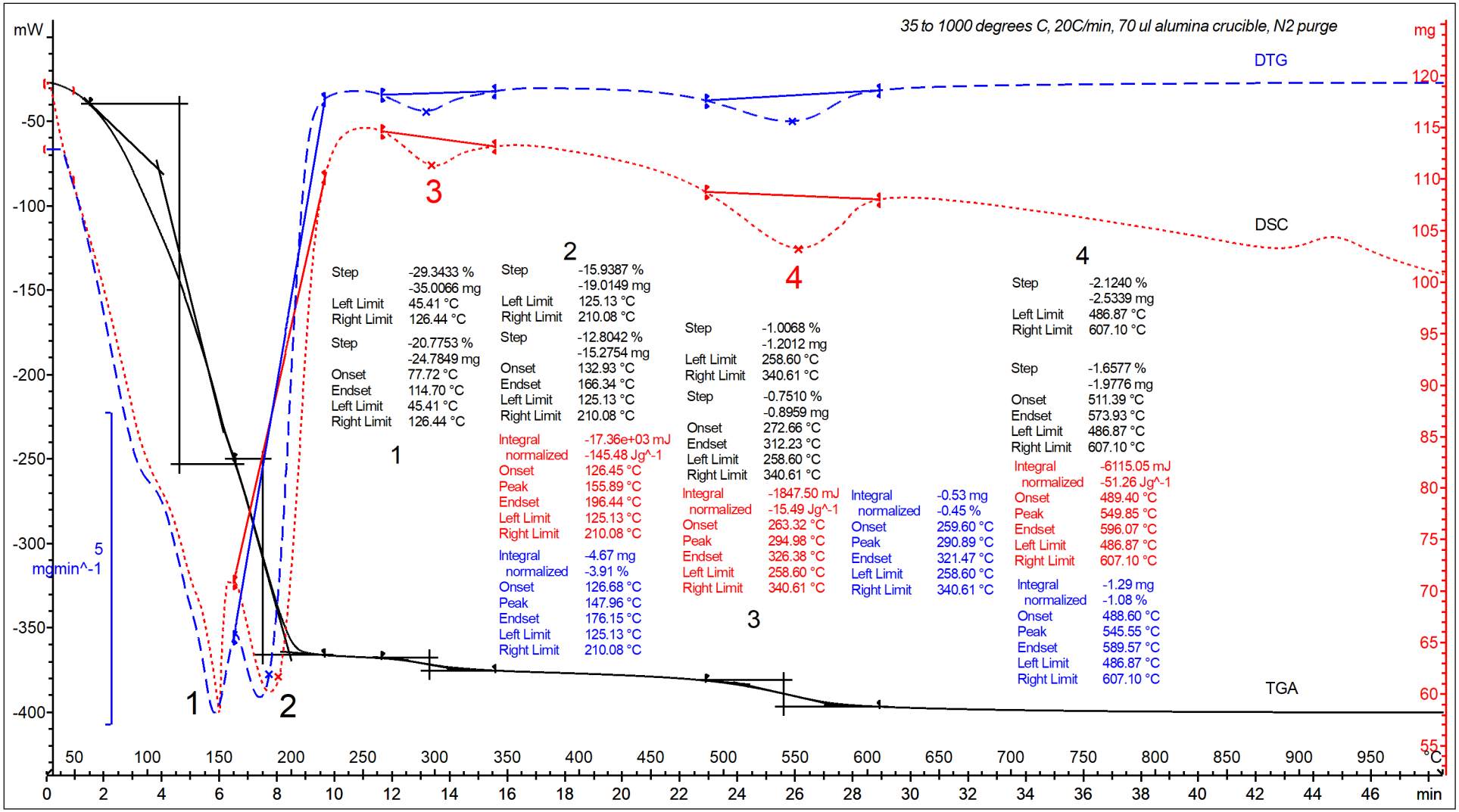


Figure 4: TGA (solid black), DSC (dotted red), and DTG (dashed blue) curves of Soil Sample: BVD 21-3, 4-8 ft. Major endotherms from decompositions (dehydroxylation) of illite-kaolinite clay minerals and other phases in soil are marked as 1 through 4. No polymorphic transition of fine clay-sized quartz particle is found at 573ºC. Results of thermal analyses are also given. Maximum weight loss from loss of free and bound moisture in illitic clay has occurred within 200ºC.

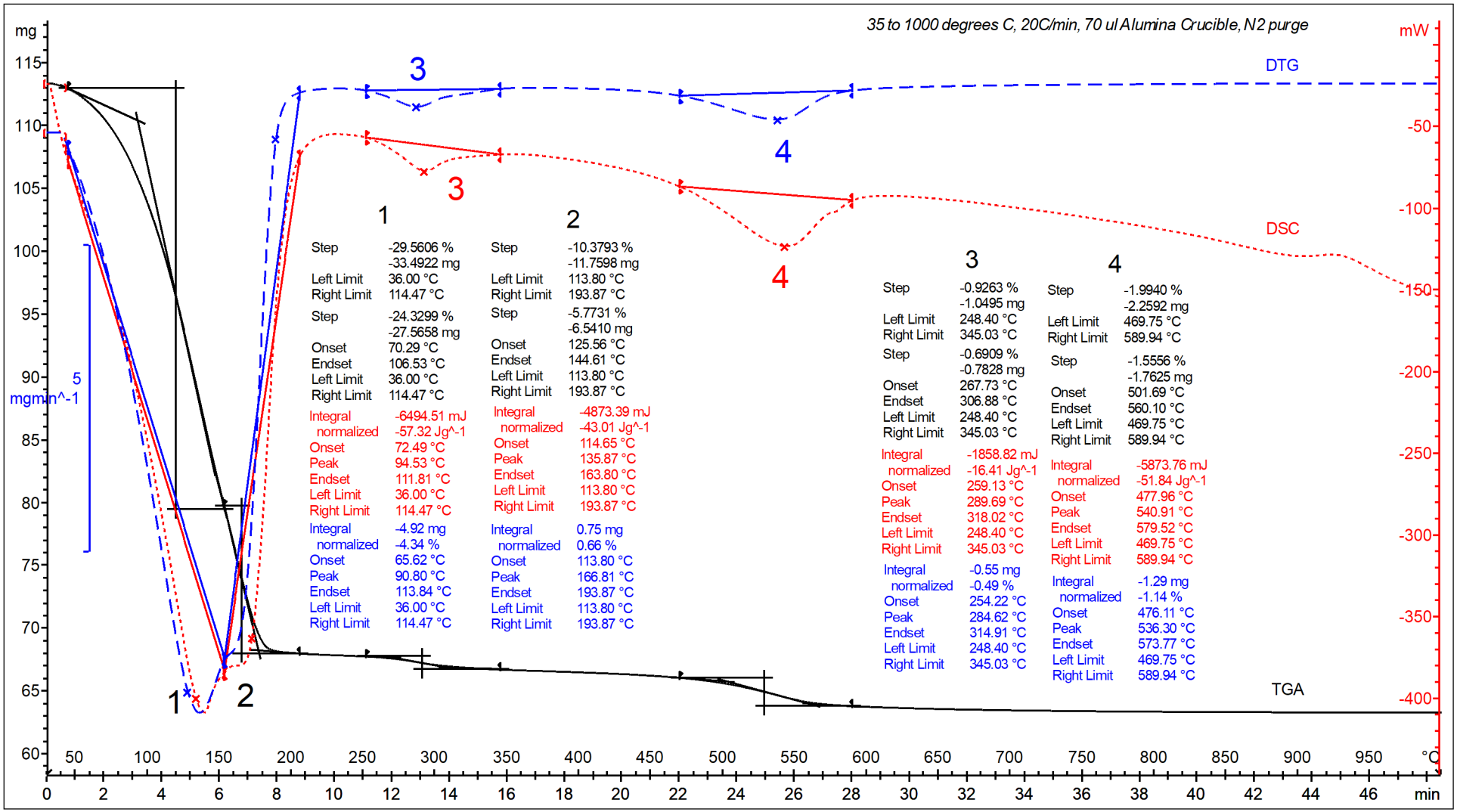


Figure 5: TGA (solid black), DSC (dotted red), and DTG (dashed blue) curves of Soil Sample: BVD 21-3, 8-12 ft. Major endotherms from decompositions (dehydroxylation) of illite-kaolinite clay minerals and other phases in soil are marked as 1 through 4. No polymorphic transition of fine clay-sized quartz particle is found at 573ºC. Results of thermal analyses are also given. Maximum weight loss from loss of free and bound moisture in illitic clay has occurred within 200ºC.

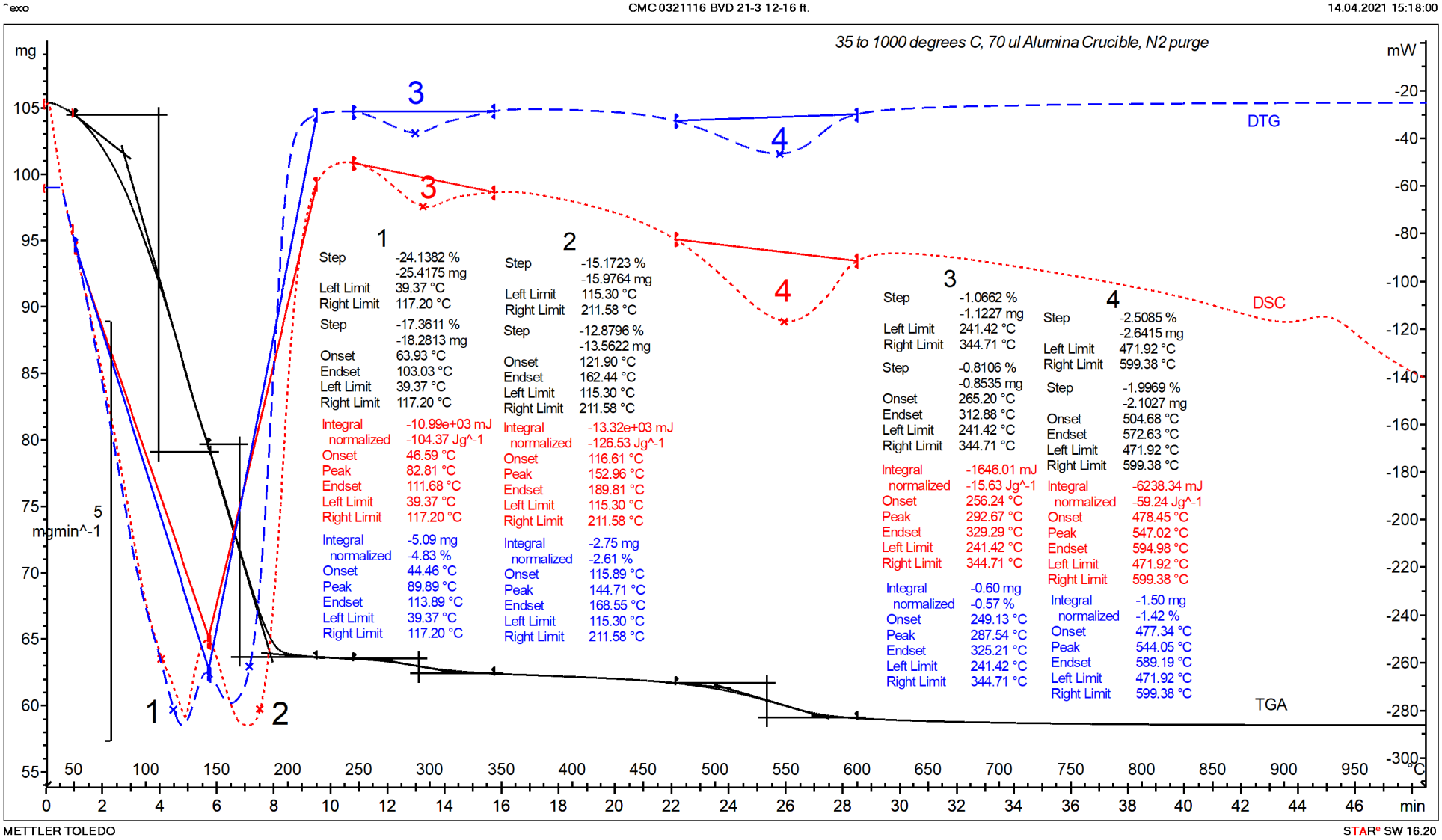


Figure 6: TGA (solid black), DSC (dotted red), and DTG (dashed blue) curves of Soil Sample: BVD 21-3, 12-16 ft. Major endotherms from decompositions (dehydroxylation) of illite-kaolinite clay minerals and other phases in soil are marked as 1 through 4. No polymorphic transition of fine clay-sized quartz particle is found at 573ºC. Results of thermal analyses are also given. Maximum weight loss from loss of free and bound moisture in illitic clay has occurred within 200ºC.

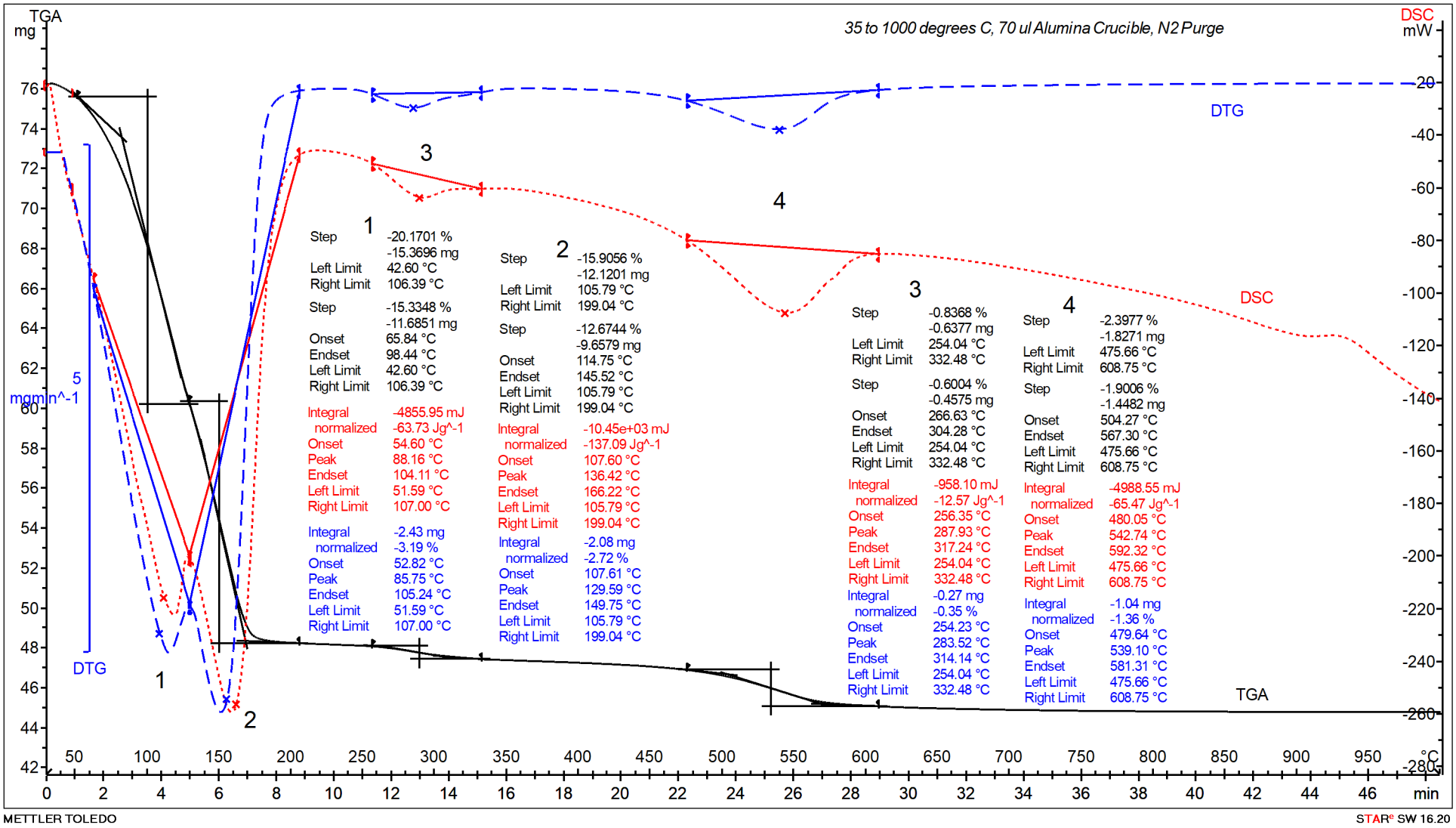


Figure 7: TGA (solid black), DSC (dotted red), and DTG (dashed blue) curves of Soil Sample: BVD 21-3, 16-20 ft. Major endotherms from decompositions (dehydroxylation) of illite-kaolinite clay minerals and other phases in soil are marked as 1 through 4. No polymorphic transition of fine clay-sized quartz particle is found at 573ºC. Results of thermal analyses are also given. Maximum weight loss from loss of free and bound moisture in illitic clay has occurred within 200ºC.

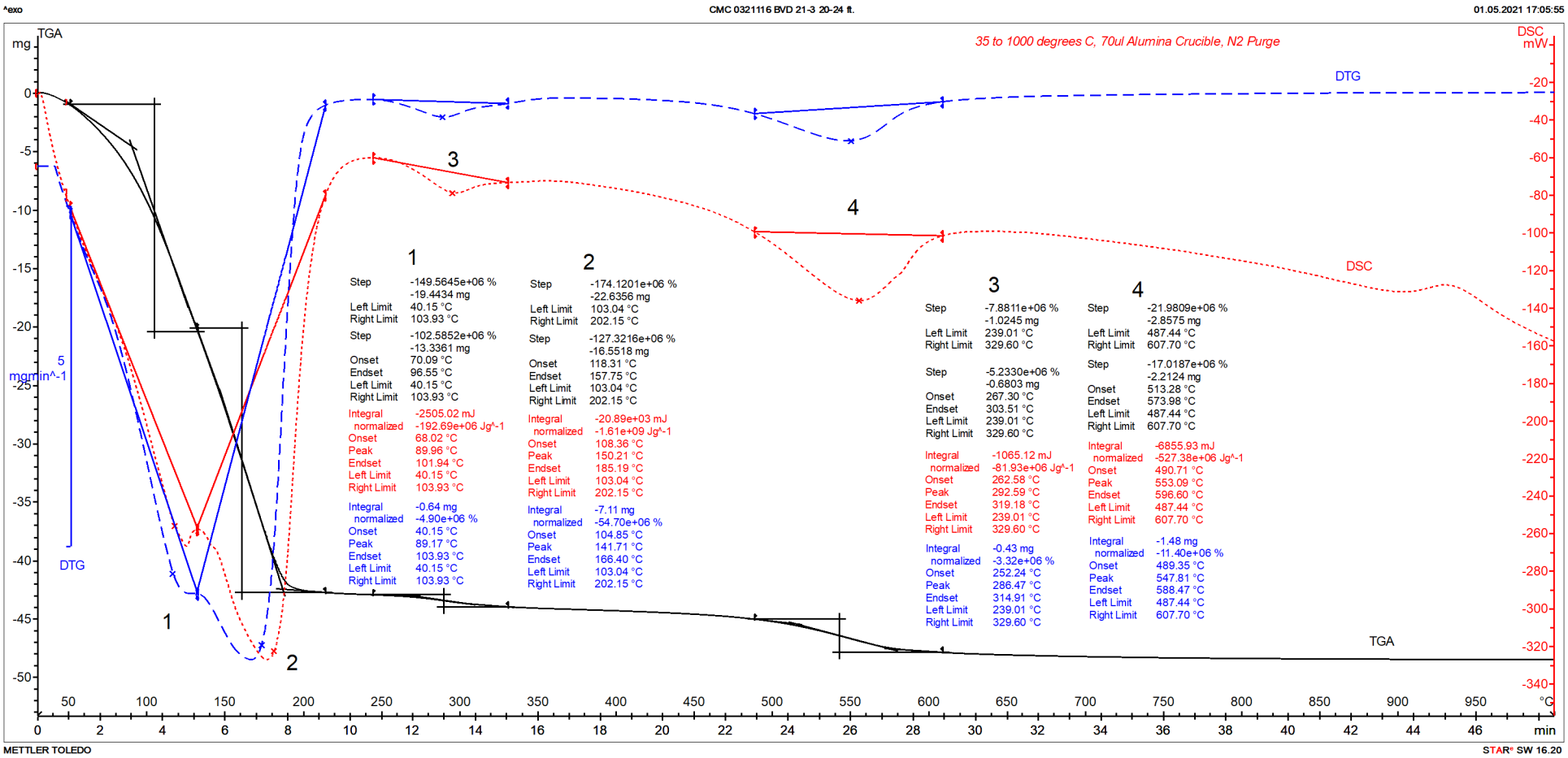


Figure 8: TGA (solid black), DSC (dotted red), and DTG (dashed blue) curves of Soil Sample: BVD 21-3, 20-24 ft. Major endotherms from decompositions (de-hydroxylation) of illite-kaolinite clay minerals and other phases in soil are marked as 1 through 4. No polymorphic transition of fine clay-sized quartz particle is found at 573ºC. Results of thermal analyses are also given. Maximum weight loss from loss of free and bound moisture in illitic clay has occurred within 200ºC.

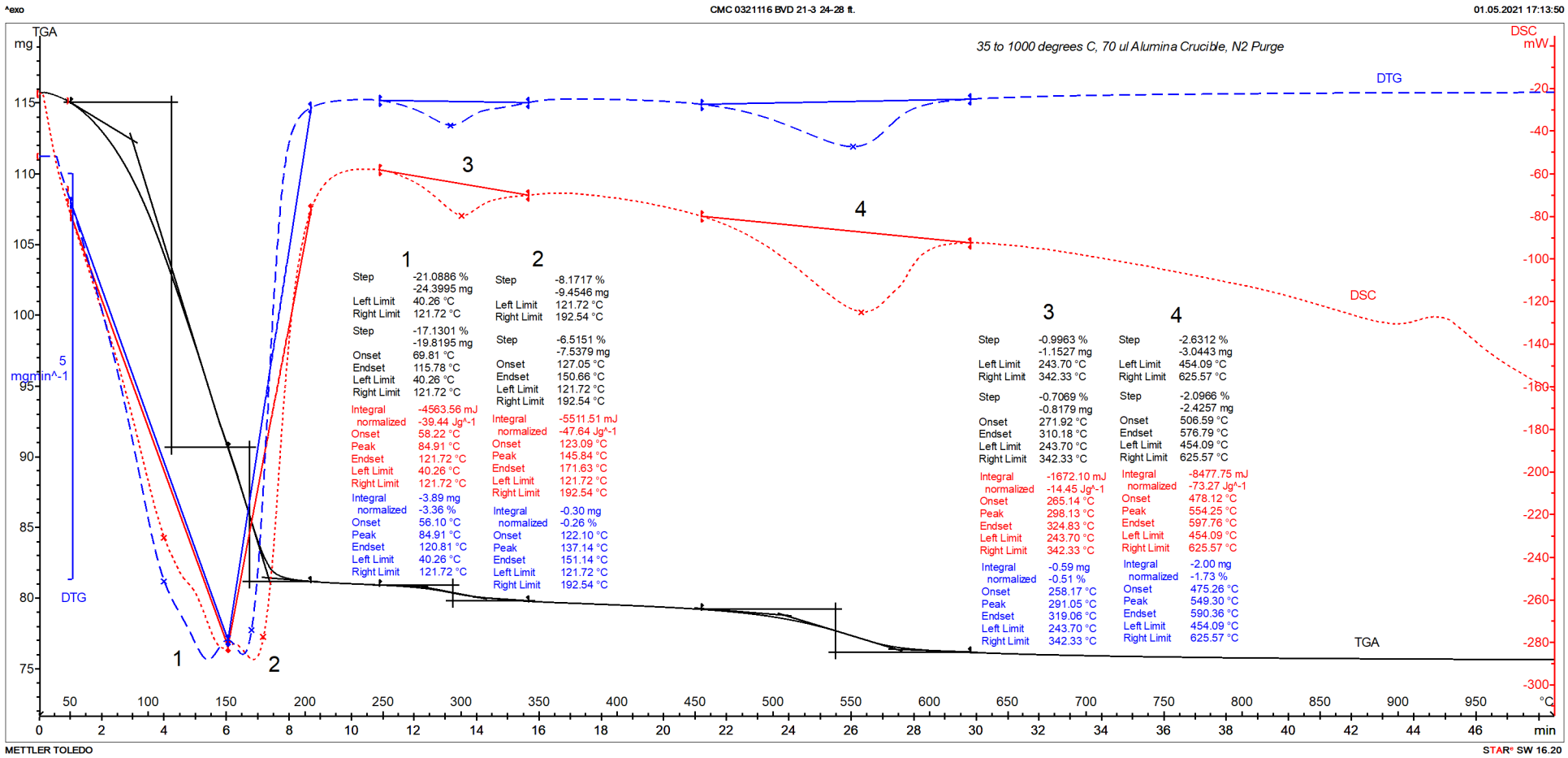


Figure 9: TGA (solid black), DSC (dotted red), and DTG (dashed blue) curves of Soil Sample: BVD 21-3, 24-28 ft. Major endotherms from decompositions (dehydroxylation) of illite-kaolinite clay minerals and other phases in soil are marked as 1 through 4. No polymorphic transition of fine clay-sized quartz particle is found at 573ºC. Results of thermal analyses are also given. Maximum weight loss from loss of free and bound moisture in illitic clay has occurred within 200ºC.

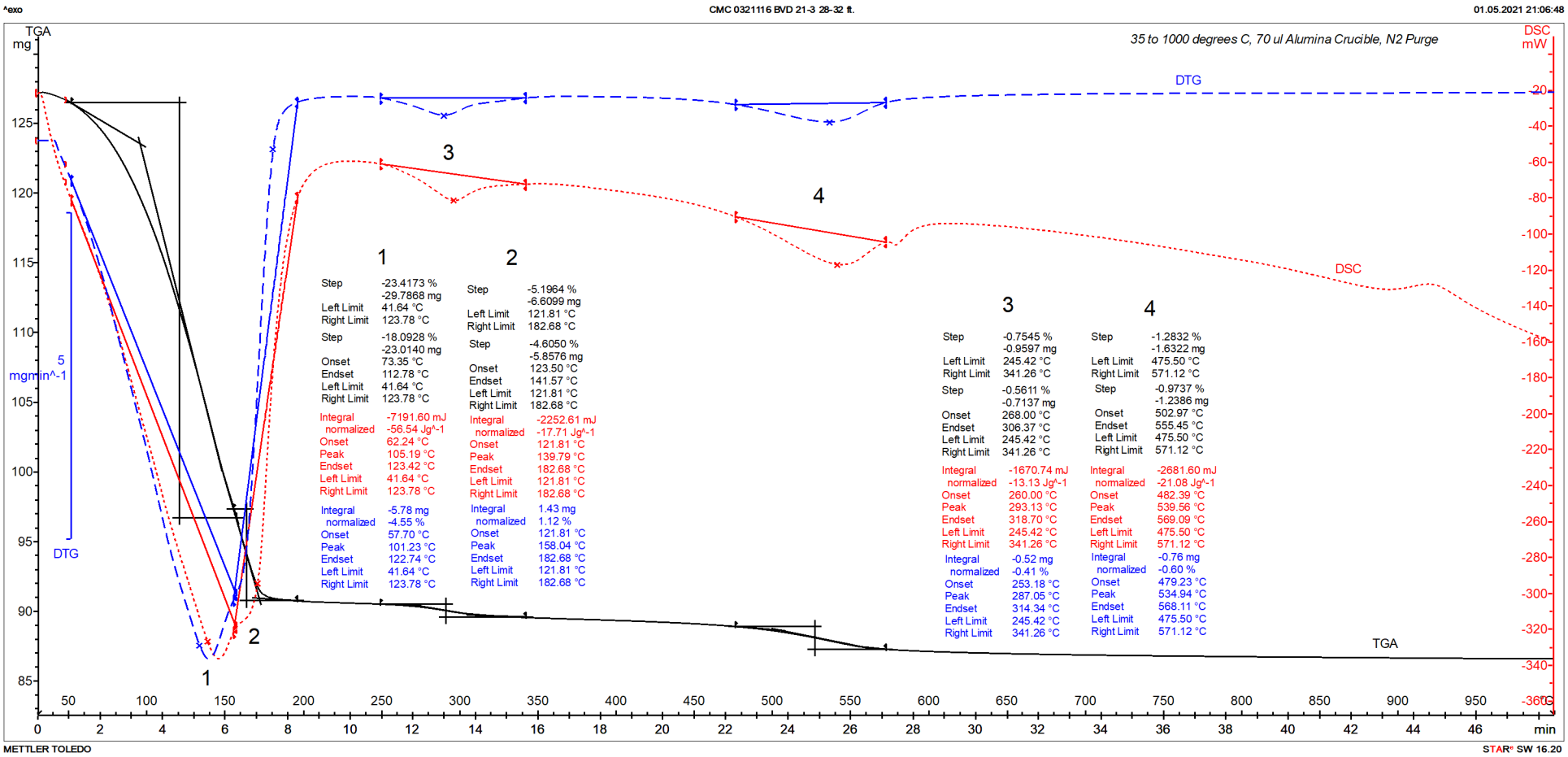


Figure 10: TGA (solid black), DSC (dotted red), and DTG (dashed blue) curves of Soil Sample: BVD 21-3, 28-32 ft. Major endotherms from decompositions (de-hydroxylation) of illite-kaolinite clay minerals and other phases in soil are marked as 1 through 4. No polymorphic transition of fine clay-sized quartz particle is found at 573ºC. Results of thermal analyses are also given. Maximum weight loss from loss of free and bound moisture in illitic clay has occurred within 200ºC.

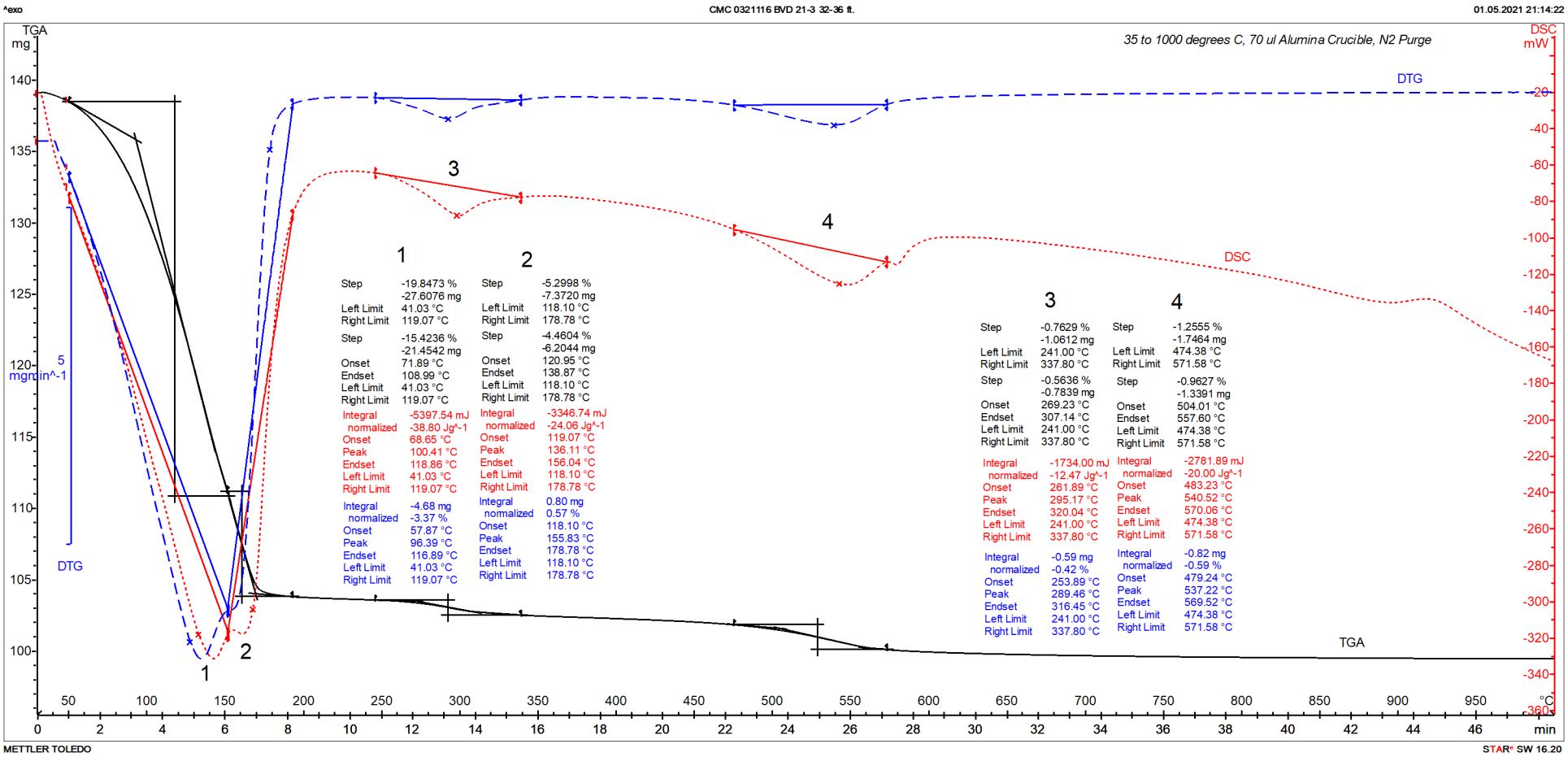


Figure 11: TGA (solid black), DSC (dotted red), and DTG (dashed blue) curves of Soil Sample: BVD 21-3, 32-36 ft. Major endotherms from decompositions (dehydroxylation) of illite-kaolinite clay minerals and other phases in soil are marked as 1 through 4. No polymorphic transition of fine clay-sized quartz particle is found at 573ºC. Results of thermal analyses are also given. Maximum weight loss from loss of free and bound moisture in illitic clay has occurred within 200ºC.

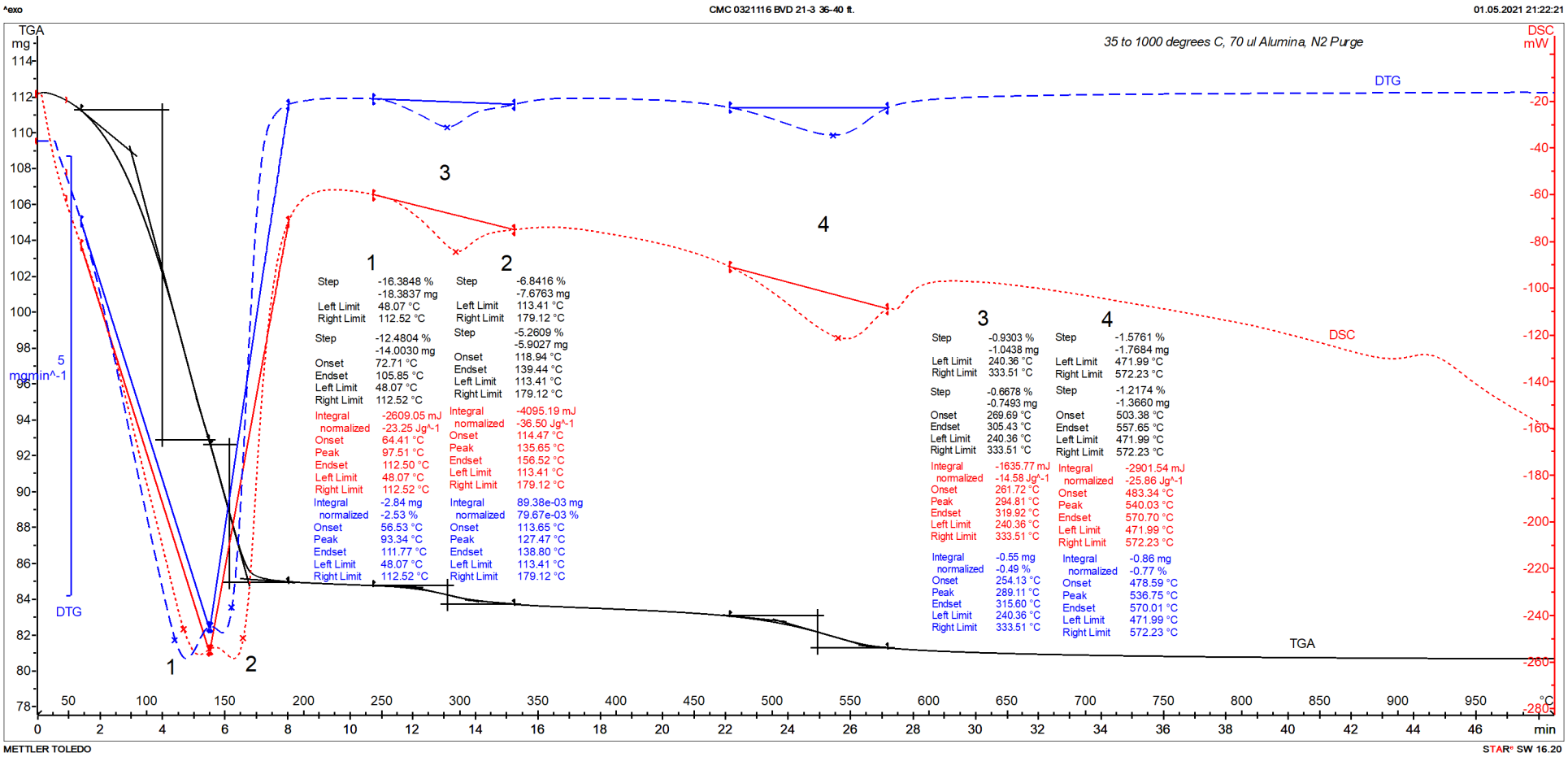


Figure 12: TGA (solid black), DSC (dotted red), and DTG (dashed blue) curves of Soil Sample: BVD 21-3, 36-40 ft. Major endotherms from decompositions (dehydroxylation) of illite-kaolinite clay minerals and other phases in soil are marked as 1 through 4. No polymorphic transition of fine clay-sized quartz particle is found at 573ºC. Results of thermal analyses are also given. Maximum weight loss from loss of free and bound moisture in illitic clay has occurred within 200ºC.

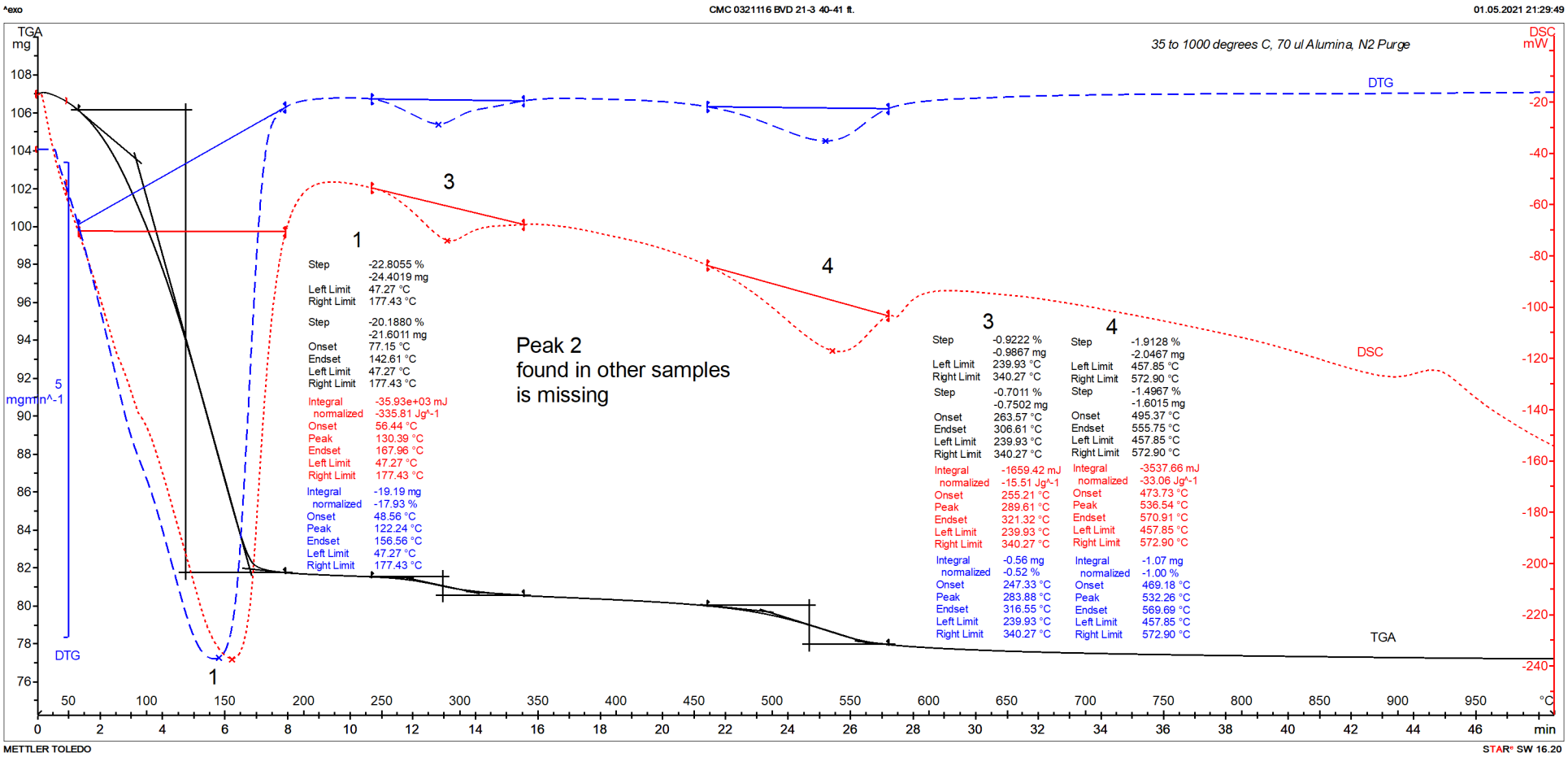


Figure 13: TGA (solid black), DSC (dotted red), and DTG (dashed blue) curves of Soil Sample: BVD 21-3, 40-41 ft. Major endotherms from decompositions (dehydroxylation) of illite-kaolinite clay minerals and other phases in soil are marked as 1 through 4. No polymorphic transition of fine clay-sized quartz particle is found at 573ºC. Results of thermal analyses are also given. Maximum weight loss from loss of free and bound moisture in illitic clay has occurred within 200ºC.

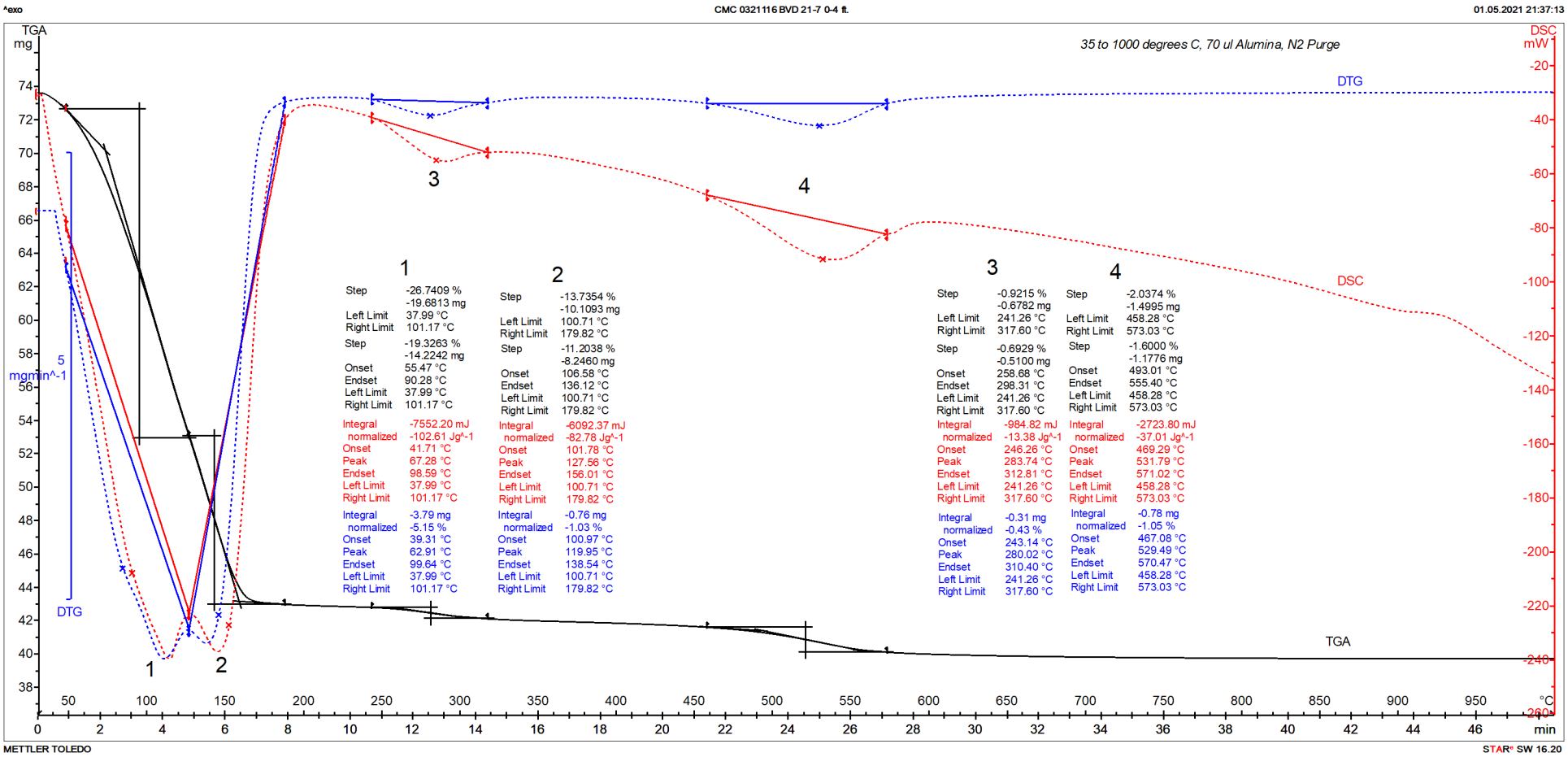


Figure 14: TGA (solid black), DSC (dotted red), and DTG (dashed blue) curves of Soil Sample: BVD 21-7, 0-4 ft. Major endotherms from decompositions (dehydroxylation) of illite-kaolinite clay minerals and other phases in soil are marked as 1 through 4. No polymorphic transition of fine clay-sized quartz particle is found at 573ºC. Results of thermal analyses are also given. Maximum weight loss from loss of free and bound moisture in illitic clay has occurred within 200ºC.

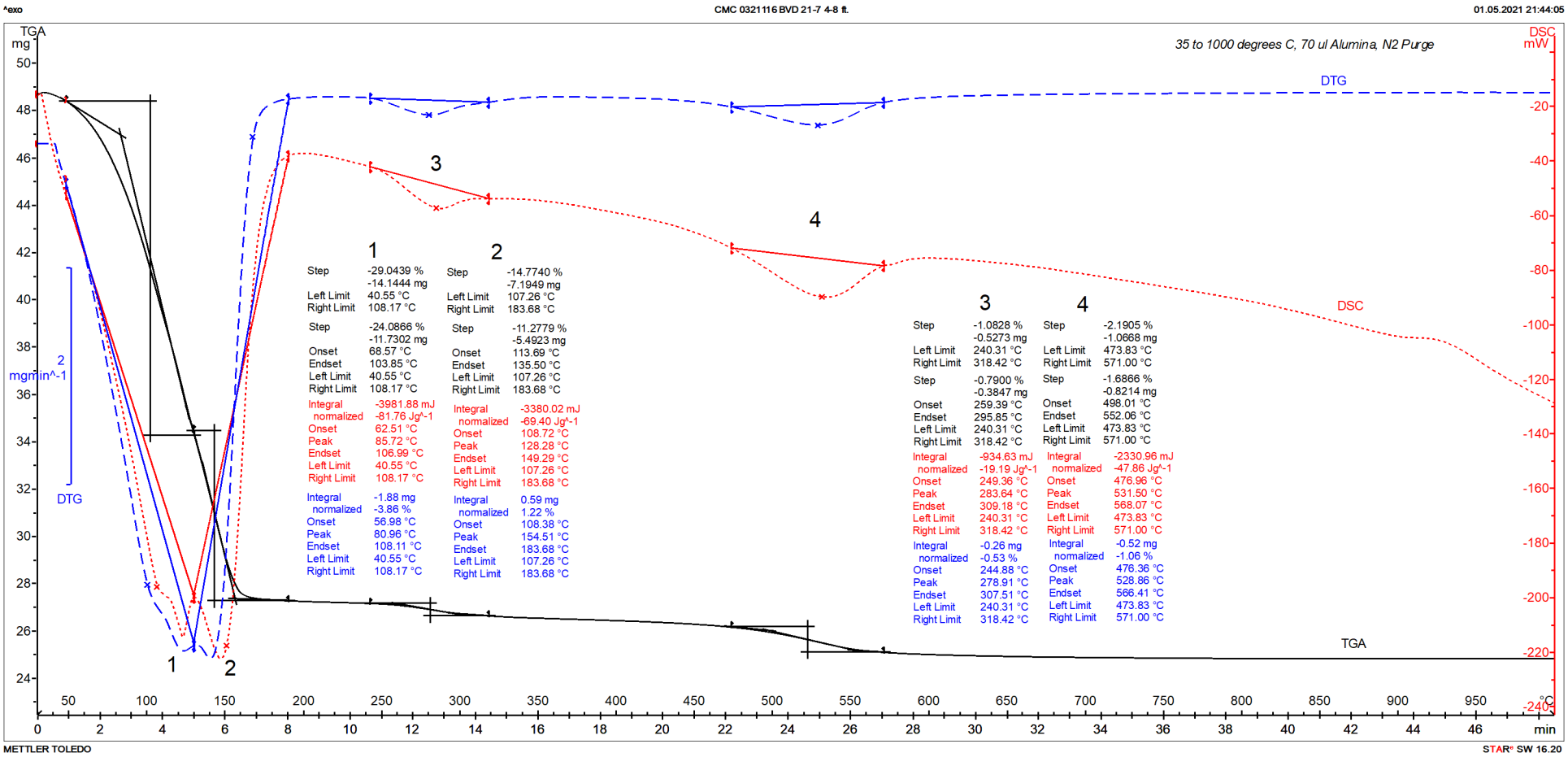


Figure 15: TGA (solid black), DSC (dotted red), and DTG (dashed blue) curves of Soil Sample: BVD 21-7, 4-8 ft. Major endotherms from decompositions (dehydroxylation) of illite-kaolinite clay minerals and other phases in soil are marked as 1 through 4. No polymorphic transition of fine clay-sized quartz particle is found at 573ºC. Results of thermal analyses are also given. Maximum weight loss from loss of free and bound moisture in illitic clay has occurred within 200ºC.

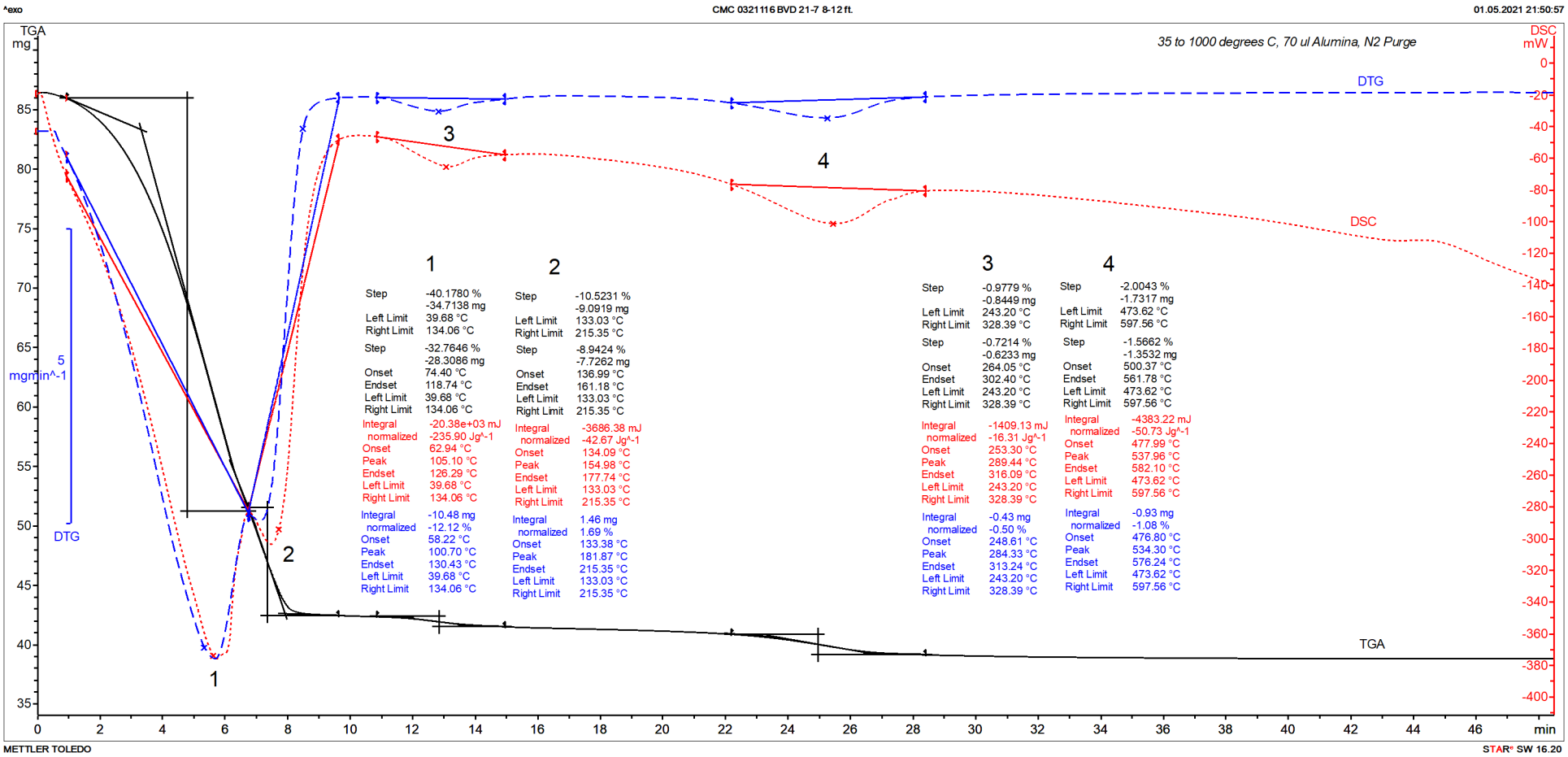


Figure 16: TGA (solid black), DSC (dotted red), and DTG (dashed blue) curves of Soil Sample: BVD 21-7, 8-12 ft. Major endotherms from decompositions (dehydroxylation) of illite-kaolinite clay minerals and other phases in soil are marked as 1 through 4. No polymorphic transition of fine clay-sized quartz particle is found at 573ºC. Results of thermal analyses are also given. Maximum weight loss from loss of free and bound moisture in illitic clay has occurred within 200ºC.

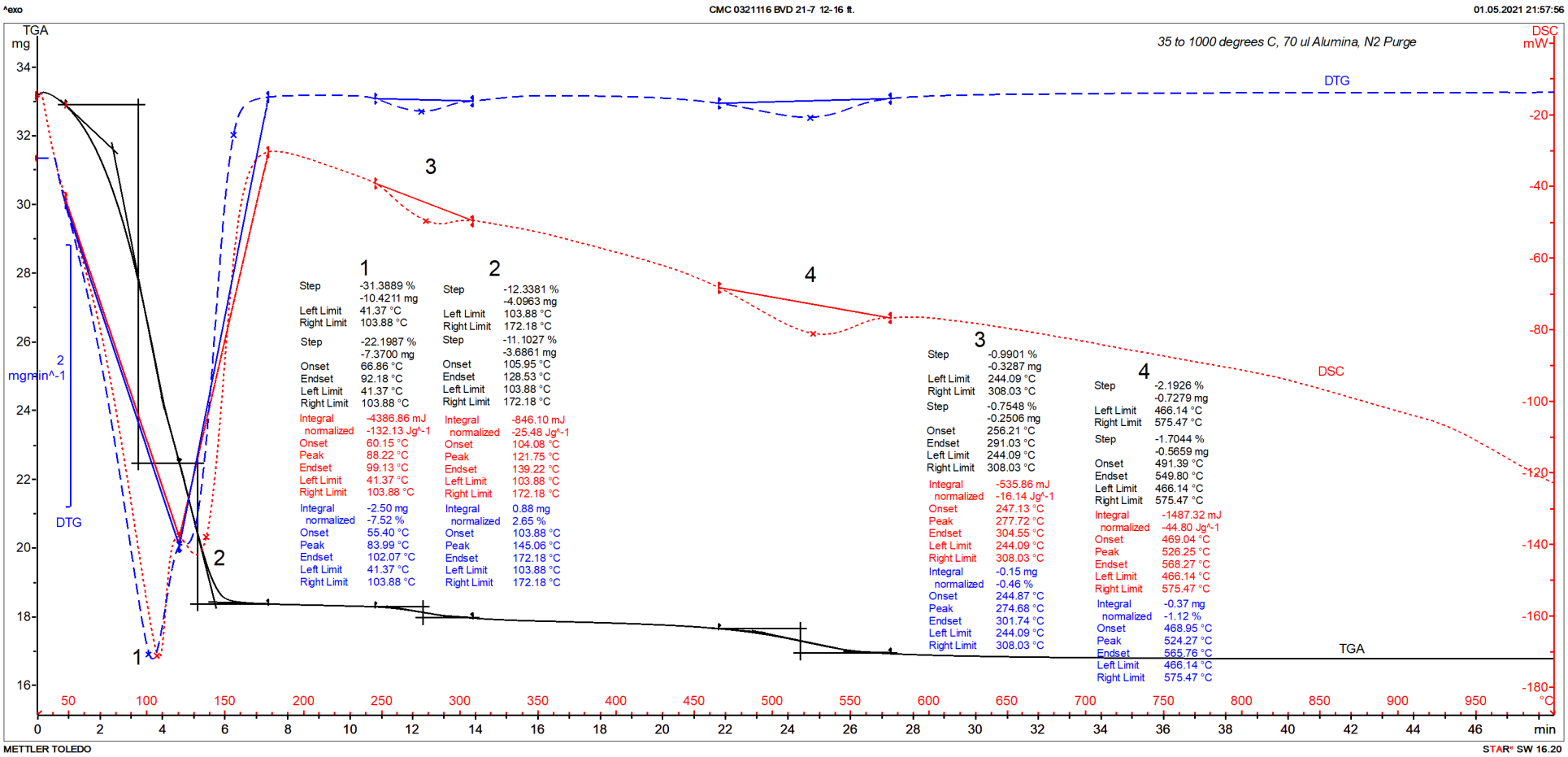


Figure 17: TGA (solid black), DSC (dotted red), and DTG (dashed blue) curves of Soil Sample: BVD 21-7, 12-16 ft. Major endotherms from decompositions (dehydroxylation) of illite-kaolinite clay minerals and other phases in soil are marked as 1 through 4. No polymorphic transition of fine clay-sized quartz particle is found at 573ºC. Results of thermal analyses are also given. Maximum weight loss from loss of free and bound moisture in illitic clay has occurred within 200ºC.

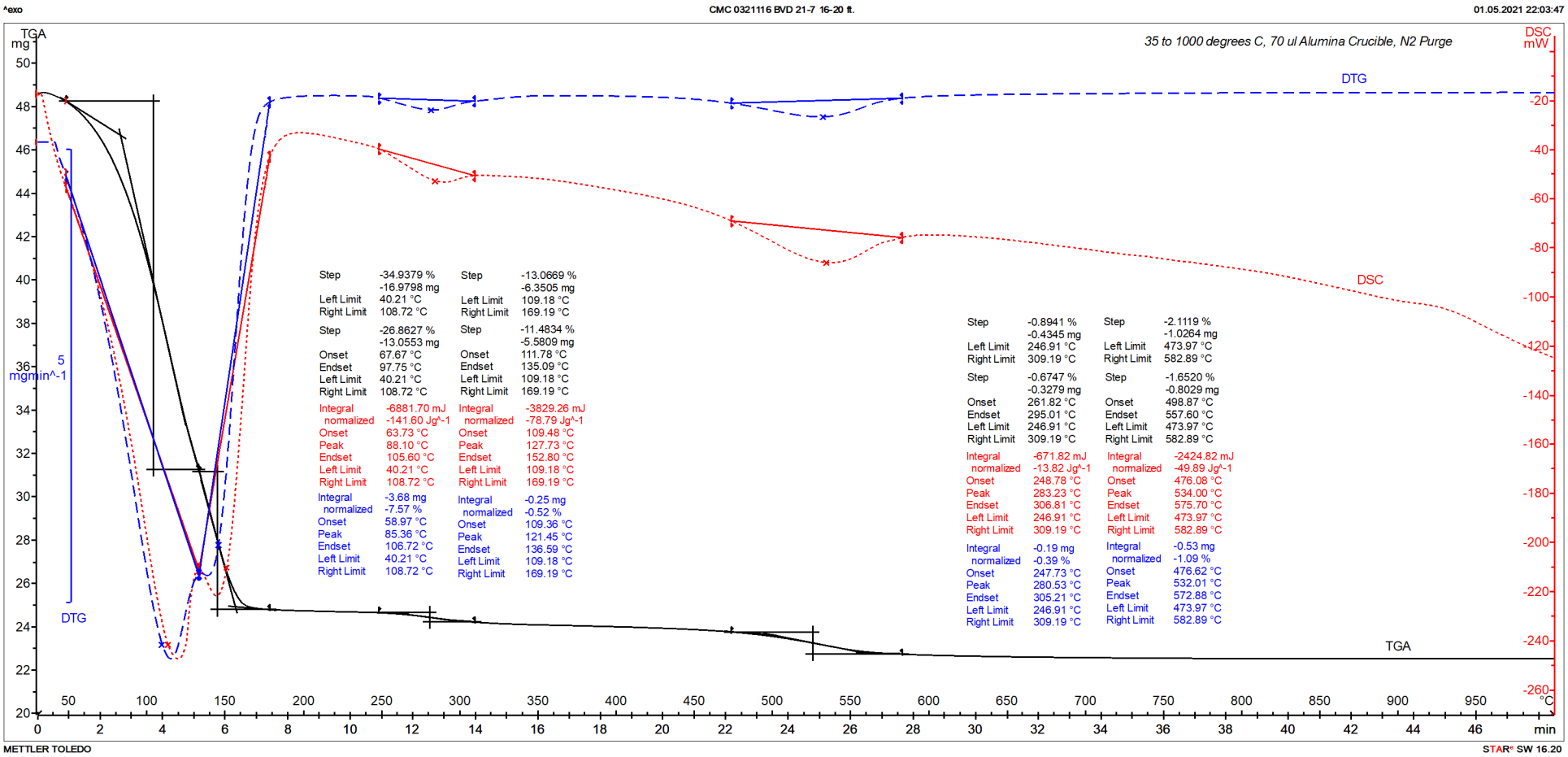


Figure 18: TGA (solid black), DSC (dotted red), and DTG (dashed blue) curves of Soil Sample: BVD 21-7, 16-20 ft. Major endotherms from decompositions (dehydroxylation) of illite-kaolinite clay minerals and other phases in soil are marked as 1 through 4. No polymorphic transition of fine clay-sized quartz particle is found at 573ºC. Results of thermal analyses are also given. Maximum weight loss from loss of free and bound moisture in illitic clay has occurred within 200ºC.

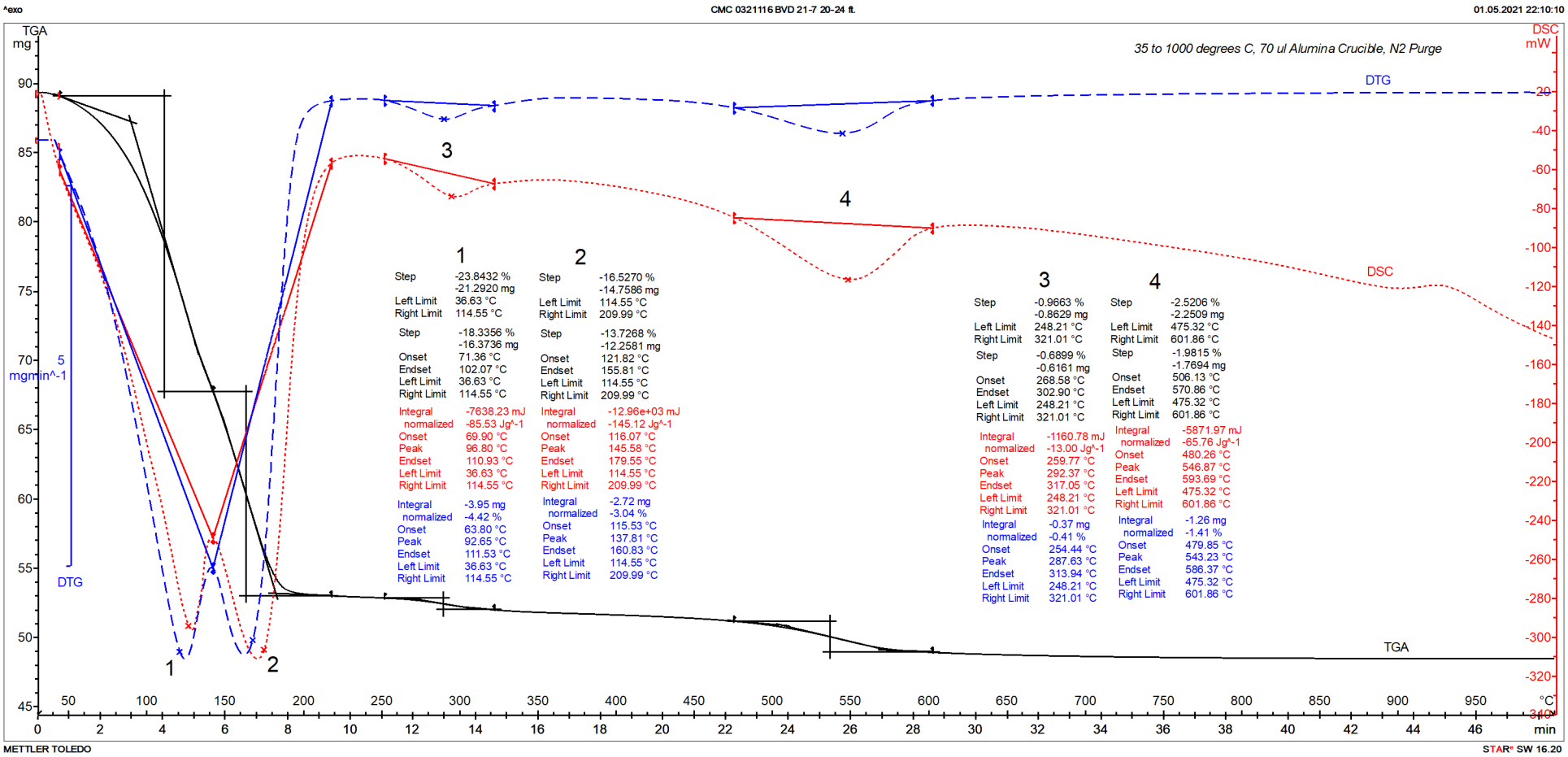


Figure 19: TGA (solid black), DSC (dotted red), and DTG (dashed blue) curves of Soil Sample: BVD 21-7, 20-24 ft. Major endotherms from decompositions (dehydroxylation) of illite-kaolinite clay minerals and other phases in soil are marked as 1 through 4. No polymorphic transition of fine clay-sized quartz particle is found at 573ºC. Results of thermal analyses are also given. Maximum weight loss from loss of free and bound moisture in illitic clay has occurred within 200ºC.

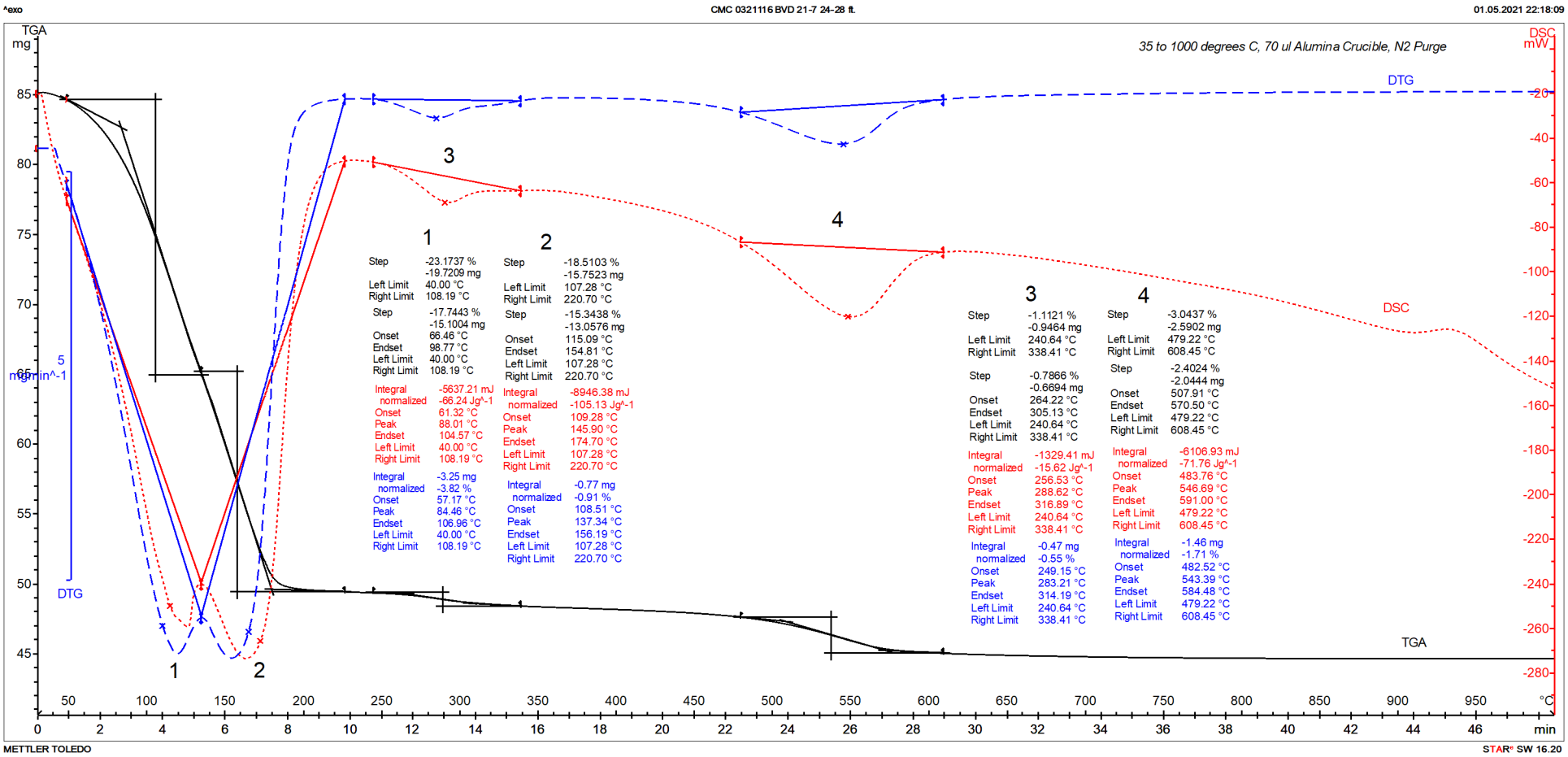


Figure 20: TGA (solid black), DSC (dotted red), and DTG (dashed blue) curves of Soil Sample: BVD 21-7, 24-28 ft. Major endotherms from decompositions (dehydroxylation) of illite-kaolinite clay minerals and other phases in soil are marked as 1 through 4. No polymorphic transition of fine clay-sized quartz particle is found at 573ºC. Results of thermal analyses are also given. Maximum weight loss from loss of free and bound moisture in illitic clay has occurred within 200ºC.

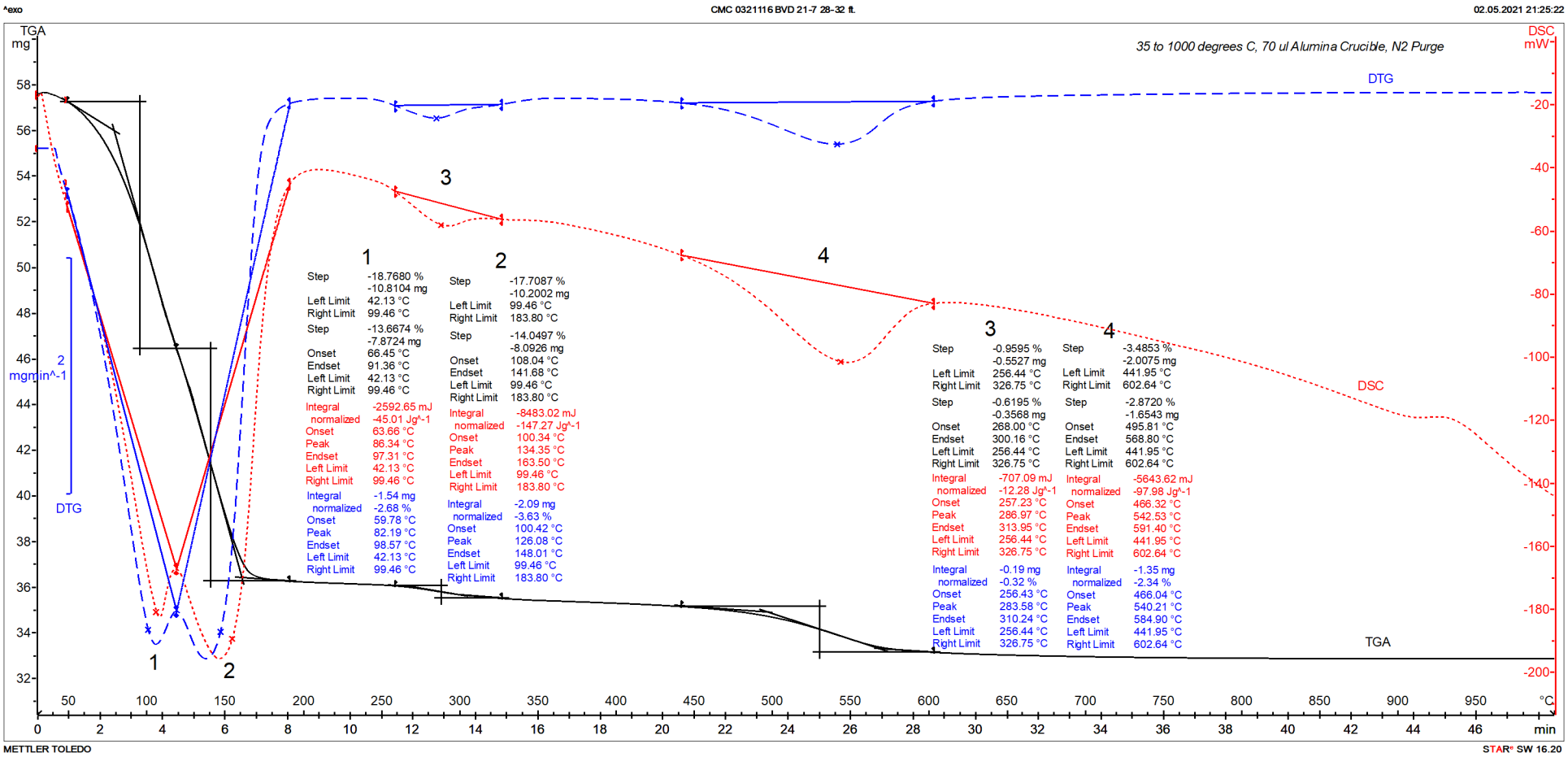


Figure 21: TGA (solid black), DSC (dotted red), and DTG (dashed blue) curves of Soil Sample: BVD 21-7, 28-32 ft. Major endotherms from decompositions (dehydroxylation) of illite-kaolinite clay minerals and other phases in soil are marked as 1 through 4. No polymorphic transition of fine clay-sized quartz particle is found at 573ºC. Results of thermal analyses are also given. Maximum weight loss from loss of free and bound moisture in illitic clay has occurred within 200ºC.

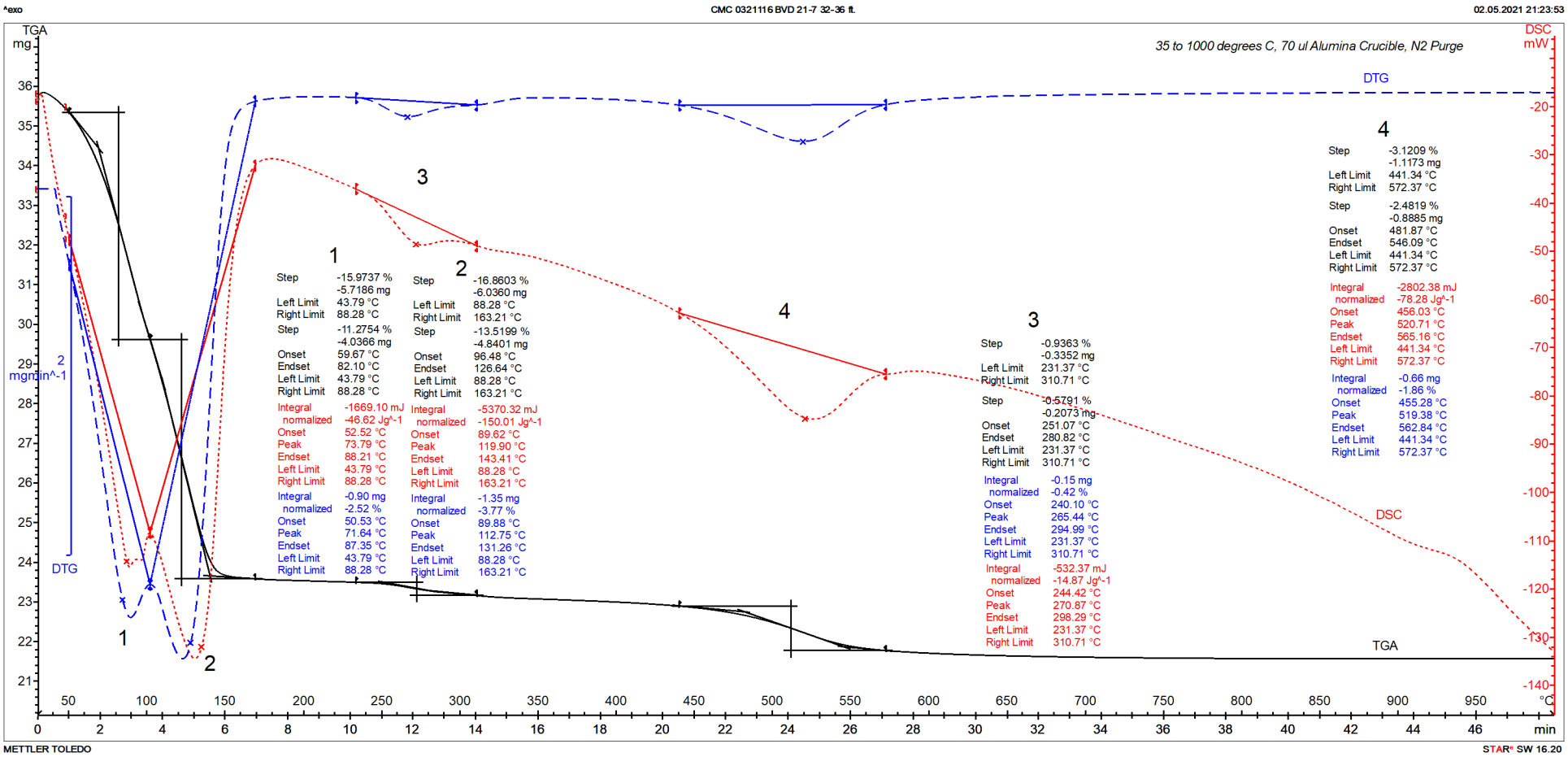


Figure 22: TGA (solid black), DSC (dotted red), and DTG (dashed blue) curves of Soil Sample: BVD 21-7, 32-36 ft. Major endotherms from decompositions (dehydroxylation) of illite-kaolinite clay minerals and other phases in soil are marked as 1 through 4. No polymorphic transition of fine clay-sized quartz particle is found at 573ºC. Results of thermal analyses are also given. Maximum weight loss from loss of free and bound moisture in illitic clay has occurred within 200ºC.

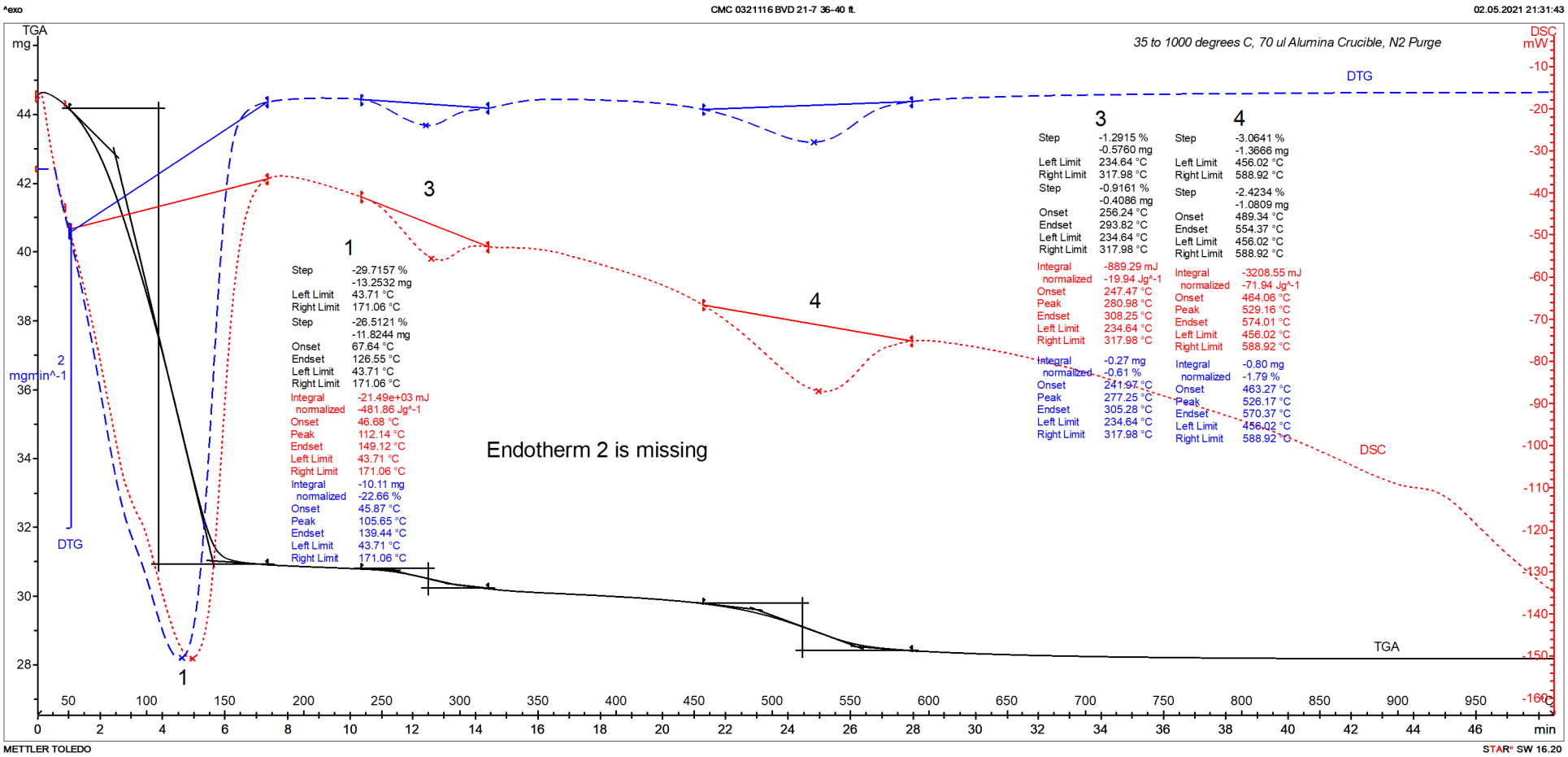


Figure 23: TGA (solid black), DSC (dotted red), and DTG (dashed blue) curves of Soil Sample: BVD 21-7, 36-40 ft. Major endotherms from decompositions (dehydroxylation) of illite-kaolinite clay minerals and other phases in soil are marked as 1 through 4. No polymorphic transition of fine clay-sized quartz particle is found at 573ºC. Results of thermal analyses are also given. Maximum weight loss from loss of free and bound moisture in illitic clay has occurred within 200ºC.

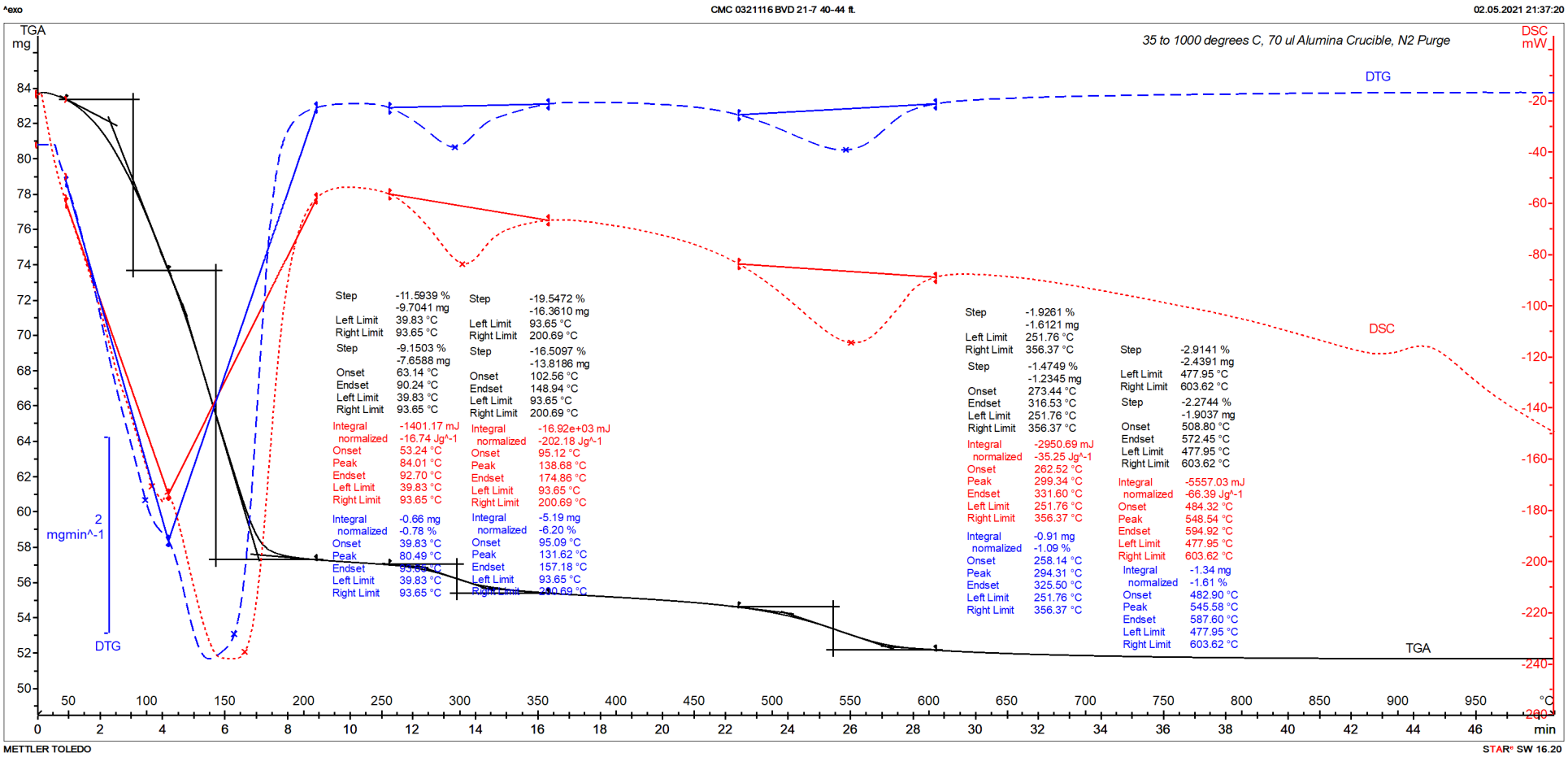


Figure 24: TGA (solid black), DSC (dotted red), and DTG (dashed blue) curves of Soil Sample: BVD 21-7, 40-44 ft. Major endotherms from decompositions (dehydroxylation) of illite-kaolinite clay minerals and other phases in soil are marked as 1 through 4. No polymorphic transition of fine clay-sized quartz particle is found at 573ºC. Results of thermal analyses are also given. Maximum weight loss from loss of free and bound moisture in illitic clay has occurred within 200ºC.

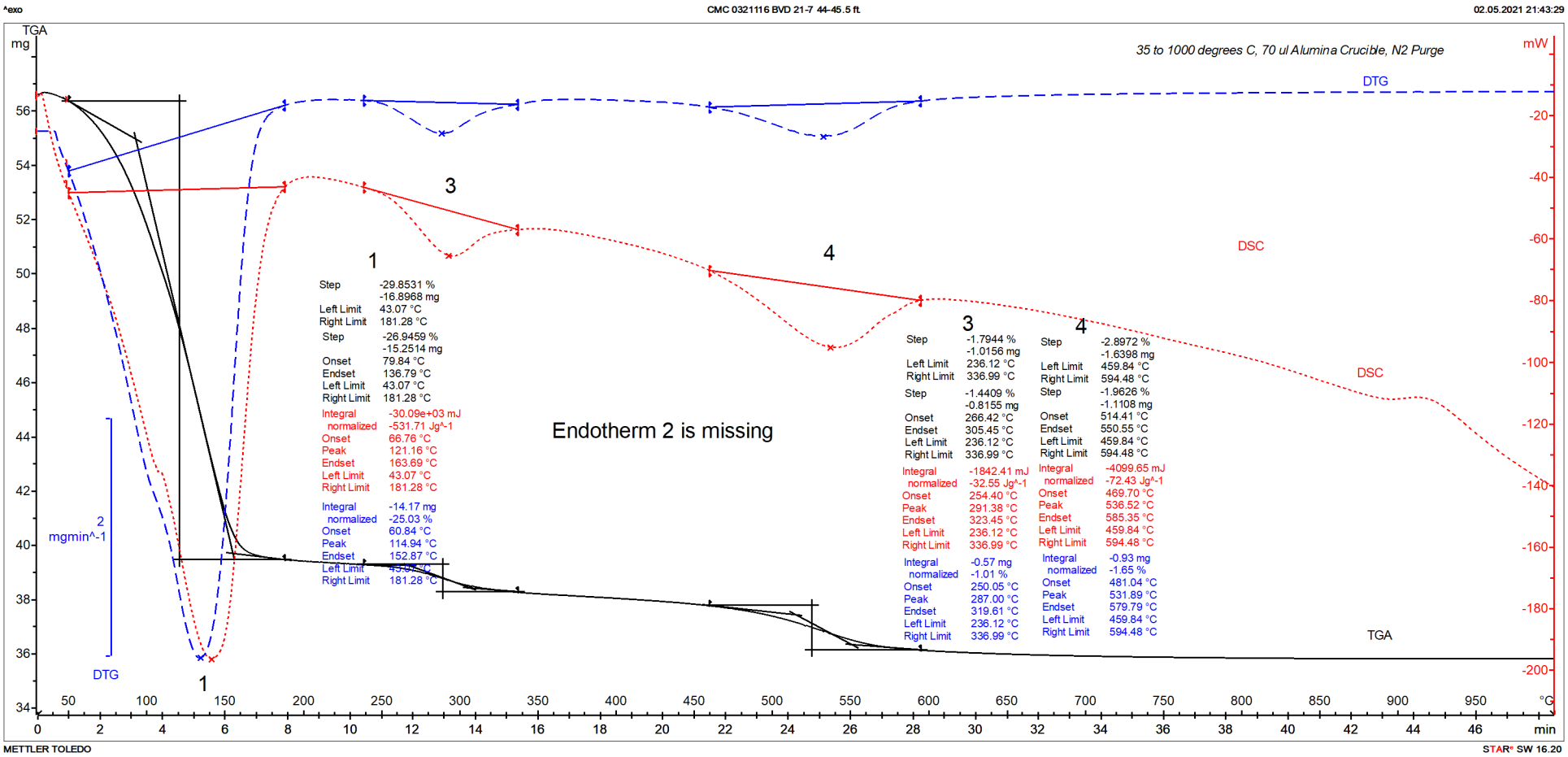


Figure 25: TGA (solid black), DSC (dotted red), and DTG (dashed blue) curves of Soil Sample: BVD 21-7, 44-45 ft. Major endotherms from decompositions (dehydroxylation) of illite-kaolinite clay minerals and other phases in soil are marked as 1 through 4. No polymorphic transition of fine clay-sized quartz particle is found at 573ºC. Results of thermal analyses are also given. Maximum weight loss from loss of free and bound moisture in illitic clay has occurred within 200ºC.

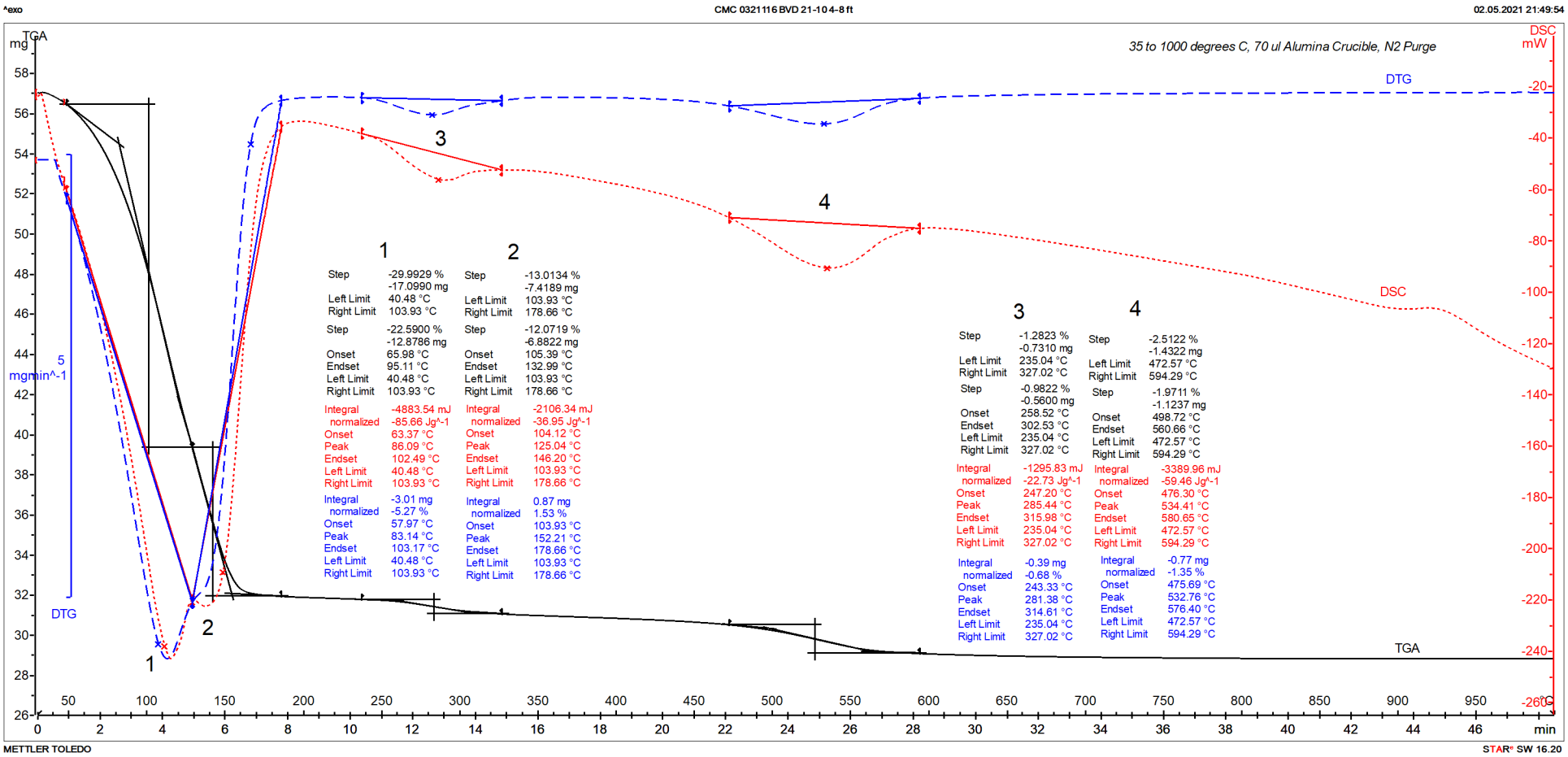


Figure 26: TGA (solid black), DSC (dotted red), and DTG (dashed blue) curves of Soil Sample: BVD 21-10, 4-8 ft. Major endotherms from decompositions (de-hydroxylation) of illite-kaolinite clay minerals and other phases in soil are marked as 1 through 4. No polymorphic transition of fine clay-sized quartz particle is found at 573ºC. Results of thermal analyses are also given. Maximum weight loss from loss of free and bound moisture in illitic clay has occurred within 200ºC.

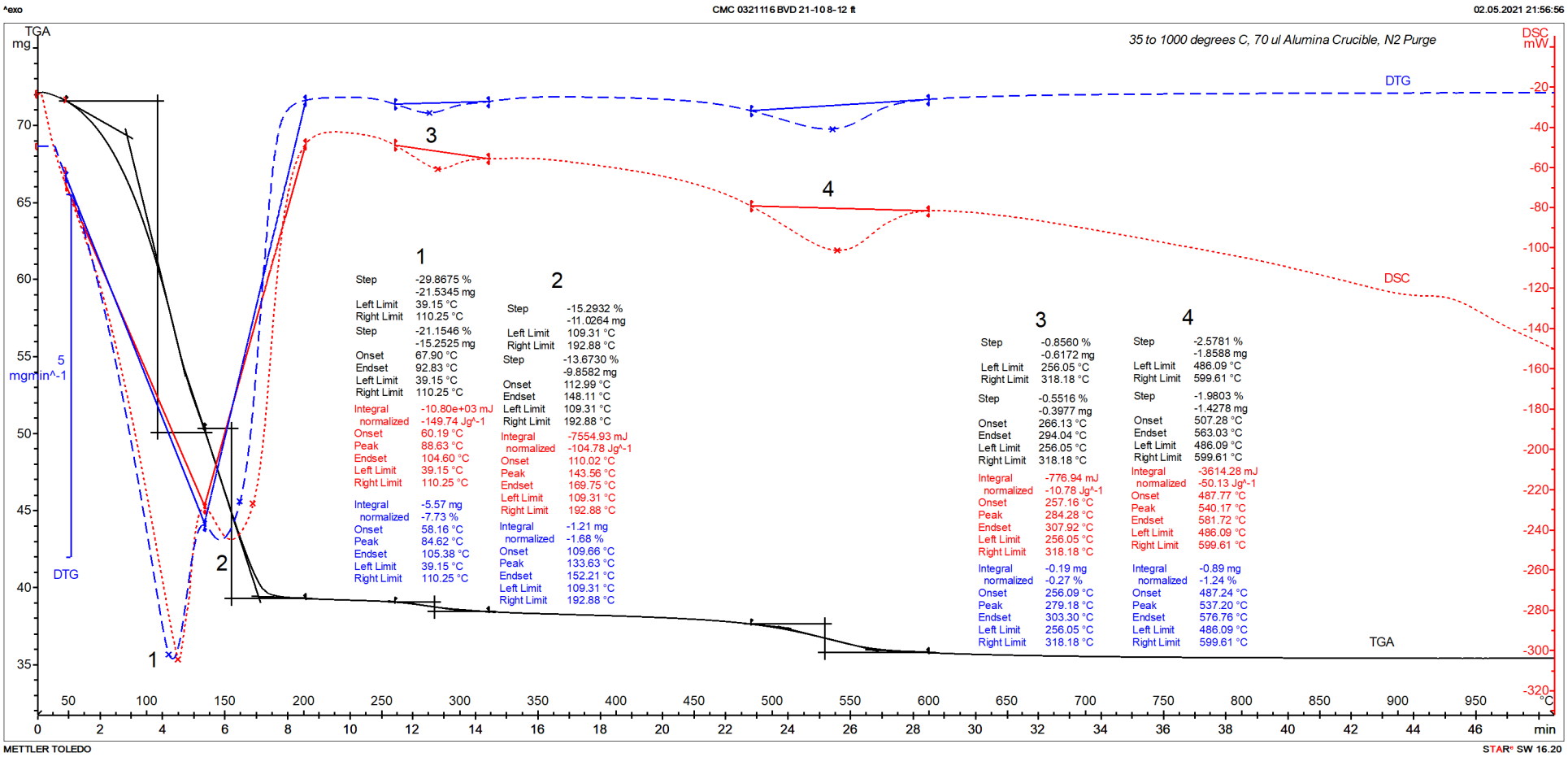


Figure 27: TGA (solid black), DSC (dotted red), and DTG (dashed blue) curves of Soil Sample: BVD 21-10, 8-12 ft. Major endotherms from decompositions (dehydroxylation) of illite-kaolinite clay minerals and other phases in soil are marked as 1 through 4. No polymorphic transition of fine clay-sized quartz particle is found at 573ºC. Results of thermal analyses are also given. Maximum weight loss from loss of free and bound moisture in illitic clay has occurred within 200ºC.

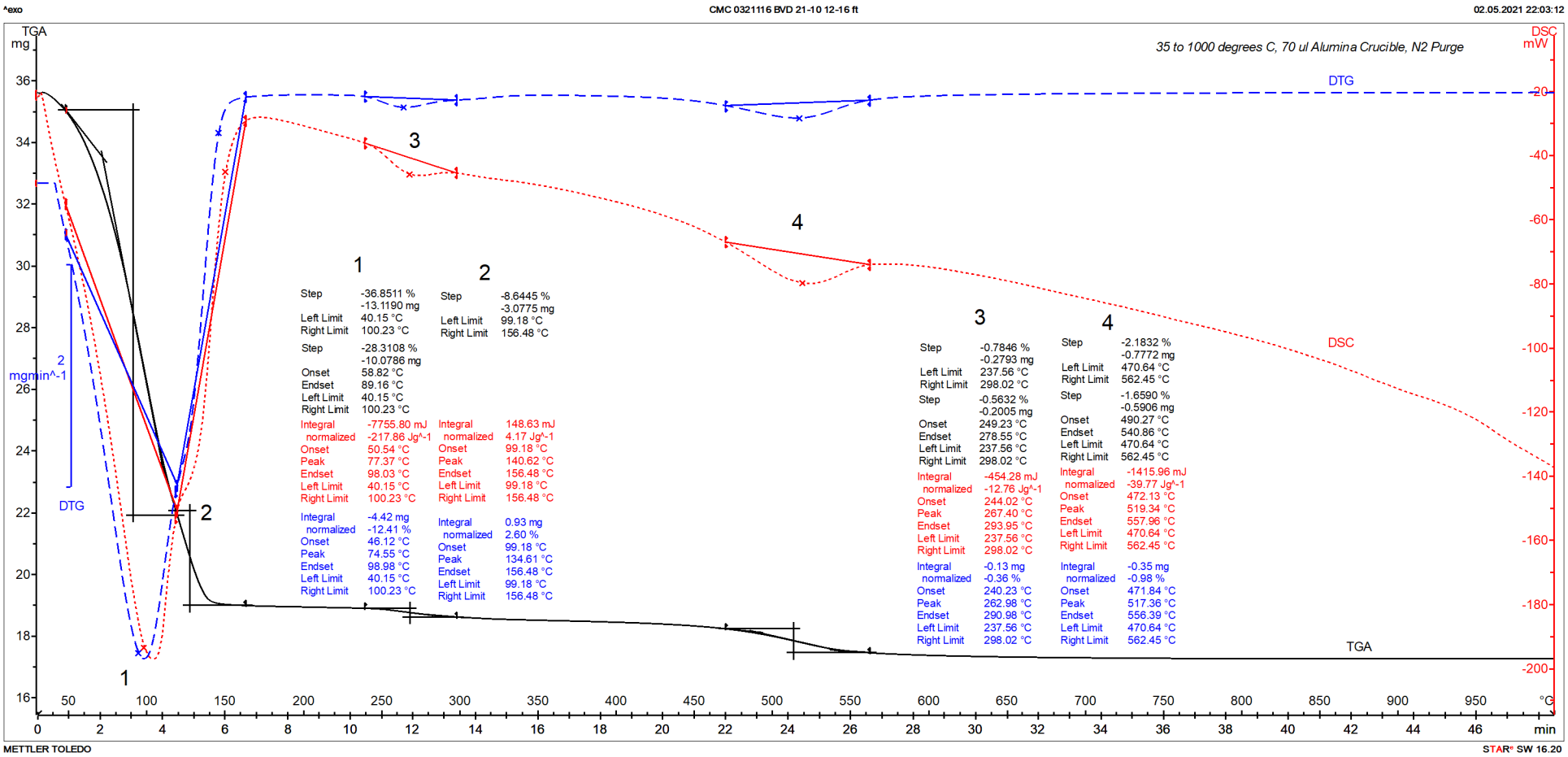


Figure 28: TGA (solid black), DSC (dotted red), and DTG (dashed blue) curves of Soil Sample: BVD 21-10, 12-16 ft. Major endotherms from decompositions (dehydroxylation) of illite-kaolinite clay minerals and other phases in soil are marked as 1 through 4. No polymorphic transition of fine clay-sized quartz particle is found at 573ºC. Results of thermal analyses are also given. Maximum weight loss from loss of free and bound moisture in illitic clay has occurred within 200ºC.

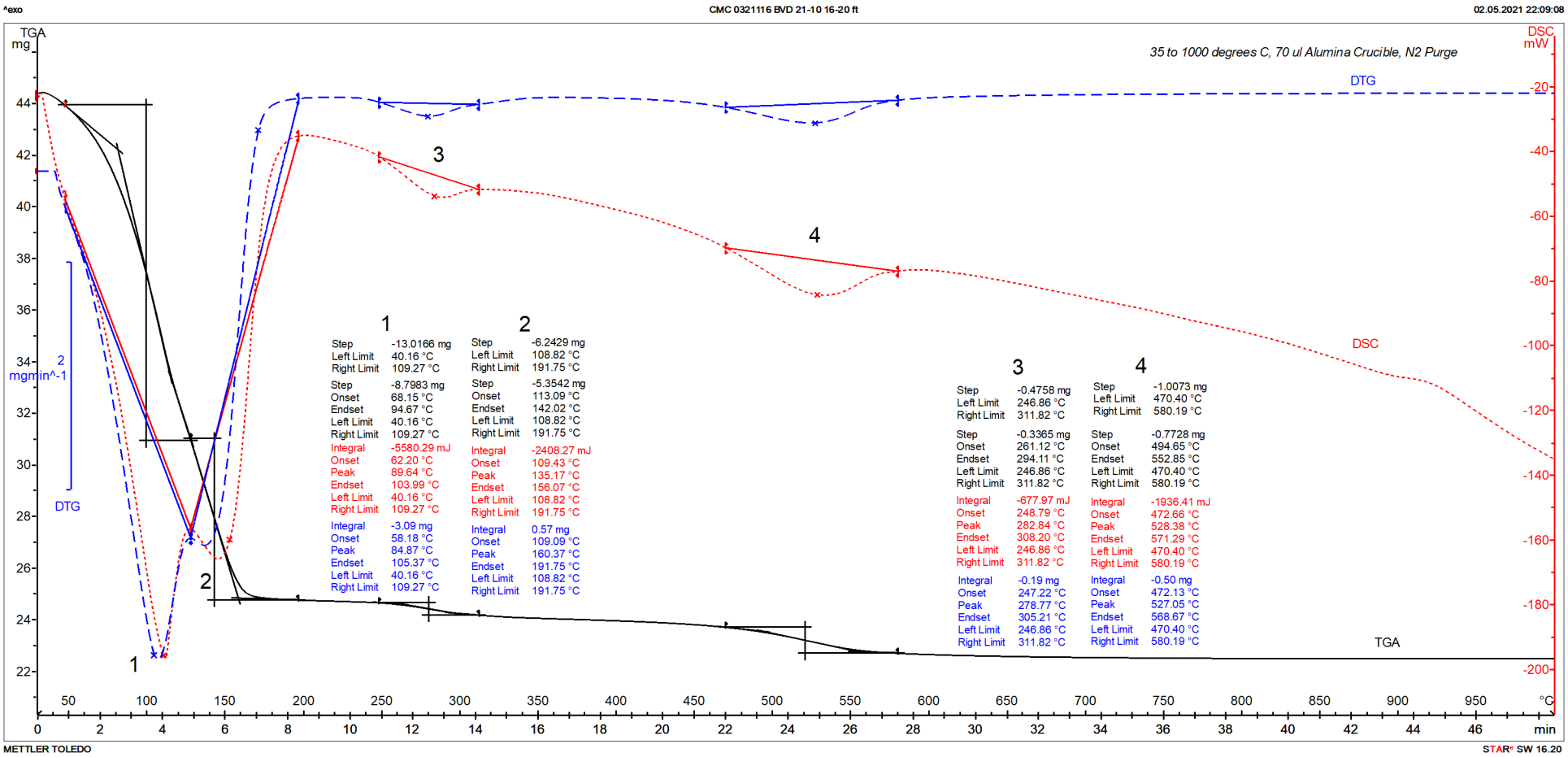


Figure 29: TGA (solid black), DSC (dotted red), and DTG (dashed blue) curves of Soil Sample: BVD 21-10, 16-20 ft. Major endotherms from decompositions (dehydroxylation) of illite-kaolinite clay minerals and other phases in soil are marked as 1 through 4. No polymorphic transition of fine clay-sized quartz particle is found at 573ºC. Results of thermal analyses are also given. Maximum weight loss from loss of free and bound moisture in illitic clay has occurred within 200ºC.

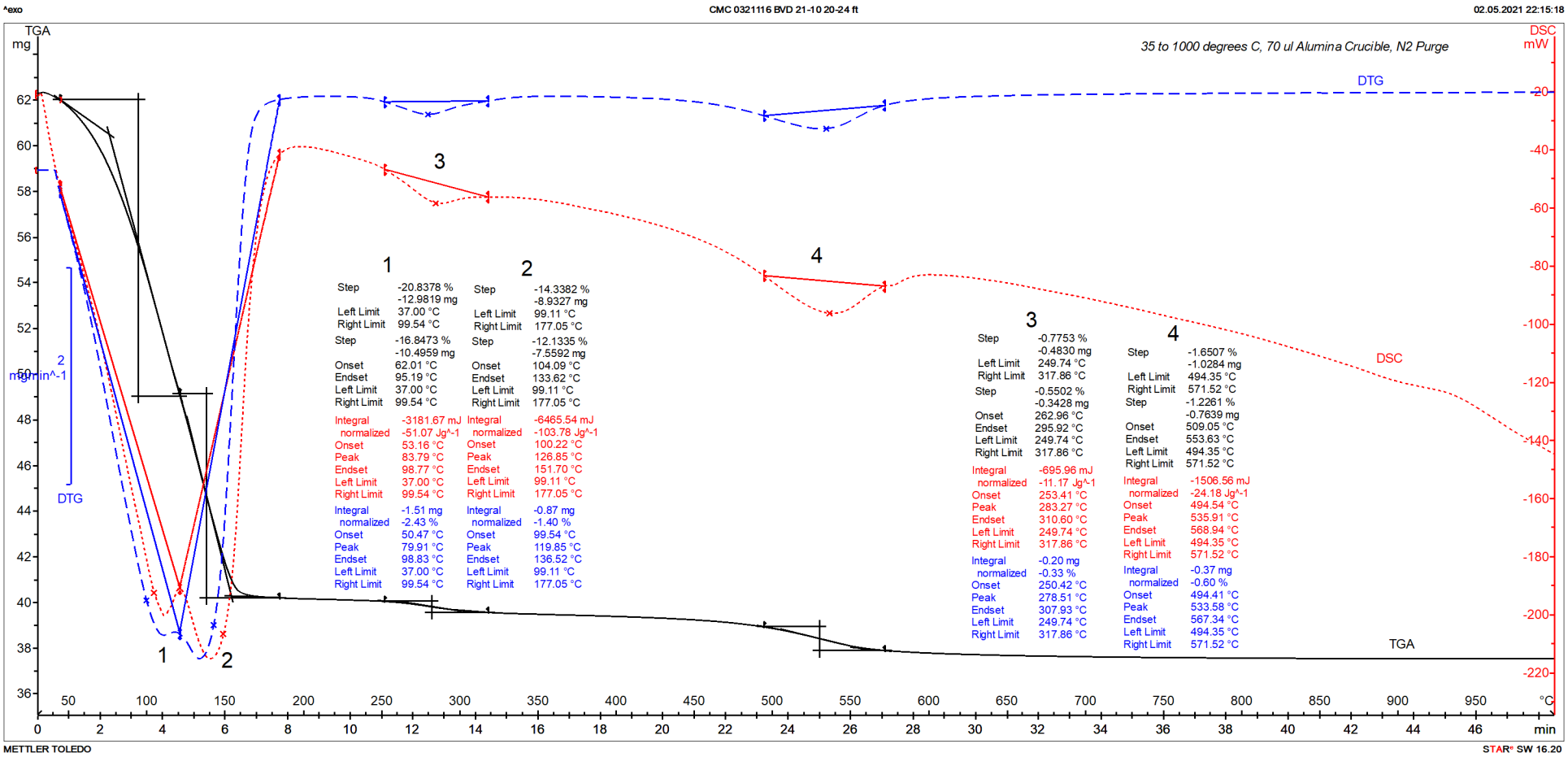


Figure 30: TGA (solid black), DSC (dotted red), and DTG (dashed blue) curves of Soil Sample: BVD 21-10, 20-24 ft. Major endotherms from decompositions (de-hydroxylation) of illite-kaolinite clay minerals and other phases in soil are marked as 1 through 4. No polymorphic transition of fine clay-sized quartz particle is found at 573ºC. Results of thermal analyses are also given. Maximum weight loss from loss of free and bound moisture in illitic clay has occurred within 200ºC.

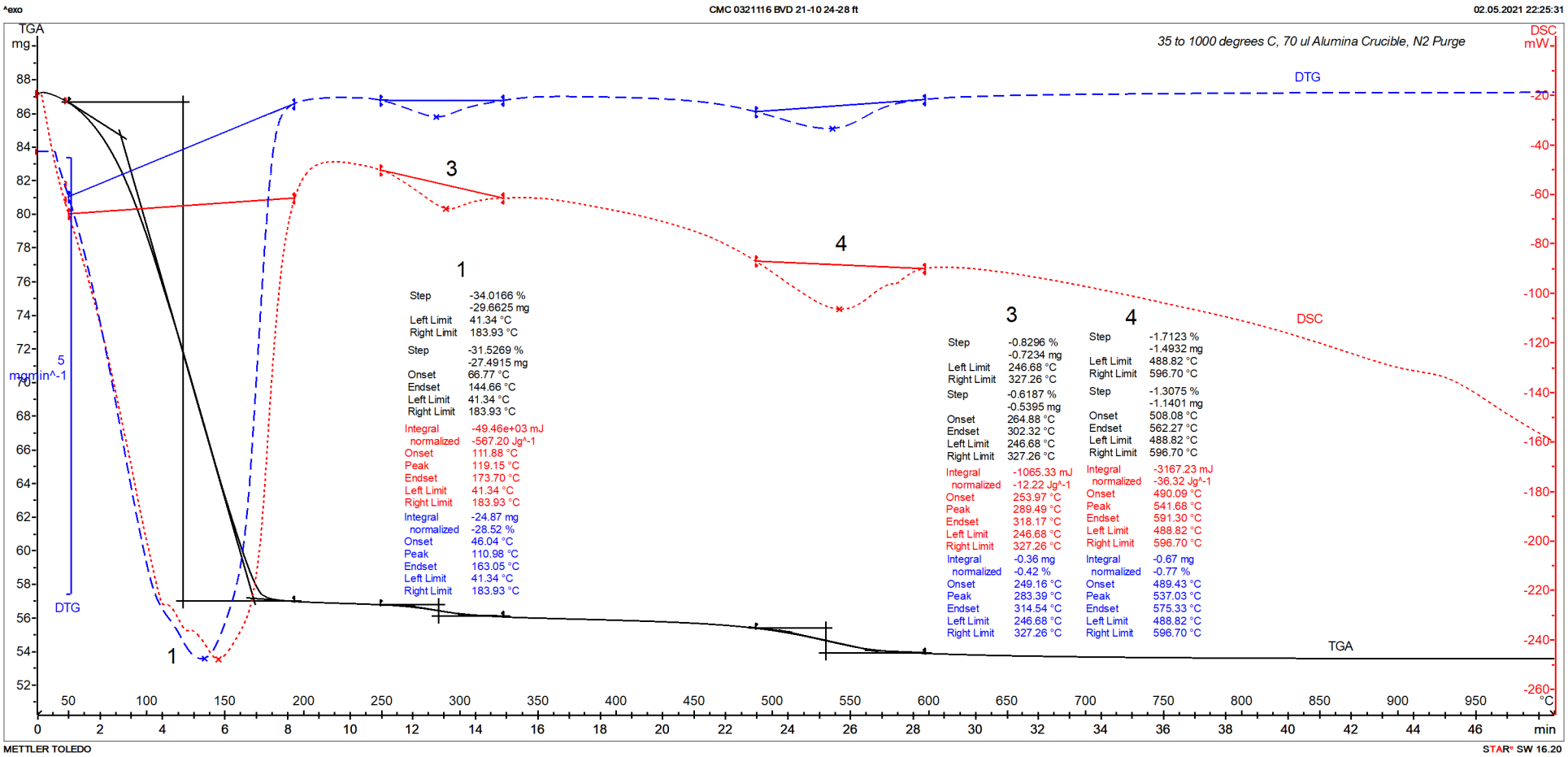


Figure 31: TGA (solid black), DSC (dotted red), and DTG (dashed blue) curves of Soil Sample: BVD 21-10, 24-28 ft. Major endotherms from decompositions (dehydroxylation) of illite-kaolinite clay minerals and other phases in soil are marked as 1 through 4. No polymorphic transition of fine clay-sized quartz particle is found at 573ºC. Results of thermal analyses are also given. Maximum weight loss from loss of free and bound moisture in illitic clay has occurred within 200ºC.

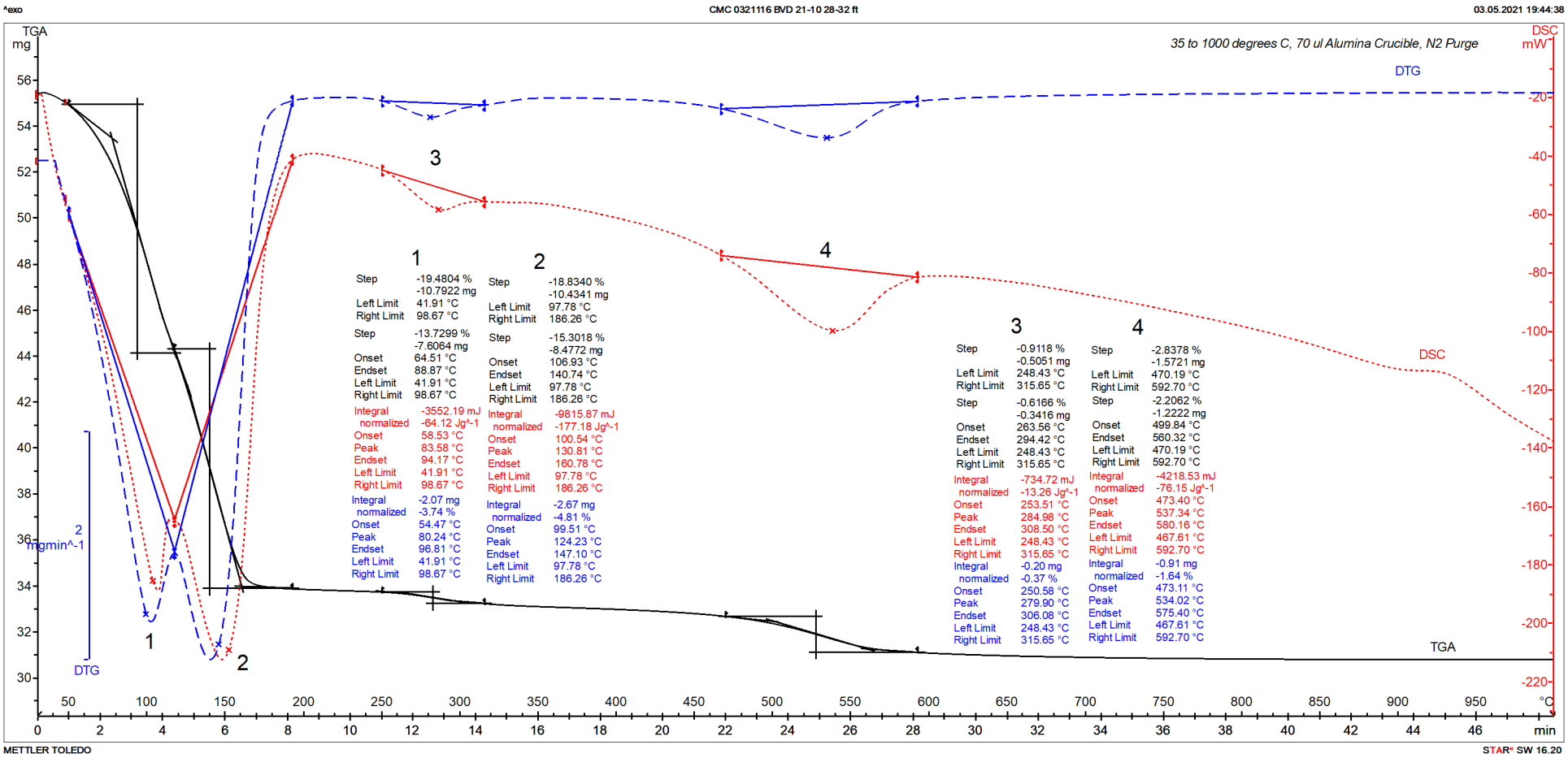


Figure 32: TGA (solid black), DSC (dotted red), and DTG (dashed blue) curves of Soil Sample: BVD 21-10, 28-32 ft. Major endotherms from decompositions (dehydroxylation) of illite-kaolinite clay minerals and other phases in soil are marked as 1 through 4. No polymorphic transition of fine clay-sized quartz particle is found at 573ºC. Results of thermal analyses are also given. Maximum weight loss from loss of free and bound moisture in illitic clay has occurred within 200ºC.

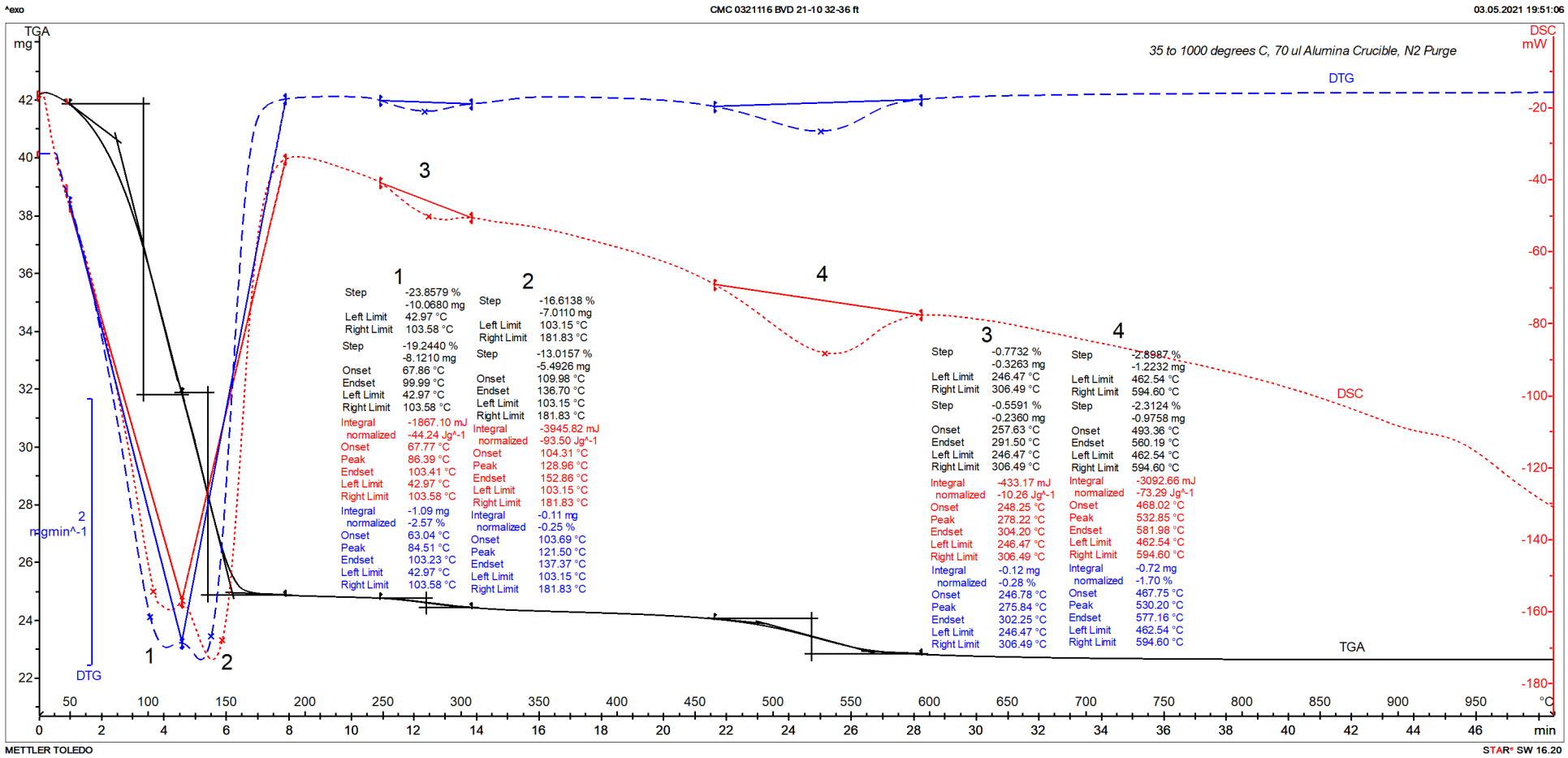


Figure 33: TGA (solid black), DSC (dotted red), and DTG (dashed blue) curves of Soil Sample: BVD 21-10, 32-36 ft. Major endotherms from decompositions (de-hydroxylation) of illite-kaolinite clay minerals and other phases in soil are marked as 1 through 4. No polymorphic transition of fine clay-sized quartz particle is found at 573ºC. Results of thermal analyses are also given. Maximum weight loss from loss of free and bound moisture in illitic clay has occurred within 200ºC.

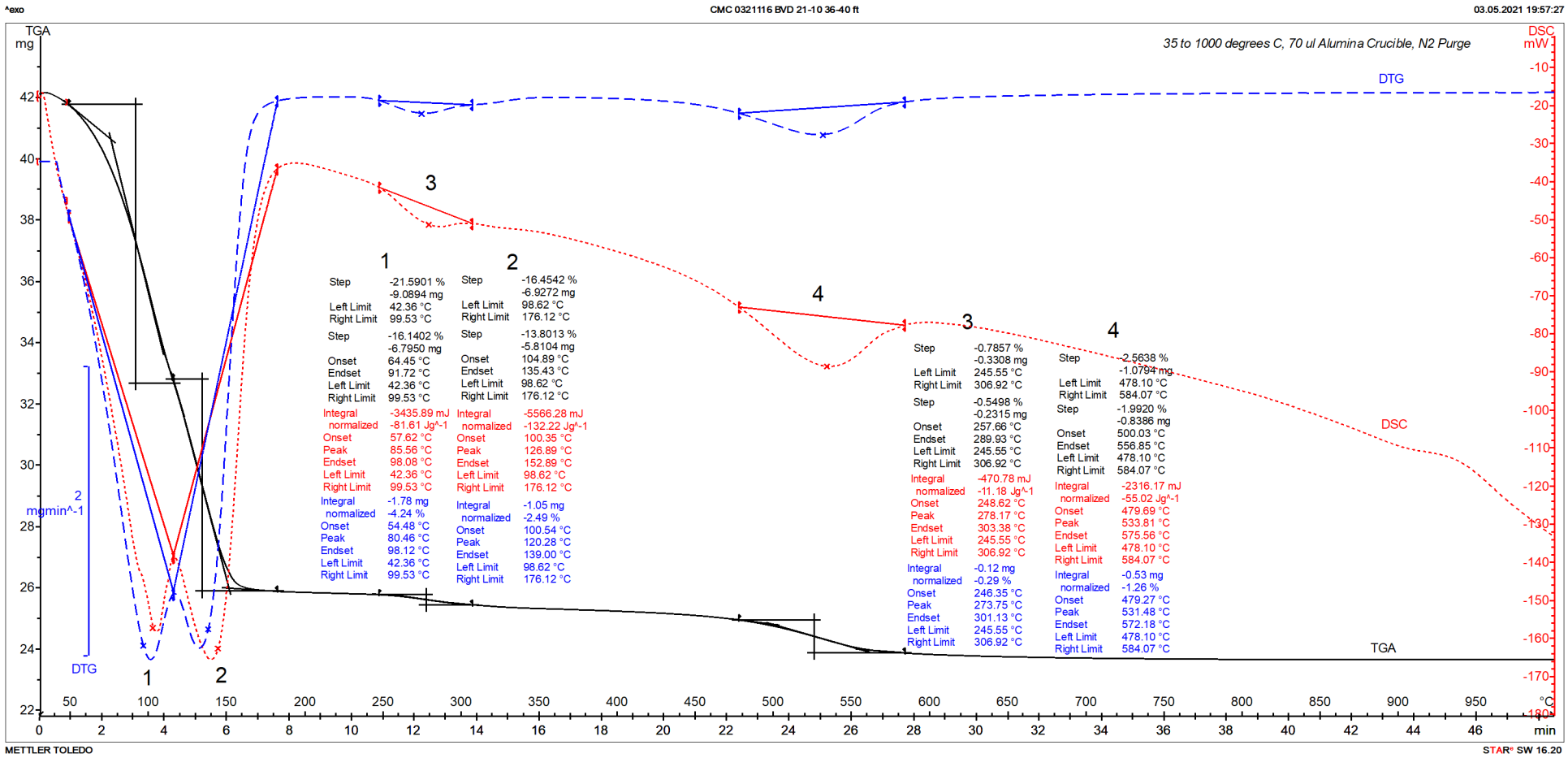


Figure 34: TGA (solid black), DSC (dotted red), and DTG (dashed blue) curves of Soil Sample: BVD 21-10, 36-40 ft. Major endotherms from decompositions (de-hydroxylation) of illite-kaolinite clay minerals and other phases in soil are marked as 1 through 4. No polymorphic transition of fine clay-sized quartz particle is found at 573ºC. Results of thermal analyses are also given. Maximum weight loss from loss of free and bound moisture in illitic clay has occurred within 200ºC.

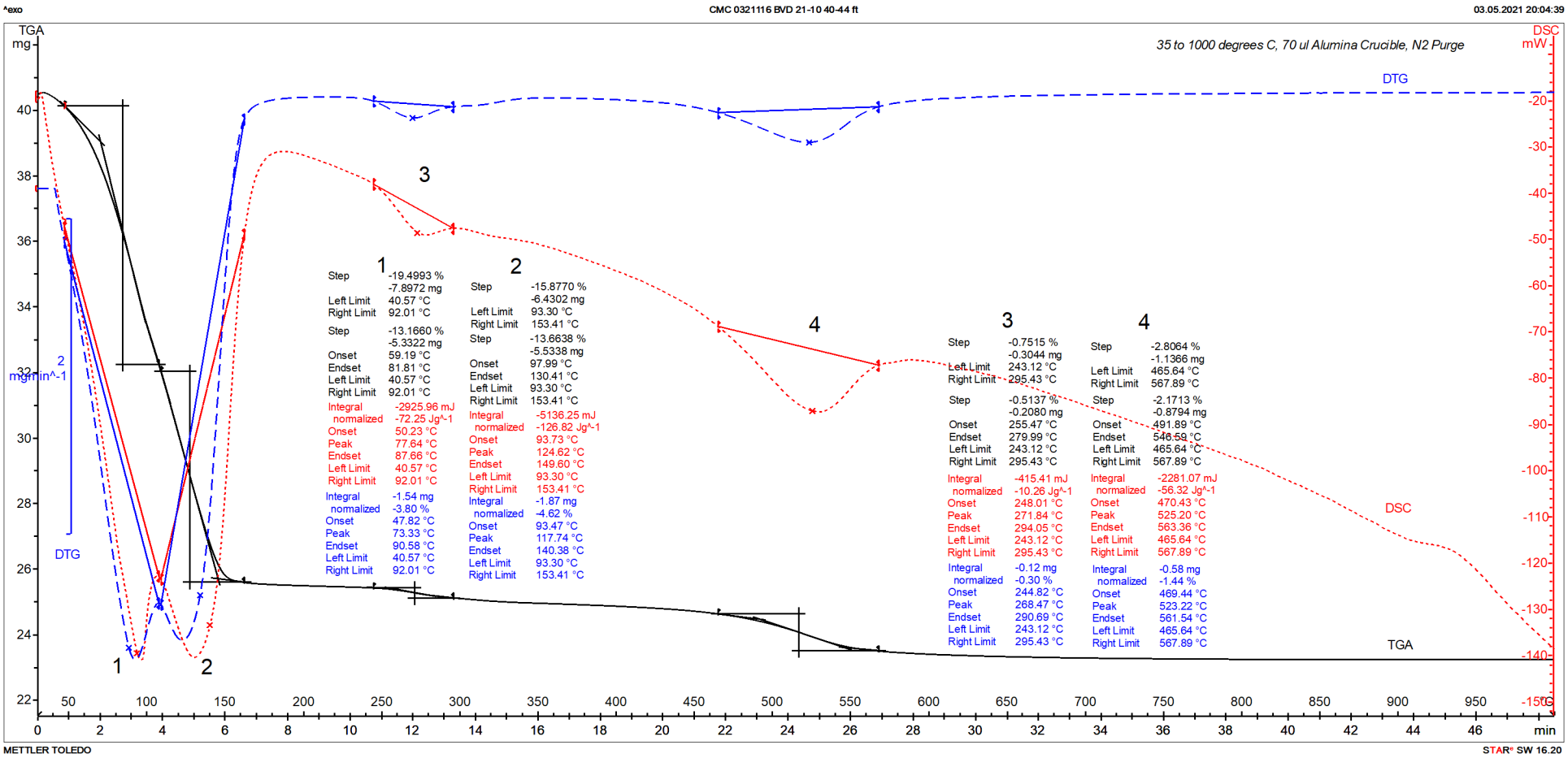


Figure 35: TGA (solid black), DSC (dotted red), and DTG (dashed blue) curves of Soil Sample: BVD 21-10, 40-44 ft. Major endotherms from decompositions (de-hydroxylation) of illite-kaolinite clay minerals and other phases in soil are marked as 1 through 4. No polymorphic transition of fine clay-sized quartz particle is found at 573ºC. Results of thermal analyses are also given. Maximum weight loss from loss of free and bound moisture in illitic clay has occurred within 200ºC.

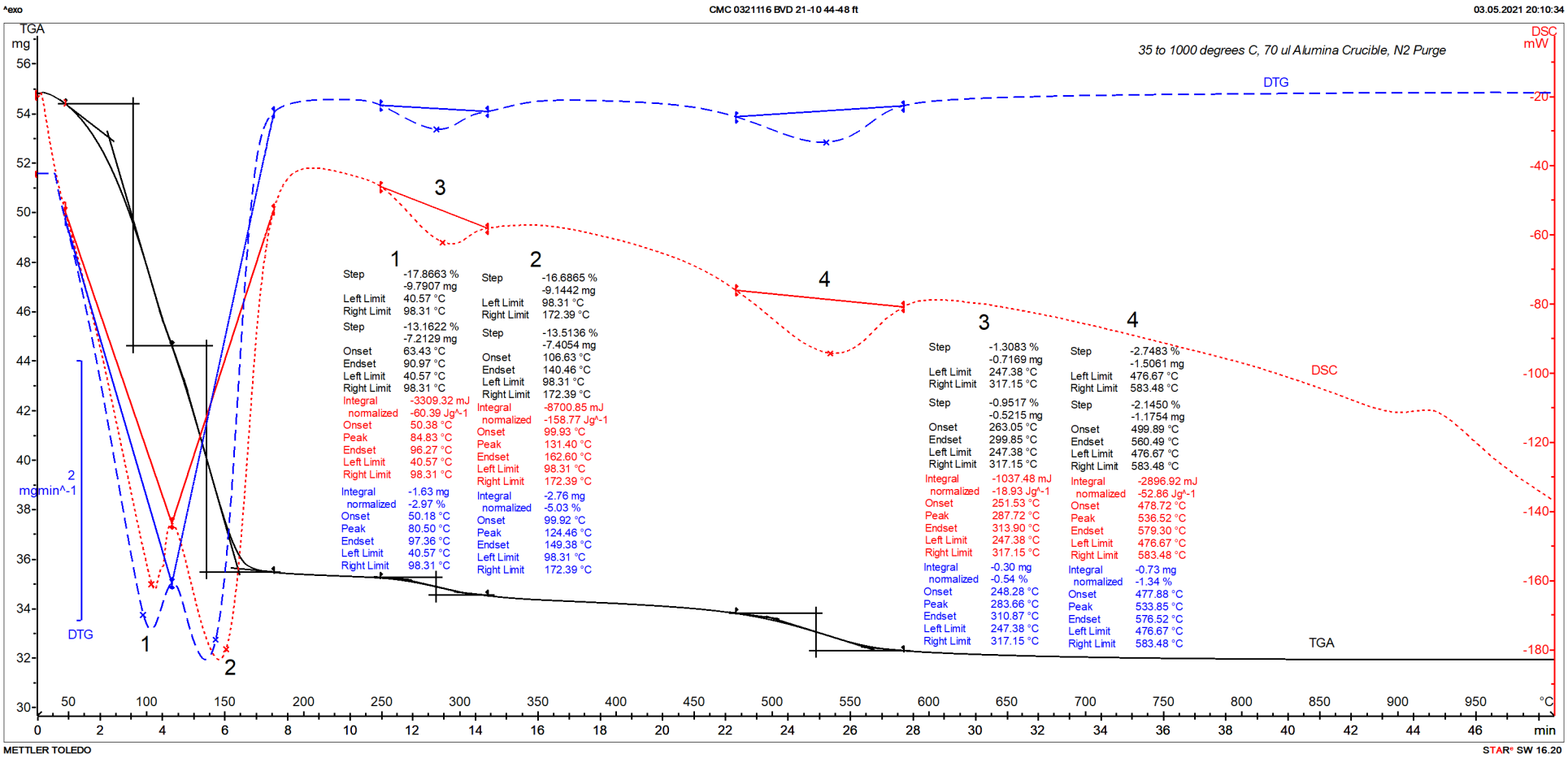


Figure 36: TGA (solid black), DSC (dotted red), and DTG (dashed blue) curves of Soil Sample: BVD 21-10, 44-48 ft. Major endotherms from decompositions (de-hydroxylation) of illite-kaolinite clay minerals and other phases in soil are marked as 1 through 4. No polymorphic transition of fine clay-sized quartz particle is found at 573ºC. Results of thermal analyses are also given. Maximum weight loss from loss of free and bound moisture in illitic clay has occurred within 200ºC.

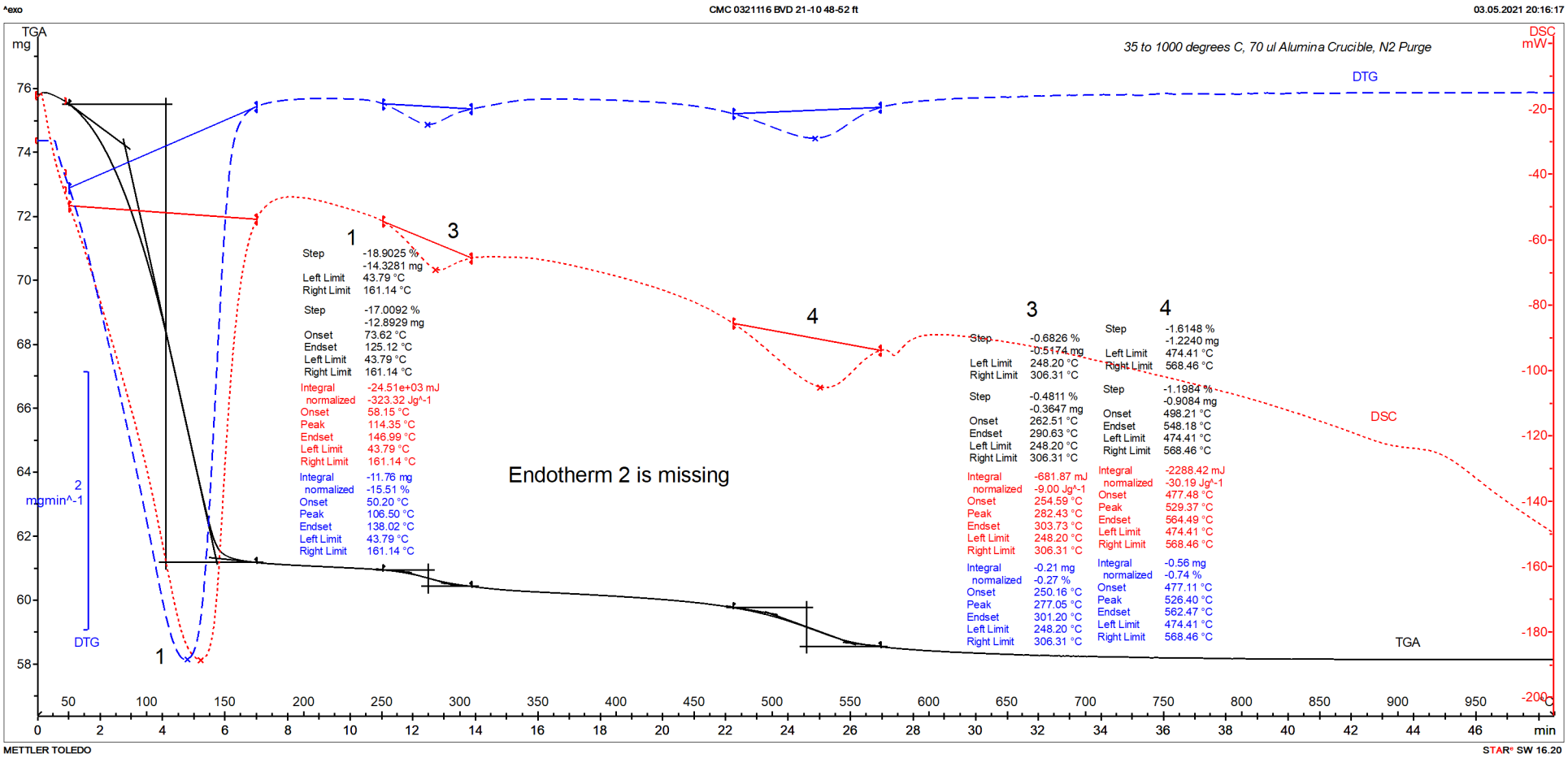


Figure 37: TGA (solid black), DSC (dotted red), and DTG (dashed blue) curves of Soil Sample: BVD 21-10, 48-52 ft. Major endotherms from decompositions (de-hydroxylation) of illite-kaolinite clay minerals and other phases in soil are marked as 1 through 4. No polymorphic transition of fine clay-sized quartz particle is found at 573ºC. Results of thermal analyses are also given. Maximum weight loss from loss of free and bound moisture in illitic clay has occurred within 200ºC.

# END OF REPORT[1]

[1] The CMC logo is made using a lapped polished section of a 1930's concrete from an underground tunnel in the U.S. Capitol.